Condition Assessment of Concrete Elements through Two Nondestructive Ultrasonic Techniques

by

María José Rodríguez Roblero

A thesis

presented to the University Of Waterloo

in fulfilment of the

thesis requirement for the degree of

Doctor of Philosophy

in

Civil Engineering

Waterloo, Ontario, Canada, 2017

Examining Committee Membership

The following served on the Examining Committee for this thesis. The decision of the Examining Committee is by majority vote.

External Examiner	DR. DANTE FRATTA Associate Professor
Supervisor(s)	DR. GIOVANNI CASCANTE Professor
	DR. MAHESH D. PANDEY Professor
Internal Member	DR. SUSAN TIGHE Professor
Internal Member	DR. JEFFREY WEST Professor
Internal-external Member	DR. KUMARASWAMY PONNAMBALAM Professor

Author's declaration

This thesis consists of material all of which I authored or co-authored: see Statement of Contributions included in the thesis. This is a true copy of the thesis, including any required final revisions, as accepted by my examiners.

I understand that my thesis may be made electronically available to the public.

Statement of contributions

One of the contributions of this research project is the improvement of a new field testing ultrasonic device to test structural elements with circular cross section called UTPole. The methodology and the software to acquire and process the data were developed during the PhD studies of a former member of the NDT group (Tallavó, 2009) to evaluate wood poles. My contribution consisted in: the management and technical assistance to the electronic specialists in charge of the development of the electronic system; the design of the transducers holders of the improved field testing device; the study of the modifications needed for the application of the system to test concrete elements; the testing of the different components of the equipment in the laboratory, and the testing of specimens of mortar and concrete in the laboratory and a sample of in-service reinforced concrete columns. The contributions from this research are:

i. The construction, testing in the laboratory and in the field of a new ultrasonic device to assess the condition of structural elements.

ii. The evaluation of the functionality of the device to test concrete elements by testing in-service reinforced concrete columns.

The experimental work done to evaluate the freezing and thawing damage of concrete specimens through nondestructive techniques has been incorporated within a paper that was co-authored by myself, my supervisors, Dr. Giovanni Cascante and Dr. Mahesh Pandey, Dr. Marcelo González and Dr. Susan Tighe. This study was also part of the experimental program of the PhD thesis of Marcelo González at the University of Waterloo under the supervision of Dr. Susan Tighe. I contributed in the concept development of the study; the fabrication of the specimens, the experimental work; the data analysis and the report writing related with the nondestructive tests. Chapter 5 includes the detailed description of this study. The contributions related with this study are:

iii. A critical evaluation of the standardized procedures to assess freeze/thaw damage in concrete.

iv. The evaluation of an alternative procedure to assess freeze/thaw damage in concrete elements based on wave attenuation estimates.

A study performed to verify if through surface wave analysis it is possible to obtain some indication of the imminence of failure of the beams that were tested under fatigue loading is included in Chapter 6. It was defined as a collaborative project with Rayed Alyousef as part of

the experimental program for his PhD thesis under the supervision of Dr. Timothy Topper and Dr. Adil Al-Mayah. My collaboration consisted in the execution of the nondestructive tests of five beams, the data analysis and the concept development of an alternative procedure for the monitoring of the progression of damage. For the evaluation of alternative techniques to process the test data, Dr. Jesús Nuño Ayón advised possible signal processing techniques that could be applicable and the computing algorithms. From this study the main contributions are:

v. The appraisal of a procedure to monitor the progression of damage in concrete elements subjected to fatigue loading based on surface wave analysis.

vi. The evaluation of the applicability of three alternative signal processing techniques for surface wave testing results.

Abstract

Reinforced concrete is one of the materials most used in civil infrastructure, and the expected service life is generally for several decades. However, as any other material, concrete performance is affected by environmental conditions, the normal use of the structure, ageing and extreme load events. All of these factors affect the elements performance and can induce damage. Since all infrastructure components deteriorate over time, it is needed to assess their actual condition. Moreover, to implement adequate corrective measures it is needed to first detect damage and quantify its extent. There are different methods that may be used to inspect concrete elements, and the selection of the adequate technique depends on the property of interest and the available resources.

Among the available inspection methods, the nondestructive techniques (NDT) are those used to detect defects, to estimate the material properties or to assess the integrity of components that do not affect the elements under evaluation. Every inspection technique has advantages and disadvantages; and consequently, the current trend is to use a combination of methods. Even though several nondestructive methods are commercially available, currently there is no comprehensive method to evaluate concrete columns. Taking in consideration these aspects, the main objective of this research was to develop a new nondestructive methodology and testing device that would allow inspecting concrete columns in a fast and reliable manner, without affecting their future performance.

The proposed methodology relies on ultrasonic tests. The condition evaluation is based on measurements of wave velocity and wave attenuation because it is known that the attenuation is more sensitive to damage than the velocity. However, wave attenuation is generally not used in site evaluations because is very difficult to ensure consistent measurements in the field. To overcome this limitation, a new ultrasonic testing device was developed and tested. To verify the applicability of the methodology, reinforced and unreinforced concrete samples were tested in the laboratory, and a sample of in-service reinforced concrete columns was also evaluated. The main contributions of the research presented in this thesis are:

- The construction of a new ultrasonic field testing device to test structural elements with circular cross section.
- The evaluation of a new methodology to evaluate concrete elements based on statistical indexes computed from wave velocity and wave attenuation by testing a sample of in-service columns.

- The new methodology allows detecting damage at earlier stages which would allow implementing opportune corrective measures.
- The proposal and evaluation of an alternative testing procedure to evaluate freeze/thaw damage in concrete specimens based on wave attenuation measurements.
- The appraisal of a new procedure to monitor progressive damage in concrete elements using surface wave measurements.
- The evaluation of alternative signal processing techniques of the signals obtained from the surface wave testing to facilitate the analysis of the results.

Acknowledgements

I would like to thank my supervisors Dr. Giovanni Cascante and Dr. Mahesh Pandey for giving me the opportunity to study in the PhD Program under their supervision, and to the members of the examining committee for their recommendations to improve the work done.

I would like to acknowledge the technical assistance of Dr. Fernando Tallavó throughout my PhD studies and to Dr. Marcelo González, Dr. Jesús Nuño Ayón and Dr. Rayed Alyousef for the opportunity to collaborate with them. Also the technical discussions with Olivier Daigle, Hassan Ali , Fredy Díaz Durán and Piotr Wiciak were essential to my research work.

I am thankful for the technical assistance from John Boldt, Rick Forgett, Mark Kuntz, Jorge Cruz and Andy Barber in the construction of the field testing device; and Richard Morrison, Douglas Hirst, Terry Ridgeway and Anne Allen for the assistance in different stages of the experimental work.

I would like to acknowledge the timely help from Daniel Parent, Don Haffner and Adam Toplician from Plant Operations, and Michael Ditty in the Faculty of Science to obtain the information and the permit for the testing of columns at the University of Waterloo campus.

I express my special thanks to my colleagues in the NDT group and in the Geotechnical group for all the good and difficult experiences shared during these years.

I am particularly thankful to the lounge group (first and second generation) and all the friends that I met in Waterloo who made this journey memorable.

I would also like to express my gratitude to Professor Carlos Fernández at the University of Costa Rica for being a mentor since my undergraduate studies.

Dedication

To my family and friends for their unconditional support, without you I would not have achieved any of my goals.

Table of Contents

List of Tables

List of Figures

List of Symbols

A_1 = amplitude of a propagating wave at the distance x_1 (for the attenuation computation)

A_2 = amplitude of a propagating wave at the distance x_2 (for the attenuation computation)

b = dimension of the cross section of the specimen transverse to the direction in which is driven (to compute the dynamic modulus of elasticity from the resonance test ASTM C215-08)

COV = coefficient of variation of the strength for the cores

$\mathrm{COV_A}$ = coefficient of variation of wave transmission calculations

$\mathrm{COV_V}$ = coefficient of variation of wave velocity measurements

$\mathrm{DIA_{\theta_r}}$ = dissimilarity index for the wave transmission in equation (3-3)

$\mathrm{DIV_{\theta_r}}$ = dissimilarity index for the P-wave velocity in equation (3-2)

DF = durability factor (ASTM C666-08)

E = Young's modulus of elasticity

E_c = modulus of elasticity of concrete from the empirical equation on ACI 318-11

E_d = dynamic modulus of elasticity computed from the dynamic tests (pulse velocity or resonance)

E_s = static modulus of elasticity computed according to ASTM C469-10

FFT = Fast Fourier Transform

f = frequency of the wave

f'_c = specified compressive strength of concrete

f_{ceq} = equivalent strength of the cores extracted (ACI 562M-13)

$\overline{f_c}$ = average core strength accounting for the diameter and moisture condition of the cores

f_x = fundamental transverse frequency after x freeze/thaw cycles (for the computation of the durability factor ASTM C666-08)

f = fundamental transverse frequency at the initial condition (for the computation of the durability factor ASTM C666-08)

$H_A(\omega)$ = transfer function of the system, ratio between the magnitude of the Fourier transform of the output signal and the Fourier transform of the input signal

H_o = null hypothesis, hypothesis test for the comparison of the strength

H_1 = alternative hypothesis, hypothesis test for the comparison of the strength

K = radius of gyration of the cross section, needed to select the correction factor T to calculate the dynamic modulus of elasticity (ASTM C215-08)

k_c = modification factor that depends on the number of cores extracted considered in the computation of the equivalent strength of the cores extracted (ACI 562M-13)

L = length of the specimen

M = mass of the specimen

M_c = constrained modulus

n = number of cores extracted to evaluate the strength of an element

n_1 = number of samples for the cylinders tested in compression (hypothesis test)

n_2 = number of samples for the cores extracted (hypothesis test)

ODI_{θ_r} = overall dissimilarity index at location r

$P_{x_i x_i}$ = auto-power spectral density of the reference signal x_i

$P_{x_j x_j}$ = auto-power spectral density of the compared signal x_j

$P_{x_i x_j}$ = cross-power spectral density of the reference signal x_i and the compared signal x_j

R_e = reflection coefficient which depends on the acoustic impedances (Z) of the materials at an interface

S_1 = the stress corresponding to a longitudinal strain of 0.000050 in the static modulus of elasticity test (ASTM C469-10)

S_2 = the stress corresponding to 40% of the ultimate load (ASTM C469-10)

s_1 = standard deviation for the cylinders tested in compression (hypothesis test)

s_2 = standard deviation for the cores extracted from the specimens (hypothesis test)

$s(\omega)$ = system function obtained by deconvolution dividing the frequency components of the received voltage $V(\omega)$ by the transfer function $H_A(\omega)$ of the system

T_r = transmission coefficient defined which depends on the acoustic impedances (Z) of the materials at an interface

T = correction factor depending on the radius of gyration and the length of the specimen specified in ASTM C215-08 to calculate the dynamic modulus of elasticity

t = dimension of the cross section of the specimen in the direction in which is driven to compute the dynamic modulus of elasticity from the resonance test (ASTM C215-08)

t_e = statistic computed for the hypothesis test

V_p = velocity of the P-waves computed from the ultrasonic pulse velocity test

V_R = Rayleigh waves velocity

V_S = velocity of the S-waves

$V(\omega)$ = frequency components of the received voltage

W = weight factor considered in the calculation of the overall dissimilarity index in equation

x = specified number of cycles at which the exposure is calculated for the durability factor (ASTM C666-08)

$x_i(f)$ = Power spectrum of the reference signal

$x_j(f)$ = Power spectrum of the compared signal

y = specified number of cycles at which the exposure is to be terminated for the computation of the durability factor (ASTM C666-08)

Z = acoustic impedance of a material which is the product of the density and the wave velocity

α_x = spatial coefficient of wave attenuation caused by the material damping

β = geometric attenuation constant

ε_2 = the strain corresponding to the stress S_2 in the static modulus of elasticity test (ASTM C469-10)

Δt_1 = total transit time before the first freeze/thaw cycle minus the transit time in the coupling medium

Δt_2 = the total transit time after n cycles minus the transit time in the coupling medium

$\Delta\varphi$ = phase difference between the signals recorded in two receivers in the Surface wave analysis method (SAWS)

Δx = receivers separation in the Surface wave analysis method (SAWS)

λ = wavelength of the ultrasonic wave

ρ = density of a material

ρ_c = density of the concrete

$\rho_{x_i x_j}$ = Pearson correlation between two signals, x_i the reference signal and x_j the compared signal

σ_{test} = average compressive strength of the cores

τ_n = relative transit time after n freeze/thaw cycles according to RILEM TC 176-IDC

$\tau_n{}^2$ = dynamic modulus of elasticity according to RILEM TC 176-IDC

μ_{A_f} = expected value of the transmission factor corresponding to the reference elements

μ_{V_p} = expected value of P-wave velocity corresponding to the reference elements

μ_1 = average strength of the cylinders tested (before freeze/thaw testing)

μ_2 = average strength of the cores extracted from the specimens (after the freeze/thaw testing)

μ_{x_i} = average of the reference signal x_i

μ_{x_j} = average of the compared signal x_j

σ_{A_f} = standard deviation for the transmission factor corresponding to the reference elements at a specific location

σ_{V_p} = standard deviation for the wave velocity corresponding to the reference elements at a specific location

σ_{x_i} = standard deviation of the signal x_i

υ = Poisson's ratio

ν = degrees of freedom for the case where the standard deviations are unequal and unknown are given by the Satterthwaite's approximation (hypothesis test)

ω = angular frequency

ξ = damping ratio (ratio between the system damping and the critical damping)

Chapter 1 Introduction

Reinforced concrete is one of the most widely used materials for building infrastructure. As any other material, concrete components deteriorate over time and it is required to assess their condition to ensure that they perform as intended in the design. Decision makers often lack of adequate information to implement suitable corrective measures to preserve infrastructure elements or to prevent failures. There is an imperative need for better assessment tools that can provide comprehensive and reliable information about the structural elements. Currently, different methods to inspect concrete elements are commercially offered; however, there is no a comprehensive method for reinforced concrete columns. The main objective of this research was to develop a new methodology and testing device that would allow inspecting concrete columns in a fast and reliable manner, without affecting their future performance.

Various methods may be used to assess the condition of in-service concrete elements, and the selection of a method is based on the scope of the investigation and the resources available. Nondestructive testing (NDT) methods are those inspection techniques used to detect defects, to estimate the material properties or to assess the integrity of components that do not affect the elements under evaluation. The NDT techniques based on the analysis of the propagation of the waves through the element under study are called stress-wave methods; and in this group are classified the ultrasonic pulse velocity and the surface waves method employed in this work. Both methods are also called ultrasonic, for the reason that ultrasonic testing refers to the use of sound waves above 16 kHz, which is considered the average person hearing range (Ensminger & Bond, 2012).

Every NDT inspection technique has advantages and disadvantages; and consequently, the current trend is to use a combination of them (Breysse, Klysz, Dérobert, Sirieix, & Lataste, 2008; Balayssac, Laurens, Arliguie, Breysse, Gernier, Dérobert, & Piwakowski, 2012). The combination of methods may have different purposes, such as to verify the results, to improve the interpretation of the testing data, to obtain a more comprehensive examination, or to correct the effect of a specific parameter in the results.

In this research project, the complementary use of ultrasonic pulse velocity testing and surface wave analysis is analyzed. Even though these two techniques have been used before to evaluate concrete, there are no reported studies of both methods used jointly. From the

surface wave analysis, a global longitudinal evaluation could be obtained, allowing identifying areas of dissimilar characteristics. Then, the areas identified as potentially damaged could be tested with the ultrasonic testing device developed to obtain a detailed evaluation of the cross section.

The most common ultrasonic test consists of the determination of the propagation velocity of the compression waves (P-waves) along the element under study. The usual testing configuration employs two sensors located at opposite sides of the element. The sensors are generally piezoelectric transducers, which are devices that convert electrical energy in ultrasonic energy and vice versa (Blitz & Simpson, 1996). One transducer emits the pulse and the other acts as a receiver. The time between the start of the pulse and the detection of the first arrival of the P-waves at the receiver is the arrival time. The ultrasonic pulse velocity (UPV) is computed dividing the distance between the transducers by the arrival time.

The surface wave analysis method is based also on wave propagation, but monitors Rayleigh waves (R-waves). These waves are those that propagate along the surface as a result of an impact. The basic configuration of the surface wave tests requires a source, two receivers and the data acquisition system. The wave speed is determined using signal processing techniques, and the elastic constants of the underlying materials are determined through an inversion process.

There are several examples in literature that demonstrate that the proposed methods may be useful for the condition assessment of concrete. Ultrasonic testing has been used for decades and is one of the most common NDT methods (ACI 228.2R-13; Breysse, 2012; Cetrangolo & Popovics, 2010; Dilek, 2007). The most recent research in the area is addressed to automation and the generation of images (Chai, Momoki, Kobayashi, Aggelis, & Shiotani, 2011; Schickert, 2012; De la Haza, Samokrutov, & Samokrutov, 2013; Nelson, Ferraro, & Algernon, 2014; Haach & Ramirez, 2016). The surface waves method has been proven useful to determine the elastic modulus of soil sites, pavements and concrete slabs (ACI 228.2R-13); to detect chemical damage in concrete (Ould Naffa, Goueygou, Piwakowski, & Buyle-Bodin, 2002), to verify the quality of the concrete of a bridge pier (Liu & Guo, 2005); to measure the crack depth of surface breaking cracks (Goueygou, Abraham, & Lataste, 2008) (Yang, Cascante, & Polak, 2009), to evaluate repair effectiveness (Aggelis, Shiotani, & Polyzos, 2009), to assess the porosity of concrete (Abraham, Piwakowski, Villain, & Durand, 2012), and to evaluate the condition of cemented materials with distributed damage (Kirlangic, 2013).

The proposed new methodology innovates in the execution of the tests. While the usual configuration uses two sensors, the new methodology is implemented using arrays. In the common ultrasonic testing configuration the results are based on measurements over a single path. It is likely that some defects may not be detected because of the orientation selected or because of the size of the defect. The use of arrays has the advantage that is possible to take different measurements from a single location (Drinkwater & Wilcox, 2006), the measurements can be used to produce visualizations of the internal condition, and there is faster data collection and better noise control. In recent years, there are reports of the successful application of ultrasonic arrays of transducers for the condition assessment of pipelines, wood poles (Tallavó, Cascante, & Pandey, 2011) and concrete elements such as slabs (Schickert, 2012) and bridge decks. Nevertheless, it has been found a limited use of arrays of transducers to evaluate in-service concrete columns.

Another contribution of this research is that the evaluation is based on the ultrasonic measurements of wave velocity and wave attenuation. Several researchers (Saint-Pierre, Rivard, & Ballivy, 2007; Chai, Momoki, Kobayashi, Aggelis, & Shiotani, 2011; Molero, Aparicio, Al-Assadi, Casati, Hernández, & Anaya, 2012; Kirlangic, 2013; Yim, Kwak, & Kim, 2012) demonstrated that wave attenuation presents higher sensitivity than wave velocity to damage. Wave attenuation is an important parameter to take into account for material evaluation, because an increase in the attenuation is an indication of degradation or loss of strength of the material (Ensminger & Bond, 2012). Nonetheless, the implementation of wave attenuation has been limited, due to the difficulty to obtain reliable measurements in the field. The main challenge in the field is to obtain a consistent coupling, which is the transmission of the waves from the transducers to the elements. This limitation was addressed by the development of a new field testing device and the testing of different couplants. Currently, there are no reported examples of the use of ultrasonic wave attenuation for the condition assessment of reinforced concrete circular columns in the field, which are the elements of interest for this project.

Based on these findings, the objectives of this research were formulated and are detailed in the following section.

1.1 Research objectives

General objective

To develop a new methodology for the condition assessment of reinforced concrete columns, using ultrasonic techniques and taking advantage of the complementary use of wave velocity and wave attenuation measurements. The novelty of the proposed methodology lies on the complementary use of wave attenuation and elastic moduli in addition to wave velocity to better evaluate damage in reinforced concrete columns.

Specific objectives

a. To understand the state-of-the art in inspection methods for concrete elements, the existing limitations of the stress-wave methods under study and the improvements required.

b. To improve the coupling between the piezoelectric transducers and the concrete elements to obtain more reliable attenuation estimates in the laboratory and in the field.

c. To investigate the effectiveness of ultrasonic pulse velocity and attenuation measurements to assess internal damage in concrete elements.

d. To perform a pilot study on the use of surface waves to assess the progression of damage of reinforced concrete elements.

e. To calibrate the new testing device (called UTPole) by testing unreinforced and reinforced concrete specimens in the laboratory.

f. To assess the functionality of the new ultrasonic device developed by testing a statistically representative sample of reinforced concrete columns in-service.

1.2 Methodology

Figure 1-1 provides a schematic representation of the methodology and the detailed description is presented in Chapter 3.

The methodology was divided in three components: the literature review, the laboratory and the field testing.

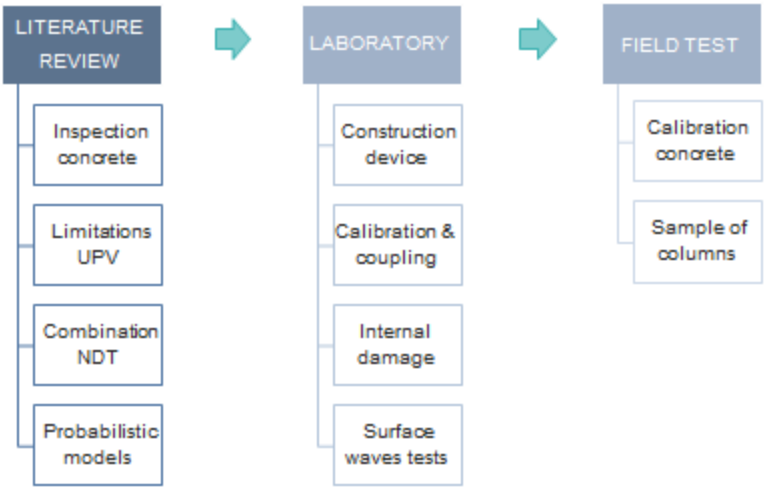

Figure 1-1: Schematic representation of the methodology

The literature review was needed to understand the state-of-the art in inspection methods for concrete elements, the existing limitations of the methods under study and the improvements required.

The laboratory testing was focused on specific aspects of the ultrasonic techniques used in the study that required improvement, according to the limitations identified in the literature review. The studies included the calibration of the transducers, the evaluation of different couplants for the field testing, the assessment of the effectiveness of the velocity and attenuation measurements to detect internal damage and the application of the surface waves method to evaluate reinforced concrete elements.

To be able of incorporating wave attenuation in the evaluation, it was necessary to build a new field testing device, so it was possible to obtain constant pressure and adequate coupling. Once the new device was built and verified in the laboratory, a sample of in-service concrete columns was tested.

The new aspects of the methodology are the proposed complementary use of the ultrasonic techniques and the testing procedure with the new field testing device developed.

1.3 Significance of the research

In this project, a new methodology to assess the internal condition of structural elements is evaluated. The methodology is non-invasive and nondestructive; therefore, the mechanical properties of the elements are not affected by the tests. It is intended to detect damage at

earlier stages, which would allow the implementation of adequate corrective measures. With the existing inspection methods, the deterioration has to be extensive to be detected. The methodology is based on the combination of nondestructive techniques and the use of a newly constructed field testing device. The field testing device allows reducing inspection time without compromising reliability of data, and provides a global and also a detailed assessment of the condition of concrete elements. A better assessment of the condition of the structural elements would result in better maintenance practices and a possible reduction in costs.

The contribution of this research work is included in four journal publications that are currently in progress:

1. "Evaluation of Freeze/Thaw Damage in Nanoconcrete through Ultrasonic Wave Velocity and Attenuation". Authors: Rodríguez-Roblero, M.J., González, M., Cascante, G., Pandey, M.D., & Tighe, S. This paper presents the study of freezing and thawing damage in concrete specimens and the complementary use of attenuation measurements to detect internal damage (Chapter 5). This paper has been submitted to the ASCE Journal of Materials in Civil Engineering.
2. "New application of the surface wave analysis to assess reinforced concrete structural elements". Authors: Rodríguez-Roblero, M.J., Alyousef, R., Nuño Ayón, J., Cascante, G., Pandey, M.D., & Topper, T. This paper presents the study of the application of surface waves to monitor fatigue damage in concrete beams and the site evaluation of a reinforced concrete dome. In addition, contains the study of the application of alternative signal processing techniques to facilitate the interpretation of the field data (Chapter 6).
3. "New Methodology for the Assessment of the Homogeneity in Concrete Columns through Ultrasonic Wave Velocity and Attenuation". Authors: Rodríguez-Roblero, M.J., Tallavó, F., Pandey, M.D., & Cascante, G. This paper describes the calibration of the UTPole software to test reinforced concrete elements and the evaluation of a sample of in-service reinforced concrete columns (Chapter 7).
4. "Study of the coupling effect on the ultrasonic measurements in the evaluation of concrete elements". Authors: Rodríguez-Roblero, M.J., Wiciak, P., Cascante, G., Polak, M., & Pandey, M.D. This paper includes the tests presented in Chapter 4 for the examination of possible couplants for testing concrete elements, and the results from the direct measurement of the ultrasonic response using a laser vibrometer.

1.4 Thesis organization

Chapter 1 presents the problem definition, the objectives and the expected contributions from the research project.

The theoretical background is presented in Chapter 2, where the main concepts of the two ultrasonic testing methods applied in the project are summarized. Also includes the literature review and a brief description of the mechanisms of deterioration of concrete.

Chapter 3 describes the methodology followed in this research project and Chapter 4 explains the calibration of the ultrasonic transducers.

Chapter 5 summarizes the results of a study on the sensitivity of the ultrasonic pulse velocity test to two types of internal damage (freeze/thaw and compression) and evaluates a possible manner of incorporating ultrasonic wave attenuation in the evaluation of concrete samples.

Chapter 6 presents the study of the application of surface waves testing to evaluate reinforced concrete elements. This study considered the testing configuration, different types of mounting of the sensors and alternative methods to process the test data.

Chapter 7 reports the results of the testing of in-service concrete columns using the field testing device built during this research project. Finally, Chapter 8 summarizes the conclusions and recommendations of the work.

Chapter 2 Background and Literature Review

2.1 Introduction

This chapter summarizes the generalities of reinforced concrete as a material and the deterioration mechanisms of structural elements. The main inspection techniques are mentioned, and the nondestructive methods for hardened concrete compared. As the testing methodology employed in this research is based on stress-wave methods, the fundamentals of wave propagation are also summarized.

2.2 Generalities of reinforced concrete

Concrete is a widely used construction material because it may be used for different applications and it presents economical and durability advantages (Kosmatka, Kerkhoff, & Panarese, 2002). It is a composite material consisting of a binding medium formed by hydraulic cement and water in which are embedded granular materials usually referred as aggregates. Concrete can also include other materials with cementing properties (for example natural pozzolans, fly ash or silica fume), admixtures or fibres. It is called reinforced concrete when includes bars, wires, fibres, strands or other slender elements embedded in the matrix to resist forces (ACI CT-13). By volume, the typical hydraulic concrete has volume fractions of aggregates in the range of 0.7 to 0.8 (Lamond & Pielert, 2006). The rest of the volume is occupied by the cement paste (water, cement, admixtures, other cementitious materials) and air voids. The aggregates are generally crushed rocks or gravels and sand, but also could be crushed hydraulic cement concrete or iron blast-furnace slag. The aggregates are usually classified as coarse and fine, being the coarse the aggregates retained in the 4.75mm (No. 4) sieve, and the fine the portion passing the 4.75 mm sieve but that are predominantly retained on the 75 mm (No. 200) sieve (ACI CT-13).

Even though an adequate selection of the materials (proportion and characteristics) is essential for the performance of reinforced concrete, this is not sufficient to ensure that the elements would have the durability expected. The production, handling, placing, finishing and curing of concrete have an important effect in the final quality of the elements. These factors and the consideration of the possible deterioration mechanisms should be analyzed in the design stage so the concrete element would perform as intended during the expected service life. Of these aspects, the most relevant for the research are the deterioration mechanisms for reinforced concrete and are summarized in the next section.

2.3 Deterioration mechanisms for reinforced concrete

Deterioration in concrete can result from external factors (environmental conditions, stress, strains) or internal to the material (concrete components). The damages can be classified as physical and mechanical damages or chemical processes.

- **Physical and mechanical damage processes:** those damages that have a physical or mechanical origin: abrasion, fire, freeze and thaw, restraining effects (shrinkage and temperature) and overloading or imposed strains.
- **Chemical damage processes:** damages caused by chemical processes originated in the environment or in the concrete matrix itself (Breysse, 2010). The main chemical processes of damage are: carbonation, chloride penetration (which lead to corrosion of the reinforcement), alkali-aggregate reaction, sulfate attack, leaching and ammonium nitrate attack.

The understanding of the deterioration processes is fundamental to identify problems, choose appropriate methods of inspection and ultimately to select adequate corrective measures. Table 2-1 summarizes the main deterioration mechanisms and the information collected in the inspections.

Table 2-1: Main deterioration mechanisms, consequences and required information (after Breysse, 2010)

Mechanism	Consequences in concrete	Required information
Overloading Restraining effects (temperature, shrinkage)	Damage, cracking	▪ If distributed damage: crack density, residual stiffness and strength ▪ If localized cracking: location, width, depth
Freeze-thaw cycles	Scaling, spalling, delamination	▪ Affected areas ▪ Depth of defect
Fire	Strength decrease, spalling	▪ Depth reached by fire effects ▪ Residual strengths at different depths
Abrasion-erosion	Material loss	▪ Residual strength of surface layer
Carbonation	Increase in density, depassivation of steel, thus, rebar corrosion	▪ Carbonation depth ▪ If corrosion: localization of active corrosion areas and corrosion rate

Table 2-1: Main deterioration mechanisms, consequences and required information (after Breysse, 2010)

Mechanism	Consequences in concrete	Required information
Chloride attack	Rebar corrosion	▪ Chloride content, chloride profile ▪ If corrosion: localization of active corrosion areas and corrosion rate
Alkali-aggregate reaction Sulphate attack	Internal expansion, generalized cracking	▪ Potential for future volume change ▪ Residual stiffness and strength
Leaching	Cement paste dissolution, increase in porosity	▪ Residual strength ▪ Porosity
Ammonium nitrate attack	Deterioration of cement paste, spalling, rebar corrosion	▪ Depth of the attack ▪ If corrosion: localization of active corrosion areas and corrosion rate

Table 2-1 describes different signs of distress that can be identified in concrete elements, and how concrete deterioration could affect the integrity and the performance of the elements. Therefore, the condition assessment of concrete elements is an essential task for every infrastructure owner. Different methods can be applied to inspect hardened concrete and the selection is based on the characteristic of interest and the type of inspection required.

2.4 Condition assessment for concrete structural elements

The expected service life of concrete elements is generally for several decades, but as any other material, concrete's performance is affected by environmental conditions, the normal use of the structure, ageing and extreme load events. All these factors can induce damage in the components and the detection of damage and its quantification is the main goal of the inspections. In addition to damage, the inherent variability in the mechanical properties of the materials and the changes during the construction stage may lead to differences between the designed and built elements. Therefore, structural elements should be inspected regularly during the service life to evaluate the current condition, and to ensure that the elements will perform as intended in the design.

Figure 2-1 shows that documentation examination, visual inspections, field testing, laboratory testing and structural analysis are the basic components for concrete evaluation.

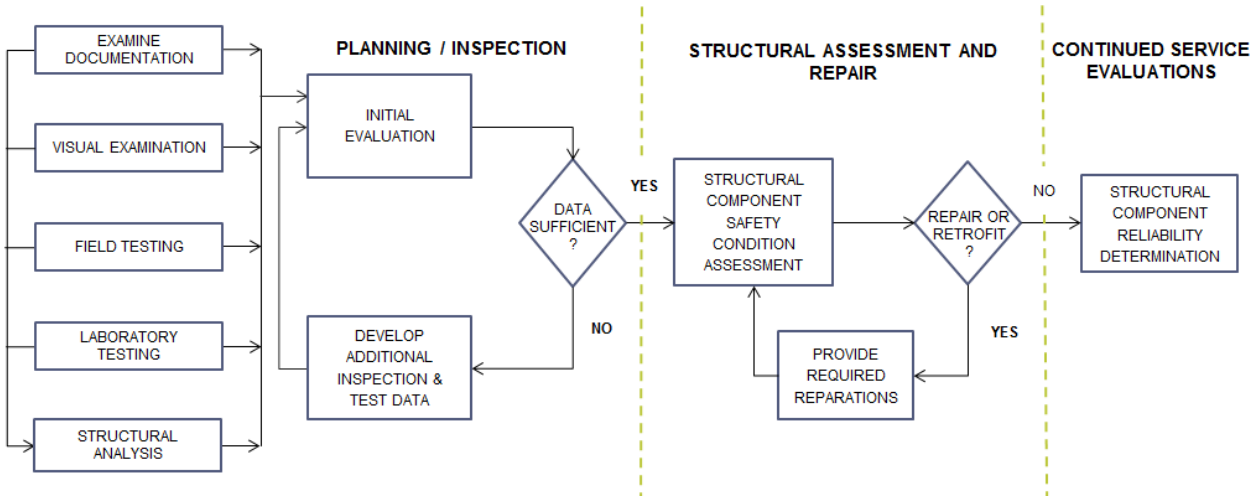

Figure 2-1: Concrete component evaluation (after ACI 365.1R-00)

ACI 365.1R-00 also highlights that the testing of the concrete components and its performance is needed in several circumstances, such as:

- Noncompliance with specifications
- Inadequate placing, compacting or curing of concrete
- There is physical (overload, fatigue, abrasion, freeze and thaw, fire, explosion) or chemical damage
- Concern about the capacity of the structure
- Verification of models, materials and environmental parameters considered in the service life prediction in the design phase, or for the optimization of the operation and maintenance.

The previous list demonstrates the importance of condition assessment techniques, and also the broad range of conditions in which they are needed. For this reason, it is considered necessary to indicate that for the purpose of this work, only the conditions related with the deterioration of columns and that are revealed in a field inspection are considered. In the following section the conditions studied are detailed.

2.4.1 Typical defects encountered in concrete columns

The defects in reinforced concrete can be classified as internal or external defects. External defects include surface air voids, shrinkage cracking, scaling, spalling and popouts. Internal

defects include honeycombing, inclusions, voids and corrosion. The definitions of the defects presented below are from the ACI Concrete Terminology (ACI CT-13):

- **Surface air voids:** refers to cavities not exceeding 15 mm in diameter, generally resulting from entrapment of air bubbles in the surface of formed concrete during placement and consolidation (Figure 2-2).
- **Shrinkage cracking:** cracking resulting from the restraint of shrinkage (decrease in either length or volume as a result of changes in the moisture content or chemical damages). This kind of cracking can present a random, polygonal or parallel pattern (Figure 2-3). They can present a width as wide as 3 mm and can be spaced few millimetres o meters apart. Usually begin as shallow cracks but can become full depth cracks during the service life (ACI 224.1R-07).
- **Scaling:** local flaking or peeling away of the near-surface portion of hardened concrete or mortar.
- **Spalling:** refers to the formation of spalls which are fragments detached from the concrete caused by weather action, a blow, expansion (Figure 2-4).
- **Popouts:** small portions of a concrete that break away due to localized internal pressure that leaves a shallow, typically conical, depression (Figure 2-7).
- **Honeycombs:** voids between the coarse aggregate that are not filled with mortar (Figure 2-6). Honeycombing can be a consequence of improper placing methods, a mixture with excess of coarse aggregate and congested reinforcement (Kosmatka et al., 2002).
- **Segregation:** separation of the coarse aggregates from the mortar and the unequal distribution of the aggregate in the mixture. The areas with less aggregate would tend to experience larger cracking, shrinkage and having poor resistance to abrasion. The other parts of the mixture that contain more coarse aggregate would be difficult to consolidate and finish and segregation would be a cause of honeycombing (Kosmatka et al., 2002).

From the aforementioned defects, the internal defects (honeycombing and segregation) are of special interest for the research because they could exist in the element without evidence in the surface. The other defects are easily identified through visual inspection. The application of the proposed methodology presents an advantage with respect to the existing technologies

because it provides a cross sectional image intended to detect internal defects and deterioration at earlier stages, which is not possible with the conventional methods.

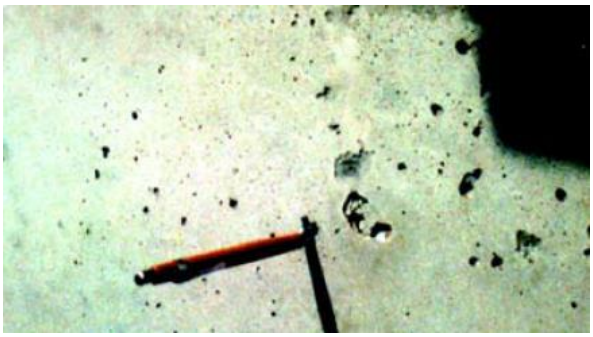

Figure 2-2: Example of surface air voids (also called bug holes, ACI 201.1R-08)

Figure 2-3: Example of shrinkage cracking (ACI 201.1R-08)

Figure 2-4: Example of medium spalling of a concrete surface (ACI 201.1R-08)

Figure 2-5: Example of concrete flaking or spalling (http://concretetoolreviews.com)

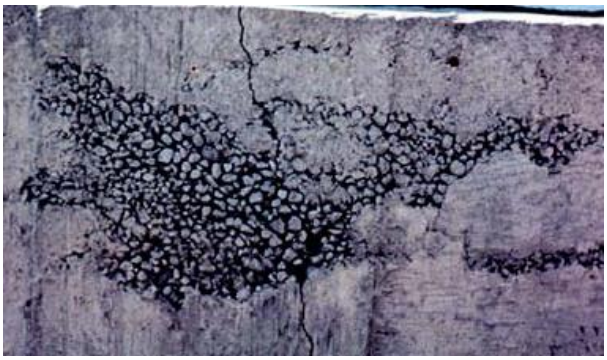

Figure 2-6: Honeycombing (ACI 201.1R-08)

Figure 2-7: Popouts (Kosmatka et al., 2002)

2.4.2 Nondestructive testing (NDT) techniques for concrete

A method is considered nondestructive when the characteristics of the element being inspected are not affected by the tests. NDT methods are used both during the construction and operation phases with different purposes: for quality control of new construction, for condition assessment of existing structures, for maintenance and rehabilitation purposes, and for quality control of repairs.

Depending on when they are applied, NDT methods for concrete are divided in two groups: methods applied in fresh concrete and in hardened concrete. This research focus is on existing reinforced concrete elements; therefore, emphasis is made on the methods for hardened concrete. The NDT methods applicable for hardened concrete are usually classified as:

- visual inspection
- stress-wave methods
- nuclear methods
- magnetic methods
- electrical methods
- methods for measuring transport properties
- infrared thermography and
- radar

This research is focused on the application of ultrasonic and surface wave methods; hence, the methods considered in detail are the stress-wave methods for structural elements.

2.4.3 Stress-wave methods

Stress-wave methods are based on the analysis of the propagation of waves through the element under study. Wave propagation refers to the transmission of a disturbance in a medium. The stress waves may be induced by impact or by a transducer, which is a device that converts energy of one kind to another. Table 2-2 summarizes the main stress-wave methods applied to assess the condition of reinforced concrete structural elements, indicating their main use, advantages and limitations. As it is indicated in Table 2-2, the standardized ultrasonic pulse velocity method is not used to identify defects because the test results only provide an estimate of the velocity of propagation. However, the generation of a new tomographic image based on statistical indexes (see Chapter 3) would allow improving the application of the method to locate and identify internal defects in the elements.

Table 2-2: Advantages and limitations of stress-wave methods for infrastructures (based on Tables 3 and 3.2.6 from ACI 228.2R-13)

Method	Principle	Applications	Advantages	Limitations
Ultrasonic pulse velocity (ASTM C597)	The travel time of a pulse of ultrasonic waves over a path of known length is measured.	To determine the relative condition or uniformity of concrete based on the measured pulse velocity.	▪ Portable equipment commercially available. ▪ Relatively easy to use.	▪ Requires access to two sides of the members. ▪ It does not provide information on the depth of the defect.
Ultrasonic echo	A transducer emits a short pulse of ultrasonic waves, which is reflected by the opposite side of the member or internal defects. The arrival time of the reflected pulse is recorded by an adjacent receiver and the round-trip travel time is determined.	To locate defects such as delaminations, voids, and honeycombing within the elements, or to measure an element thickness.	▪ It is needed access only to one face of the element. ▪ It provides information on the depth of the defect. ▪ The method based on S-wave point transducers and SAFT (Synthetic Aperture Focusing Technique) permit construction of 3-D tomographic images.	▪ Applicable to limited member thickness. ▪ An experienced operator is required.
Impact-echo (ASTM C1383)	A receiver adjacent to the impact point monitors the arrival of the stress wave, as it undergoes multiple reflections between surface and the opposite side of plate-like member or from internal defects. From frequency analysis it is possible to determine the distance to the reflector if the wave speed is known.	To locate defects such as delaminations, voids, honeycombing, or to measure element thickness.	▪ Access to only one face is needed. ▪ Equipment is commercially available. ▪ Capable of locating a variety of defects. ▪ Does not require coupling material.	▪ An experienced operator is required. ▪ Current instrumentation limited to testing members of maximum thickness of 1 m.
Spectral analysis of surface waves	A surface wave is generated through impact and two receivers monitor the surface motion. Using signal analysis the wave speed is determined as a function of wavelength. The elastic constants of the layers are determined through an inversion process.	▪ To determine the stiffness profile of a pavement system. ▪ To assess the depth of deteriorated concrete.	Capable of determining the elastic properties of layered systems, such as pavements, interlayered good and poor quality concrete.	▪ An experienced operator is required. ▪ Involves complex signal processing.
Impulse response (ASTM C1740)	The surface of the element tested is struck with an instrumented hammer and adjacent transducers measure the dynamic response. Through signal analysis it is possible to determine the characteristics of the tested element.	To locate anomalous regions in plate-like structures; voids below slabs on ground; cracks, and constrictions in deep foundations. It may provide information on low-strain dynamic stiffness of shaft/soil systems.	▪ Access to only one face is needed. ▪ Equipment is commercially available. ▪ Does not require coupling materials. ▪ Large areas tested in short time.	▪ An experienced operator is required. ▪ Thickness limitation of 1 m.

2.5 Background information

In this section, the wave propagation fundamentals and the principles of the nondestructive test methods employed in the project are briefly described.

2.5.1 Wave propagation fundamentals

The two methods studied in this research project are based on the propagation of stress waves in the material. Therefore, in this section the fundamental concepts of wave propagation in elastic media are briefly presented.

Ultrasonics refers to the use of ultrasound in different scientific applications, where ultrasounds are those sounds that exceed human hearing range, generally considered as above 18 kHz (Blitz & Simpson, 1996) or 16 kHz (Ensminger & Bond, 2012). Since ultrasonics is the application of a specific range of sound waves, the fundamentals of wave propagation are the basis for any ultrasonic method.

Wave propagation is the transmission of a disturbance in a medium to other parts of the medium without mass transport. Sound waves are stress waves, which mean that they can only exist in mass media, they cannot propagate in a vacuum and the transmission is by contact (Ensminger & Bond, 2012). The waves are elastic when the induced stresses in the material do not exceed its elastic limit and the material behaviour follows Hooke's Law.

Based on their oscillatory pattern, waves are described as P-wave, S-waves, R-waves or L-waves. P-wave and S-waves are body waves, since they travel through the internal volume of the elastic media. R-waves and L-waves are called surface waves because the propagation occurs in the surface of the elastic medium. The surface in this case refers to a maximum depth of one wavelength (λ), that is the distance between two planes in which the particles are in the same state of motion (two compression zones, for example). It is the distance that the sound will move in the direction of propagation in a given material at a specific frequency. The depth that is affected depends on the frequency of the wave propagating and the velocity of propagation in the specific material (2-4). Figure 2-8 illustrates the basic types of waves in solids and the main characteristics of each type of wave are summarized below.

- **P-wave:** are the waves associated to the propagation of normal stresses and are compressional or dilatational waves. They are also called longitudinal waves or primary waves, since in solids they are the fastest mode of propagation.

- **S-wave:** correspond to the transmission of shear strain without volumetric deformation. The particle motion is perpendicular to the direction of propagation and as they propagate slower than P-waves, they are known as secondary waves.

- **R-wave:** or Rayleigh waves are surface waves because their motion is restricted to surface of the medium (one wavelength). The particle motion is retrograde.

- **L-waves:** Love waves propagate in a horizontal plane and the particle motion is perpendicular to the direction of propagation.

- **Lamb waves:** also known as plate waves, they occur when a medium has two free surfaces and the thickness is approximately one wavelength. They can be generated only at particular values of frequency, angle of incidence and material thickness. The velocity of the wave depends on the mode of propagation and the product of the material thickness and the examination frequency (Hellier, 2001).

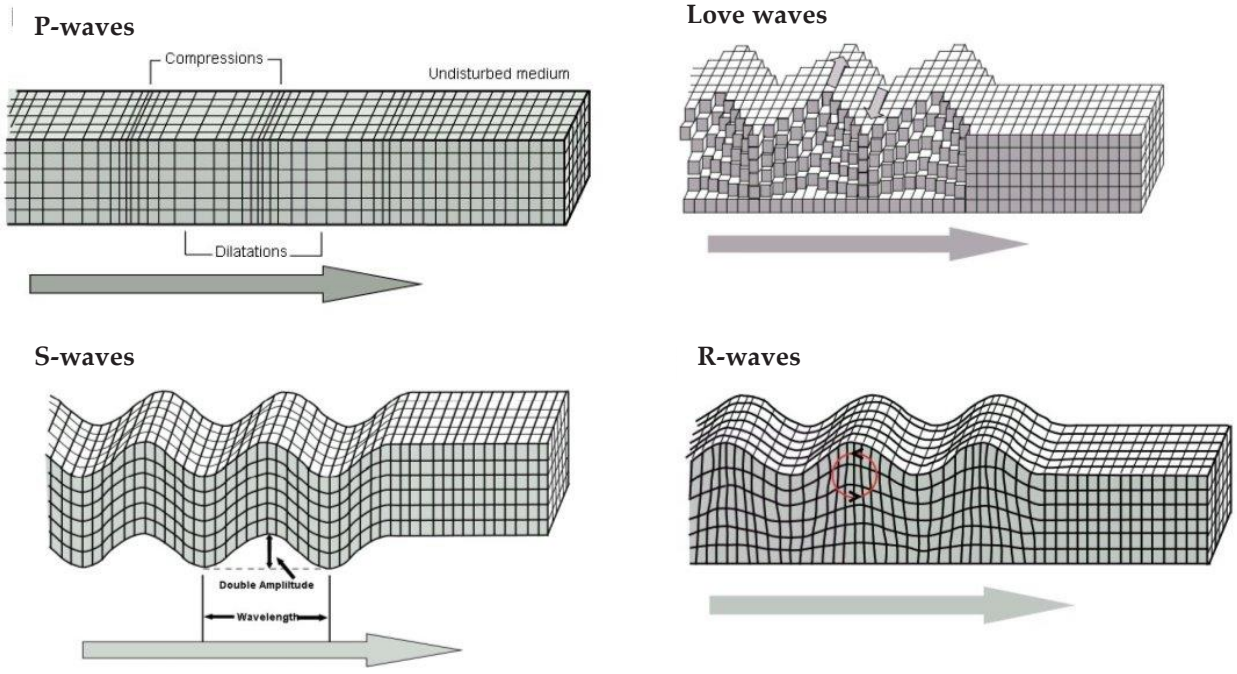

Figure 2-8: Type of waves in solids
(http://kiska.giseis.alaska.edu/input/west/guides/amato_faulting/wave_types.jpg)

The velocity of propagation of a wave depends on the medium properties (modulus of elasticity, Poisson's ratio, density); consequently, the stress-wave propagation behaviour may be used to infer characteristics of a material. For example, the **speed of a P-wave** (V_p) is given by the relation of the Young's modulus (E), Poisson's ratio (υ) and the density (ρ) as follows:

$$\mathrm{V_p} = \sqrt{\frac{\mathrm{E}(1-\upsilon)}{\rho(1+\upsilon)(1-2\upsilon)}} \tag{2-1}$$

The **velocity of the S-waves** (V_s) depends only on the density and on the shear modulus (G), as it is shown in the next equation:

$$V_s = \sqrt{\frac{G}{\rho}} \tag{2-2}$$

The ratio between the velocity of the S-waves and the surface waves, specifically Rayleigh waves, is given by equation (2-3):

$$\frac{V_R}{V_S} = \sqrt{\frac{(1-2\upsilon)}{2(1-\upsilon)}} \tag{2-3}$$

In addition to the wave velocity (V), two wave properties that have a significant effect in the testing results are the wavelength (λ) and the frequency (f). Both properties are related to the velocity by the following expression:

$$V = f \cdot \lambda \tag{2-4}$$

The **frequency** (f) of a wave is the number of oscillations per second and the units of frequency are hertz (Hz). The frequency is the inverse of the time period (T) and it is related with the angular frequency (ω) as follows:

$$f = \frac{1}{T} = \frac{\omega}{2\pi} \tag{2-5}$$

A wave can also be characterized by the **wave number** (k) defined in relation with the wavelength:

$$k = \frac{2\pi}{\lambda} \tag{2-6}$$

As a wave propagates in a medium, it interacts with discontinuities and the boundaries of the elements, which results in the partition of the acoustic energy. Depending on the type of incident wave and the acoustic properties of the media, a portion of the incident wave is reflected and part is transmitted. The **reflection** (R_e) and **transmission** (T_r) **coefficients** for an incident wave are given by:

$$R_e = \frac{1 - \frac{Z_1}{Z_2}}{1 + \frac{Z_1}{Z_2}} \tag{2-7}$$

$$T_r = \frac{2\frac{Z_1}{Z_2}}{1 + \frac{Z_1}{Z_2}} \tag{2-8}$$

where Z_1 is the acoustic impedance of material 1 and Z_2 the acoustic impedance of material 2.

The **acoustic impedance** of a material is the product of the density and the wave velocity:

$$Z = \rho \cdot V \tag{2-9}$$

Table 2-3 shows the typical values for the acoustic impedances of the materials of interest for reinforced concrete elements. It indicates the relatively low acoustic impedance of air. When a wave is traveling in concrete or steel, and it encounters an air interface, the reflection coefficient is approximately 1.0, which means that there is almost total reflection. For this reason it is possible to use NDT stress-wave methods to locate voids or other defects within the concrete.

Table 2-3: Typical values for the acoustic impedance (ACI 228.2R-13)

Material	**Acoustic impedance** $\frac{\mathbf{kg}}{(\mathbf{m^2 s})}$
Air	0.4
Water	1.5×10^6
Concrete	7 to 10 $\times 10^6$
Steel	47×10^6

The acoustic impedance also explains the convenience of the use of wave attenuation. Although a thin crack would not produce a measureable change in wave velocity, it will produce a significant change in the wave amplitude because of the impedance mismatch (Berubé, 2008). The **wave attenuation** is a factor that describes the decrease in wave intensity or pressure as the wave propagates in a medium. There are different ways of expressing the attenuation, but normally is expressed in decibels per unit length (Hellier, 2001; ASTM E1316-11b). The attenuation may also be expressed in nepers (Np) per unit length. The value in decibels is equal to 8.68 times the value in nepers for a given distance or time. If the amplitude is been reduced by one neper, it means that the amplitude has fallen to 1/e of its initial value, where e is the base of the natural logarithm. The total attenuation of a propagating wave is defined as:

$$\frac{A_1}{A_2} = \left(\frac{x_1}{x_2}\right)^{\beta} e^{\alpha_x(x_1 - x_2)} \tag{2-10}$$

where A_1 and A_2 are the amplitudes at the distances x_1 and x_2, β is the geometric attenuation constant and α_x is the spatial coefficient of wave attenuation caused by the material damping. Expressing equation (2-10) in terms of the attenuation coefficient:

$$\alpha_x = \frac{1}{x_2 - x_1}\left[\ln\left(\frac{A_2}{A_1}\right) - \beta \ln\left(\frac{x_2}{x_1}\right)\right] \tag{2-11}$$

Attenuation results from different factors: wave spreading, scattering, absorption and mode conversion. The combined loss of scattering and absorption is known as the material attenuation, and the loss from the wave spreading is usually referred as geometric attenuation. The dispersion, deflection or redirection of the energy in an ultrasonic beam caused by small reflectors (interface at which there is a change in acoustic impedance) is known as scattering (ASTM E1316-11b). Depending on the feature size and the wavelength of the radiation there are different scattering regimes known as Rayleigh scattering, mid-frequency scattering and long wavelength scattering (Ensminger & Bond, 2012):

- **Rayleigh scattering:** it is present for small features, where dimensions are a small fraction of the wavelength.
- **Mid-frequency scattering or stochastic:** it occurs when the features are of the order of the wavelength.
- **Long wavelength scattering or diffusive:** where dimensions are several wavelengths.

Scattering is a common cause of ultrasonic attenuation. There are different relationships for the attenuation depending on the scattering regime (Table 2-4). In this table, λ is the wavelength of the ultrasonic wave, D is the average grain diameter, α is the ultrasonic attenuation, f is the ultrasonic frequency, A_1, A_2 and A_3 are the coefficients that depend on the elastic moduli of the material tested. Also is included the relationship in terms of the damping factor (ξ) because it is a manner of expressing the attenuation more common in structural analysis. The damping factor can also be expressed in terms of the coefficient of attenuation α and the wavelength λ as follows (Cascante, 1996):

$$\xi = \frac{\lambda \cdot \alpha}{2\pi} \tag{2-12}$$

From equation (2-4) it follows that the wavelength could be expressed as:

$$\lambda = \frac{\mathrm{V}}{\mathrm{f}} \tag{2-13}$$

Replacing λ and the expressions for α in Table 2-4 in equation (2-12), it is obtained the relationship between the damping coefficients as a function of the frequency presented in the same table.

Table 2-4: Relationships for the attenuation for the different scattering regimes (Ensminger & Bond, 2012)

Scattering of ultrasonic waves	**Relation between the wavelength and the target dimension**	**Attenuation**	**Damping**
Rayleigh	$\lambda \gg D$	$\alpha = A_1 D^3 f^4$	$\xi = \frac{V \cdot A_1 D^3 f^3}{2\pi}$
Stochastic	$\lambda \approx D$	$\alpha = A_2 D f^2$	$\xi = \frac{V \cdot A_2 D\mathrm{f}}{2\pi}$
Diffusive	$\lambda \ll D$	$\alpha = A_3 D$	$\xi = \frac{V \cdot A_3 D}{2\pi}$

In NDT the consideration of the scattering characteristics of the materials is very important, since it defines the sensitivity of the method and the frequency that should be used for the testing.

The **sensitivity** is usually referred as the smallest reflector that produces a discernible signal on the display of an ultrasonic system (Hellier, 2001). As it may be noticed from Table 2-4, for the

three scattering regimes, the size of the grain of the material has an effect on the scattering. In the case of concrete, which is a heterogeneous material formed by particles of different sizes, the scattering is an important aspect to take into account to ensure the effectiveness of the NDT test.

There are different parameters that can be used to estimate the coefficient of attenuation α_x, for example in the time domain the peak-to-peak amplitude (PTP) or ratio between amplitudes. In the frequency domain two common methods are the maximum magnitudes or the spectrum area (Kirlangic, 2013). The method considered in this work to quantify the material attenuation is by comparing the area below the frequency spectra computed from the ultrasonic measurements. The attenuation is quantified as the ratio of the area below the frequency spectrum (in the frequency bandwidth of interest) after a specific type of action (freeze/thaw or compressive loading), and the area below the spectrum at the baseline condition. Since the apparent wave attenuation includes the losses caused by the instrumentation, the specimen configuration, sound directivity and the measurement procedure (ASTM E1316-11b), the computation of the areas of the spectra requires first to identify the frequencies related to the instrumentation and the frequencies corresponding to the specimen. The identification of these frequencies can be done normalizing the frequency response of the system formed by the specimen and the testing setup, by the transfer function obtained placing the transducers face-to-face. The system function $s(\omega)$ can be obtained by deconvolution dividing the frequency components of the received voltage $V(\omega)$ by the transfer function $t_A(\omega)$ of the system:

$$s(\omega) = \frac{V(\omega)}{t_A(\omega)} \tag{2-14}$$

The transfer function is the ratio between the magnitude of the Fourier transform of the output signal and the Fourier transform of the input signal. This procedure can be applied because the system is linear, and a linear system may be characterized by its frequency response.

It is recommended that the transfer function $t_A(\omega)$ is obtained from any calibration setup that can be modeled explicitly which would include the effect of the electrical and mechanical components (Schmer & Song, 2007). However, the effect of the coupling with the specimen is not accounted for directly with this procedure and a more thorough of the effect of coupling on the ultrasonic measurements is needed.

2.5.2 Test methods

2.5.2.1 Ultrasonic pulse velocity method

Ultrasonic pulse velocity (UPV) is one of the most common nondestructive testing (NDT) methods employed for the condition assessment of structural concrete elements. Some of the applications of the pulse velocity method are: to assess the uniformity and the relative quality of the concrete, to indicate the presence of voids and cracks, and to evaluate the effectiveness of crack repairs (ACI 228.2R-13). Another important use of UPV is to assess the damage in concrete caused by freeze/thaw cycles.

According to the standard ASTM C597-16, the scope of UPV test is the determination of the propagation velocity of the longitudinal (P-waves) through concrete. It is of interest to calculate the pulse velocity of the longitudinal stress waves because the velocity is related to the density and the elastic properties of the material. Consequently, the stress-wave propagation behaviour may be used to infer characteristics of a material (2-1).

The pulse velocity (V_p) is calculated dividing the distance between the centers of the ultrasonic transducers faces by the transit time, which corresponds to the time taken by a pulse to travel from the transmitter to the receiver through the concrete specimen. As an example, Figure 2-9 shows the setup used to perform the pulse velocity test for concrete cylinders.

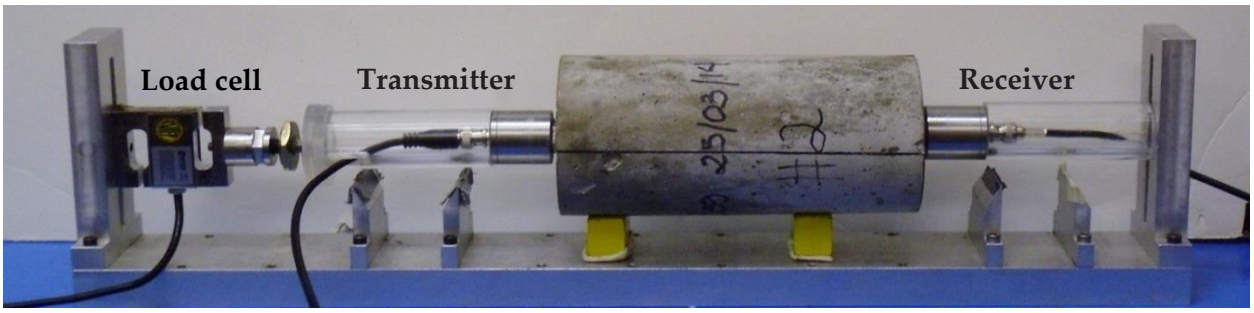

Figure 2-9: Setup to measure the pulse velocity through concrete cylinders

The transit time is defined as the time from the start of the triggering of the pulse emitted by the transmitter, to the detection of the first arrival of the longitudinal waves. To estimate the exact time it is necessary to subtract the delay caused by the transducers and the electronic equipment. The delay can be defined placing the transducers face to face as shown in Figure 2-10.

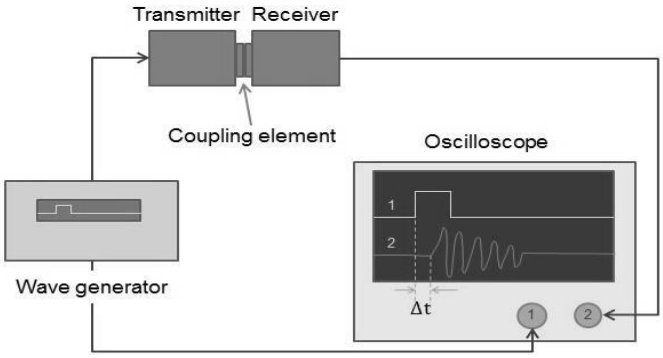

Figure 2-10: Testing setup to measure the delay caused by the electronics

In the recommendations from the International Union of Laboratories and Experts in Construction Materials (RILEM, from the name in French), the pulse velocity method is the reference method to evaluate the frost resistance of concrete (RILEM TC 176-IDC, 2004). The evaluation in accordance to these recommendations is not directly through the velocity, but based on the change in the relative transit time τ_n after n freeze/thaw cycles calculated from equation (2-15):

$$\tau_n = \frac{\Delta t_1}{\Delta t_n} \tag{2-15}$$

where τ_n is the relative transit time, Δt_1 is the total transit time before the first freeze/thaw cycle minus the transit time in the coupling medium; and Δt_n is the total transit time after n cycles minus the transit time in the coupling medium.

It is not recommended to consider the pulse velocity as a means to directly assess the compressive strength of the concrete (ASTM C597-16), because there are several factors that affect pulse velocity (for example the type and amount of aggregate, the moisture content, the amount and orientation of the reinforcement) that may overshadow the changes in the strength (ACI 228.1R-03). In addition, as the pulse velocity is proportional to the square root of the elastic modulus, and the elastic modulus is proportional to the square root of the compressive strength, as the maturity of the concrete increases, large changes in compressive strength produce only minor changes in pulse velocity (ACI 437R-03; ACI 228.1R-03). Pulse velocity method is suitable to locate regions where the concrete is of different quality or where there may be internal defects, but the nature of those defects cannot be determined based on the measured velocity

(ACI 437R-03). The ASTM standard of the ultrasonic pulse method explicitly states: "The results obtained by the use of this test method are not to be considered as a means of measuring strength nor as an adequate test for establishing compliance of the modulus of elasticity of field concrete with that assumed in the design" (ASTM C597-16).

For the reasons exposed, the pulse velocity method is considered in this research as a method to locate defects, such as honeycombing or cracking, but it is not intended to use the measurements of pulse velocity to estimate the strength of the concrete elements.

2.5.2.2 *Analysis of surface waves*

The Spectral Analysis of Surface Waves (SASW) is a method that was developed to determine the thickness of the layers and the elastic stiffness of soils and pavements (ACI 228.2R-13).

Figure 2-11 illustrates the general test configuration. Rayleigh waves are generated by impacting the surface of the tested element, and two receivers are used to monitor the motion of the waves as they propagate along the surface. The stresses generated from the impact contain a range of frequency components; therefore, the R-waves have different frequencies that in a layered medium will propagate with different phase velocities.

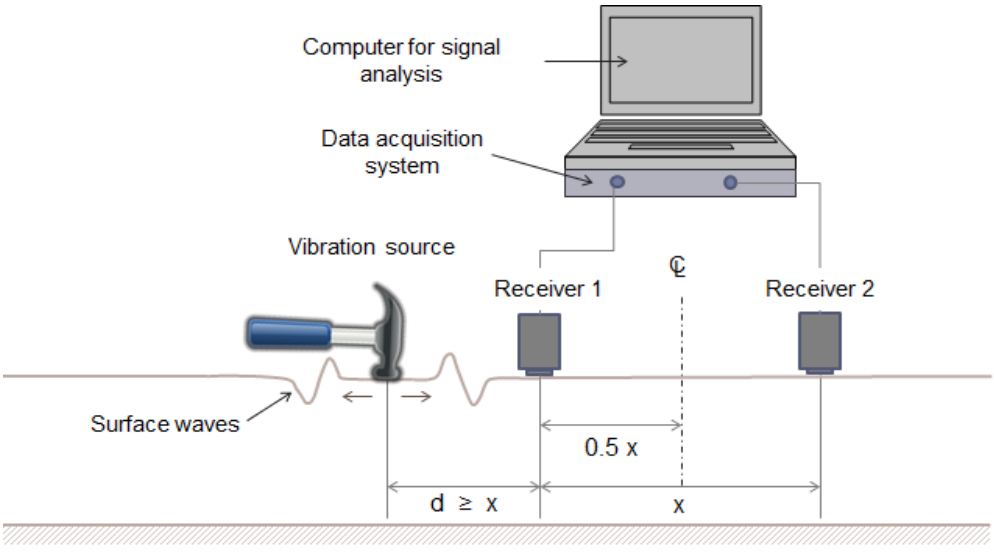

Figure 2-11: Schematic representation of the SASW method (after ACI 228.2R-13)

The surface wave analysis has three main steps: the execution of the test or data gathering, the construction of the experimental dispersion curve and the inversion of the dispersion curve. It is

called dispersion curve the plot of the phase velocity versus the wavelength or frequency. Another representation is the frequency spectrum, in which the frequencies are represented as a function of the wave number (k). The frequency spectrum is also called F-K plot.

Phase velocities are calculated by determining the travel times for each frequency (or wavelength) component between the two receivers. The travel times are determined from the phase difference of the frequency components arriving at the receivers. The phase difference is computed from equation (2-16):

$$\Delta\varphi = Phase(FT_2) - Phase(FT_1) \tag{2-16}$$

where $\Delta\varphi$ is the phase difference, FT_2 and $FT_1$are the Fourier transform of the signals recorded by the receivers and Phase (FT_2) and Phase $(FT_1)$are the unwrapped phase of the respective Fourier transform. The phase velocity for each frequency may be calculated from equation (2-17)

$$V_{ph}(\omega) = \omega\frac{\Delta x}{\Delta\varphi} = 2\pi f\frac{\Delta x}{\Delta\varphi} \tag{2-17}$$

where $V_{ph}(\omega)$ is the phase velocity for the specific frequency ω, Δx is the receivers spacing and $\Delta\varphi$ is the phase difference calculated from equation (2-16).

The dispersion curve of the experimental data can be computed using equation (2-17). A theoretical dispersion curve is determined assuming a layered system that represents the test site, which is modelled as layers of varying thickness, with an assigned density and an elastic constant. The theoretical curve is compared with the experimental dispersion curve until there is a satisfactory agreement between the curves.

Given that SASW configuration uses only two receivers, the test needs to be repeated several times to perform an evaluation. To facilitate the testing, the method called Multi-channel analysis of surface waves (MASW) was developed (Kirlangic, Cascante, & Polak, 2015). The method follows the same procedure than SASW, but instead of two receivers it is used an array of equally spaced receivers. In addition to faster data collection and better noise control (Wu, 2012), MASW has the advantage that is able to identify and separate different modes in the R-waves. In this project, a method based on MASW testing is used. The procedure followed in this work differs from the standard method in the type of source (ultrasonic source instead of a hammer) and the material studied. MASW is typically used in geotechnical exploration and in this research is employed to evaluate reinforced concrete elements. The analysis of surface

waves method has the potential to detect damage that could be visually undetected because the surface wave velocity decreases in damaged concrete (Kalinski, Stokoe II, Jirsa, & Roesset, 1994).

2.6 Combination of NDT methods

Every NDT method has some advantages and some limitations that make a method preferable for specific applications. Currently, the common practice is to use a combination of methods; thus, a second method is used to provide additional information that may overcome the limitations of the first method. According to (Breysse, Klysz, Dérobert, Sirieix, & Lataste, 2008), NDT methods can be considered in four types of combinations:

- **Type A:** the results from two or more methods are compared to confirm the measurements and variations recorded.
- **Type B:** the results from two or more techniques are compared with the purpose of improving the interpretation of the results.
- **Type C:** one technique is used for a rough mapping of the elements and a second technique is applied in the potential areas of concern identified with the first technique.
- **Type D:** a second technique is used to correct the effect of a specific parameter affecting the first technique.

In this research project, the use of two nondestructive methods is studied: the surface waves analysis and ultrasonic transmission. The combination investigated could be classified as type C, because the surface waves analysis is intended to be used to identify areas of dissimilar characteristics in the columns. Then, these areas are tested with an ultrasonic testing device developed in the research group.

The foreseen application of the methodology is for the preliminary investigation of reinforced concrete columns. The preliminary investigation is essential to establish the general condition of the elements, to define the number of tests needed and the location of the tests. The selection of the samples taken to characterize the concrete of the elements under study depends on a preliminary investigation (ASTM C823 -12).

2.7 Use of arrays and tomographic techniques

There are different methods to generate ultrasonic waves: piezoelectric transducers, lasers, electromagnetic and mechanical transmitters (Ensminger & Bond, 2012). In ultrasonic testing piezoelectric transducers are used typically to induce the ultrasonic waves. A piezoelectric

transducer is a device that converts electrical energy in ultrasonic energy and vice versa (Blitz & Simpson, 1996). This type of transducer needs to be in contact with the object tested, and must be attached using a couplant, for example grease or gel. A couplant is a substance used between the transducer and the object tested to permit or improve transmission of the ultrasonic energy (Hellier, 2001). The coupling material and the applied forces to place the transducers have an important effect on the wave amplitude; therefore, are two important factors that should be taken into account for field testing. The transducers also must be calibrated for the specific material under study to ensure the required precision and accuracy.

The most common transducers for testing concrete are the transducers with a resonant frequency of 50 kHz (ACI 228.2R-13). The standard (ASTM C597-16) establishes that the transducers should have a resonant frequency in the range of 20 kHz to 100 kHz. The selection of the transducers is based mainly on the element being tested, and in the size of the defect or feature that is under investigation.

The usual configuration for pulse velocity testing consists of two transducers located at opposite sides of the element being tested (see for example Figure 2-9). One transducer emits the ultrasonic wave pulse, and the other receives the pulse. The time between the start of the pulse and the detection at the receiver is termed the arrival time. Since the path between the transmitter and the receiver is known, the wave velocity can be computed dividing the distance by the arrival time. As the wave propagation depends on the elastic properties of the material, the wave velocity is used as a means of characterization of the material. If the only parameter considered in the test is the wave velocity, this configuration may provide reliable results. Nevertheless, some researchers have demonstrated that wave velocity is not as sensitive as wave attenuation to inhomogeneities (Prada, Fratta, & Santamarina, 2000; Chai, Momoki, Kobayashi, Aggelis, & Shiotani, 2011; Kirlangic, 2013). The attenuation is the factor that describes the decrease in ultrasound intensity or pressure with distance, and normally expressed in decibels per unit length (Hellier, 2001). Given that attenuation measurements are more sensitive to material damage, several researchers (Prada et al., 2000; Chai et al., 2011; Aggelis et al., 2009; Yim et al., 2012) suggest the complementary use of velocity and attenuation. On the other hand, the determination of the attenuation is more affected by the coupling conditions, which are difficult to control in the field.

Another problem of the usual testing configuration is that the results are based on measurements over a single travel path. It is likely that some defects may not be detected

because of the orientation selected or because of the size of the defect, because the influence of some defects on the transit time measurements is relative to the position of the defect and the travel path considered (ASTM C597-16). A manner of addressing these problems is using ultrasonic arrays. An ultrasonic array is a patterned arrangement of elements (ASTM E1316-11b, 2011), and a basic classification is made depending on their configuration as one-dimensional (1-D), two dimensional (2D) and annular. Arrays have the advantage that is possible to take different measurements from a single source location, and can be used to produce images for the visualization of the internal structure of a component (Drinkwater & Wilcox, 2006). This visualization may be obtained through tomographic techniques (Prada et al., 2000; Kim, Fratta, & Pincheira, 2011).

Since 1990s phased array ultrasonics has been in continuous progress and actually there are available commercial systems that provide tomographic images of concrete components. As an example, the patented devices MIRA™ and EyeCON™ by Germann Instruments, shown in Figure 2-12, have been used to generate 2D and 3D tomographic images of concrete elements.

Figure 2-12: Examples of commercially available tomographers for concrete by Germann Instruments, MIRA™ on the left and EyeCON™ on the right (De la Haza et al., 2013)

Both systems use dry point contact (DPC) transducers that transmit shear waves into concrete. They are called dry point transducers because there is no need of a coupling fluid, and the transducers are spring loaded to ensure sufficient coupling to irregular surfaces. MIRA™ consists on a 2D array of 48 transducers in a 4 by 12 configuration (Figure 2-12). On the other

hand, EyeCON™ uses a rectangular array of 24 transducers. These two systems generate the tomographic images from the arrival time of shear waves.

In recent years, several researchers have investigated the application of ultrasonic arrays and imaging techniques for concrete elements: (Krause et al., 2001; Kim et al., 2011; Chai et al., 2011; Schickert, 2012; Molero et al., 2012; De la Haza et al., 2013; Nelson et al., 2014, Haach, 2016). There are reports of successful applications of imaging techniques for the evaluation of grouted beams, concrete dams (Chai et al., 2011), freeze and thaw damage (Molero et al., 2012) and for the detection voids in metallic ducts in post-tensioned bridge beams (Forde, 2013). In the cases mentioned the tomographic image is based on the ultrasonic velocity distribution. The cross section under study is divided in a rectangular mesh and several travel paths are defined. The localized wave velocity in each region is determined from a procedure to invert the travel time tabulated as a function of distance for the pulse velocity. Different properties of the concrete and several types of elements may be studied through imagining techniques; however, it has been mainly applied to flat reinforced elements as slabs and beams. Furthermore, the imaging techniques are mostly based on arrival time measurements. The measurements of the attenuation are not usually taken because of the difficulty to obtain reliable measurements in the field.

2.8 NDT testing of wood poles (UTPole system)

An important antecedent for this research project is the research conducted at the University of Waterloo to assess the condition of wood poles. For details of the project refer to (Tallavó, 2009) and (Tallavó, Cascante, & Pandey, 2011). The final result of the research on wood poles mentioned was the UTPole system. UTPole is a nondestructive ultrasonic testing device, software and assessment method, developed for the condition evaluation of in-service wood poles that is based on ultrasonic and statistical measurements. The system consists of three components: the electronics (the batteries, data acquisition system, pulse generation system and the signal amplifier), the transducers array and the software that controls the execution of tests, the data acquisition and the processing of the data (Figure 2-13). The picture shows the current state of the system. However, as it is indicated in the Statement of contributions and in section 3.3.2, the construction of the field testing device was done as part of the project presented in this thesis. At the beginning of this research, the UTPole system consisted of the software and a different array of transducers. The field testing was done using laboratory equipment, and the

portable electronic system was only conceptually designed. As it is described in section 3.3.2, the final prototype is the final result of the work done to test wood and concrete elements.

Figure 2-13: UTPole system

The testing is performed using a calibrated annular array of eight piezoelectric transducers with a nominal frequency of 82 kHz evenly spaced around the pole cross-section as shown in Figure 2-14. In the figure, the letters indicate the position of the receivers.

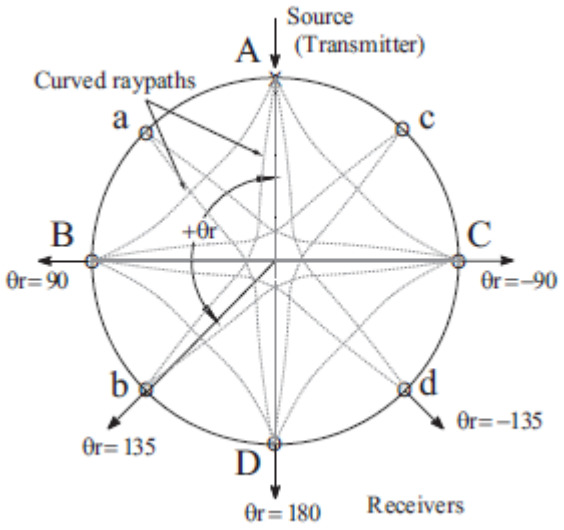

Figure 2-14: Location of the ultrasonic transducers (Tallavó et al., 2012)

The array is a customized belt that can be adjusted to test elements of different diameters. In each test, one of the transducers functions as a transmitter and the other seven as receivers. The signals received are recorded and processed using software developed specifically for the system. The times signals are then used to compute the velocity, the attenuation and the statistical indexes from which is performed the assessment of the condition. The explanation of the computation of the dissimilarity index is presented in section 3.4.2.

The UTPole system presents several advantages:

a) The method is based on statistical indexes calculated from the ultrasonic measurements of wave velocity, wave attenuation and the elastic moduli, not only on wave velocity.

b) The statistical indexes computed provide a means to quantify the extent of the damage in the cross section being tested.

c) It takes into account the variability of the material properties that influence the ultrasonic wave velocity. In order to obtain reliable ultrasonic measurements, it is needed to take into account the intrinsic variability of the parameters that affect wave velocity and to assess the effect of that variability in the estimation of wave velocity.

d) The statistical indexes computed from the ultrasonic measurements allow a tomographic image of the cross section to be generated. The tomograms are useful tools to visualize the extent of deterioration and also are suitable to track the progression of the damage. Figure 2-15 presents two examples of the tomograms obtained from UTPole in wood poles.

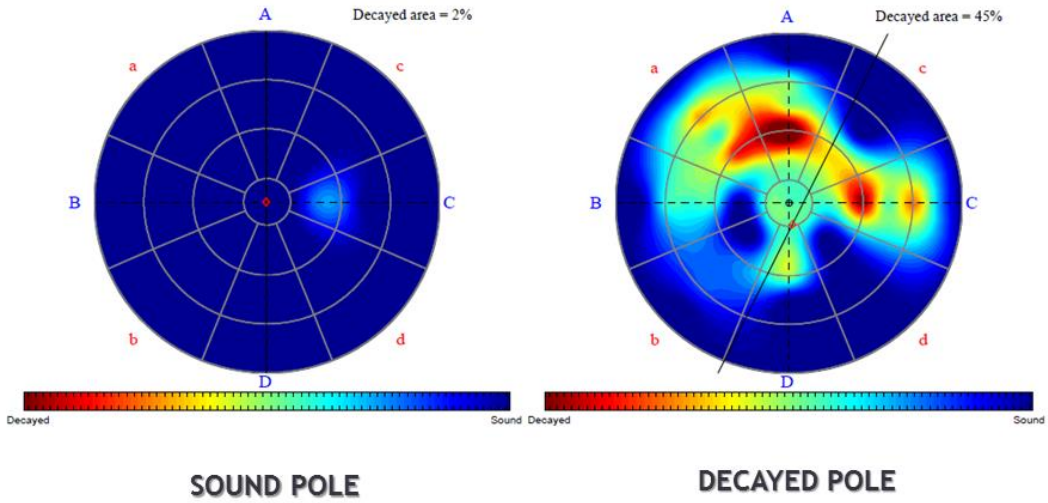

Figure 2-15: Example of the tomographic images obtained from UTPole system

2.9 Summary

This chapter included the main findings of the literature review and the background information needed to explain the methodology and the results of the research project. This comprised the fundamentals of wave propagation, the explanation of the different stress-wave nondestructive testing techniques applicable for the assessment of hardened concrete, and a brief description of the mechanisms of deterioration of concrete. Furthermore, reference was made to the current practice of combination of nondestructive methods and the use of tomographic techniques to improve the assessment of structural elements. Finally, the description of the testing system for wood poles that is a precedent for this research was presented.

Chapter 3 Methodology

3.1 Introduction

This chapter describes the components of the methodology followed in this research project, aimed to develop a testing system that could be used for the assessment of the uniformity of reinforced concrete circular columns.

3.2 Literature review

The literature review was needed to understand the state of the art in inspection methods for concrete elements, the existing limitations of the methods under study and the improvements required.

Ultrasonic pulse velocity (UPV) or transmission through has been used for decades and is one of the most common NDT methods (ACI 228.2R-13, 2013; Breysse, 2012; Cetrangolo & Popovics, 2010; Dilek, 2007; Naik, Malhotra, & Popovics, 2004). Due to the large amount of available literature on this topic, it was decided to limit the literature review to four topics:

i. Inspection methods for concrete elements in service;

ii. Applications and limits of the ultrasonic pulse velocity test;

iii. Combination of nondestructive methods; and,

iv. Capacity models for evaluation of columns.

The outcome of the literature review was the identification of the main limitations of the application of ultrasonic pulse velocity to assess concrete columns. Taking into consideration these findings, the following characteristics of the research project were defined:

a. The available pulse velocity systems rely mainly on measurements of the arrival time of P-waves and alternative procedures are needed. The methodology proposed is based on measurements of velocity and attenuation.

b. Every NDT method has some advantages and some limitations. Currently, the common practice is to use a combination of methods. For this project, the complementary use of two stress wave methods (surface wave analysis and direct transmission ultrasonic pulse velocity) was investigated.

c. A probabilistic approach is needed, because there are many sources of uncertainty in the materials, testing procedures and results. Also, the probabilistic approach would make

possible to deliver quantitative data that may be used for the analysis of the actual capacity of the columns.

The literature review also facilitated the identification of the fundamental aspects that needed to be addressed in the subsequent experimental work.

3.3 Experimental component

The experimental component consists of the investigation in the laboratory of specific aspects of the methodology and the construction of the field testing device. Once the field testing device was built and tested, a sample of in-service columns was evaluated.

3.3.1 Laboratory testing

The laboratory testing comprised three groups of tests that were intended to study specific aspects of the methodology: the sensitivity of the pulse–velocity method to detect internal damage, the application of surface–waves method to reinforced concrete elements and the verification of the functioning of the complete system. Since the purpose of this chapter is to give an overview of the methodology, only a brief description is made. The details are presented in chapters 5, 6 and 7.

- **Freeze/thaw and compression damage:** the purpose of these tests was to evaluate the sensitivity of the ultrasonic pulse velocity method to two types of internal damage. Also, to assess the adequacy of the attenuation computations to complement the information obtained from the velocity. The description of the tests and the main findings can be found in Chapter 5.

- **Surface wave testing of reinforced concrete elements:** five beams were evaluated using the surface wave method to experiment different testing configurations and to evaluate alternative signal processing techniques. The results related with the surface wave testing are presented in Chapter 6.

- **Verification of the field testing system:** the construction of the field testing tool is described in section 3.3.2. However, is considered as part of the laboratory experimentation the verification of the response of the different components (electronic boards, data acquisition system and transducers array) separately and then jointly. Also

the evaluation of the results of the testing of a cylindrical mortar sample of known properties reported in Chapter 7. This testing was done before using the device in the field.

3.3.2 Construction of the field testing device

As it was indicated in section 2.8, this research project contributed in the construction of the UTPole portable ultrasonic device (Figure 3-1), which consists of:

- **Portable electronics apparatus:** case comprising the batteries (two 12 V rechargeable batteries), the pulse generation system (high voltage board), the signal amplifier (low voltage board) and the data acquisition system (NI USB-6356 Data Acquisition Card).
- **Transducer array:** formed by eight piezoelectric transducers with nominal frequency of 82 kHz, the transducer holders and an adjustable band.
- **UTPole software:** it is the software that controls the execution of the tests, the data acquisition and the processing of the data.

Figure 3-1: UTPole system

A significant contribution of the project is the collaboration in the development of the portable system. The collaboration consisted in the following main tasks: the management and technical assistance to the electronic specialists in charge of the development of the electronic system; the

construction of the electronics apparatus, the design of the transducers holders and the testing of the components and the whole system before the field work. In addition, field testing of wood poles and concrete columns was conducted to as part of the collaboration.

Portable electronics apparatus

Figure 3-2 shows the electronic boards, the boards connected to the data acquisition system during the verification in the laboratory and a top view of the apparatus. The construction of this apparatus was essential to make the system portable and adequate for field testing.

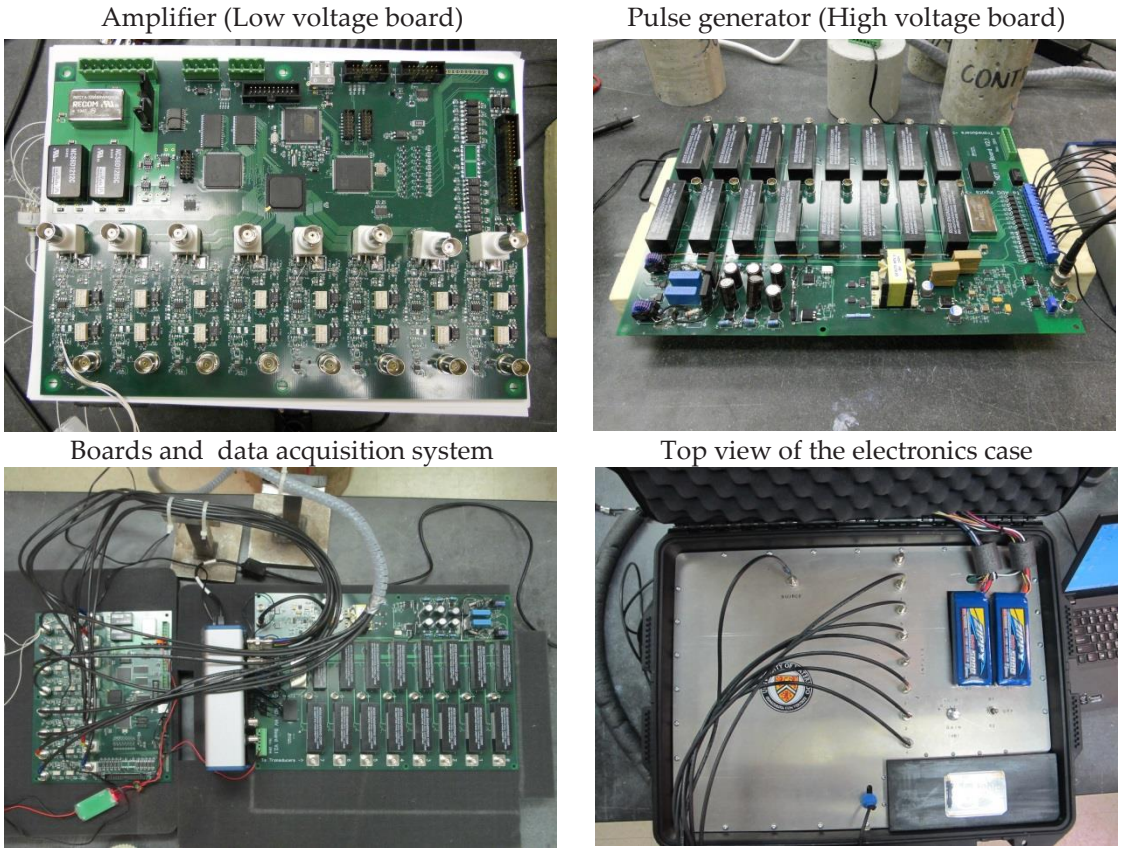

Figure 3-2: Portable electronics apparatus

Transducer array

For the construction of the transducer array, several prototypes were fabricated using different materials and methods (machining and 3D printing). The modification of the device was necessary:

i. To improve the portability of the system,

ii. To reduce the time to perform each test, and

iii. To ensure an adequate coupling between the sensors and the elements being tested.

The original sensor array is shown in Figure 3-3. In Figure 3-4 and Figure 3-5 are illustrated some of the transducers holders evaluated, and in Figure 3-6 and Figure 3-7, the complete arrays using a ratchet system and elastic bands. The ratchets and the elastic bands were evaluated because they allow adjusting the sensors around the element under study. Also they ensure a consistent pressure to enhance wave transmission (coupling).

Figure 3-3: Original sensors array

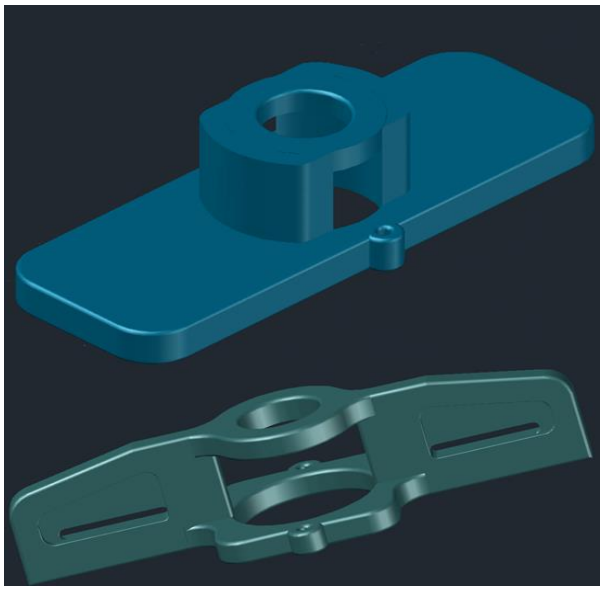

Figure 3-4: Models for the transducer holders using ratchets

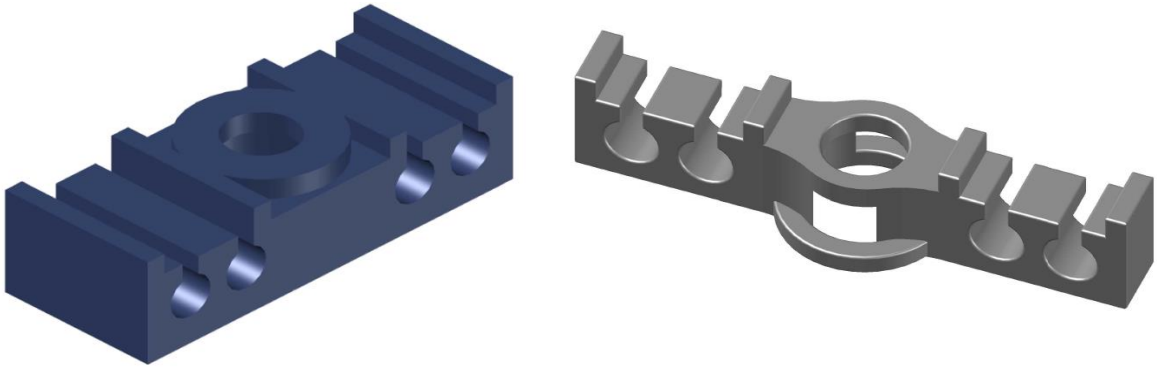

Figure 3-5: Models of the transducers holders for the system using elastic bands

Figure 3-6: Examples of adjustable systems evaluated

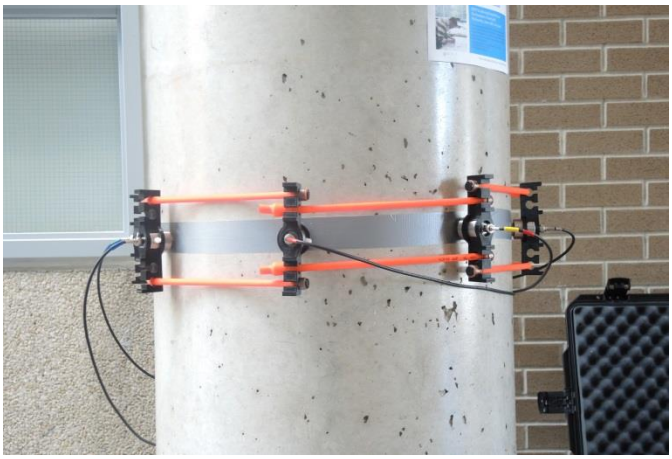

Figure 3-7: Final design of the adjustable sensors array

As soon as the field testing device was finished and verified in the laboratory, the calibration of the transducers and the study of the coupling were done. The description of the procedure followed for the study of the coupling and the calibration of the transducers is included in Chapter 4. However, the calibration of the whole system was also required and is explain in the next section.

3.4 Field testing for calibration of UTPole for concrete

The assessment performed with the UTPole system is based on the concept of dissimilarity indexes (section 3.4.2), which can be adapted to any material, not only wood as it was initially intended. Therefore, the final step of the methodology is the calibration of the UTPole system to evaluate reinforced concrete columns using the data collected from existing columns.

3.4.1 Wave propagation modeling in UTPole software

UTPole software uses the arrival times measured to solve numerically the velocities of propagation of P-waves in a cylindrically orthotropic medium excited by an impulsive force. The simplified model considers the medium as an elastic material with mechanical properties defined as random variables. The results of the analysis are the probability density function for the velocity, and the radial (E_r) and transverse (E_t) moduli of elasticity (Tallavó, 2009).

In the software, the circular cross section is divided in 25 regions and considers 28 independent ray paths between the transducers (Tallavó, Cascante, & Pandey, 2011) as shown in Figure 3-8.

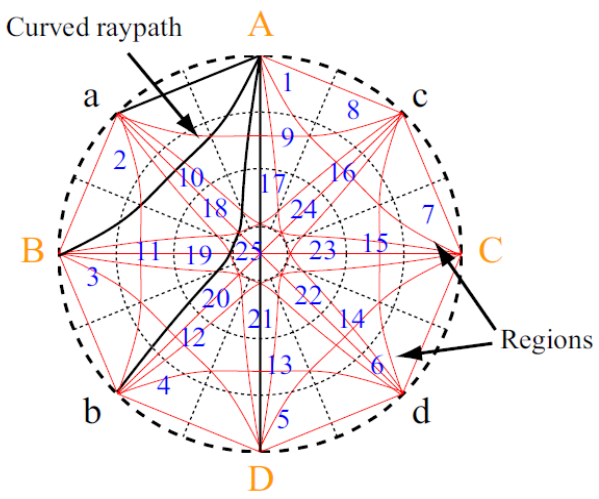

Figure 3-8: Discretization and ray paths considered for the analysis of the wave propagation in the UTPole software (figure from Tallavó et al., 2011)

For each region, the wave velocity is computed solving the inverse problem from the travel time measurements of the compression waves using the least squares method for each ray path. Inverse problems are those that solve the input or the properties of the system from the information of the output by assuming a model that relates the two (Santamarina & Fratta, 2005). The solution of the distribution of the velocities in this case is an inverse problem because the measured quantities are the arrival times, the assumed relation is the computation of the velocity and the unknowns are the velocities. The distances are defined for each ray path in terms of the regions that they are crossing.

3.4.2 Definition of the dissimilarity indexes

The UTPole system identifies potentially damaged sections using the overall dissimilarity index (ODI_{θ_r}), computed at each transducer location according to the following expression:

$$\mathrm{ODI}_{\theta_r} = \mathrm{DIV}_{\theta_r} \cdot \mathrm{W} + \mathrm{DIA}_{\theta_r} \cdot (1 - \mathrm{W}) \tag{3-1}$$

where DIV_{θ_r} is the dissimilarity index for the wave velocity (3-2), DIA_{θ_r} the dissimilarity index for the transmission factor (3-3) and W is a weight factor calculated from equation (3-4):

$$\mathrm{DIV}_{\theta_r} = \frac{\mathrm{V_p} - \mu_{\mathrm{V_p}}}{\sigma_{\mathrm{V_p}}} \tag{3-2}$$

where V_p is the P-wave velocity calculated from the ultrasonic test, μ_{Vp} the expected value of the pulse velocity (corresponding to a specific material), and σ_{Vp} the standard deviation for the wave velocity at the same receiver location.

The dissimilarity index for the transmission factor (DIA_{θ_r}) is defined as:

$$\mathrm{DIA}_{\theta_\mathrm{r}} = \frac{\mathrm{A_f} - \mu_{\mathrm{A_f}}}{\sigma_{\mathrm{A_f}}} \tag{3-3}$$

where A_f is the measured transmission factor (reciprocal of the attenuation factor) computed in the frequency domain, μ_{A_f} is the expected value and σ_{A_f} is the standard deviation.

The weight factor (W) is defined as:

$$\mathrm{W} = \frac{1}{1 + \frac{\mathrm{COV_V}}{\mathrm{COV_A}}} \tag{3-4}$$

where $\mathrm{COV_V}$ represents the coefficient of variation in the velocity measurements and $\mathrm{COV_A}$ the coefficient of the variation in the attenuation calculations.

Then, the parameters needed for a specific material are the coefficients of variation (COV) and the expected values for the wave velocity and attenuation. In the next section is presented the derivation of these parameters for concrete.

3.4.3 Expected values and coefficients of variation for UPV in concrete

Many factors affect the expected value of the pulse velocity in reinforced concrete, such as: the relative proportions of concrete components (aggregates, water, cement) (Blitz & Simpson, 1996); the degree of saturation of the element may increase pulse velocities up to 5% (ASTM C597-16); the velocity through steel is greater than in concrete and the measurements in heavily reinforced members would be greater especially when the measurement is parallel to reinforcing bars (Blitz & Simpson, 1996); and in deteriorated concrete the differences in UPV tests results could be as large as 20% (ASTM C597-16).

On the other hand, the test is reported to have low within-test variation. ACI 228.1R-03 compared the within-test coefficient of variation (COV) reported by several researchers and the maximum COV reported was 1.9%. This value is consistent with the value of 2% of repeatability for different operators using the same instrument, or one operator using different instruments, according to ASTM C597-16. The low within-test variability and the difficulty to estimate an

expected value of the velocity support the postulate that the data from the velocity test should be analyzed in a relative sense. For this purpose the dissimilarity index is adequate, but a baseline condition or calibration is needed.

3.4.4 Calibration of UTPole system for reinforced concrete circular columns

The calibration of the UTPole system to evaluate reinforced concrete columns can be divided in three steps:

I. Testing of in-service columns

II. Estimation of the elastic moduli and the probability distribution of wave velocity

III. Computation of expected values of the reference condition

I. Testing in-service columns

The testing of representative columns in sound condition is needed to establish the base line condition. As it was explained before (3.4.2), the dissimilarity indexes are relative results to the expected values for an element in sound condition. The measurements performed on the reference elements provide the arrival times that the software needs to compute the average velocities in the regions in which is divided the cross section (Figure 3-8).

The details of the testing of the in-service columns for the calibration are included in section 3.4.4.1.

II. Estimation of the elastic moduli and probability distribution of wave velocity

To estimate the elastic moduli and the probability distributions of the parameters needed to model the propagation velocity of P-waves, the cross section is divided in twenty five regions (r_i) and twenty eight ray paths. The average velocity in each region ($\overline{V_{r_i}}$) is obtained numerically from the wave propagation model as explained in section 3.4.1 assuming curved ray paths. Then, the density and Poisson's ratio are modeled as random variables. The elastic moduli are calculated from the equation of P-wave velocity (2-1) using the expected values of the density and Poisson's ratio calculated from the derived probability distributions and the velocities computed from the measurements before. Once the elastic moduli are calculated, all variables can be modelled as random variables. Monte Carlo simulations are implemented to estimate the distributions for the P-wave velocity grouping the receivers at 90°, 135° and 180°. Section 3.4.4.2 describes the derivation of the probability distribution of the wave velocity.

III. Computation of expected values of reference condition

The expected mean (μ_{Vp}) and standard deviation (σ_{Vp}) of the reference condition needed to calculate the dissimilarity indexes when testing other columns of the same characteristics are calculated from the probability distributions of the wave velocity.

To summarize, Figure 3-9 shows a schematic representation of the calibration using the information collected in the field testing. On the left are indicated the main assumptions considered in the software and in the right the results obtained at each step.

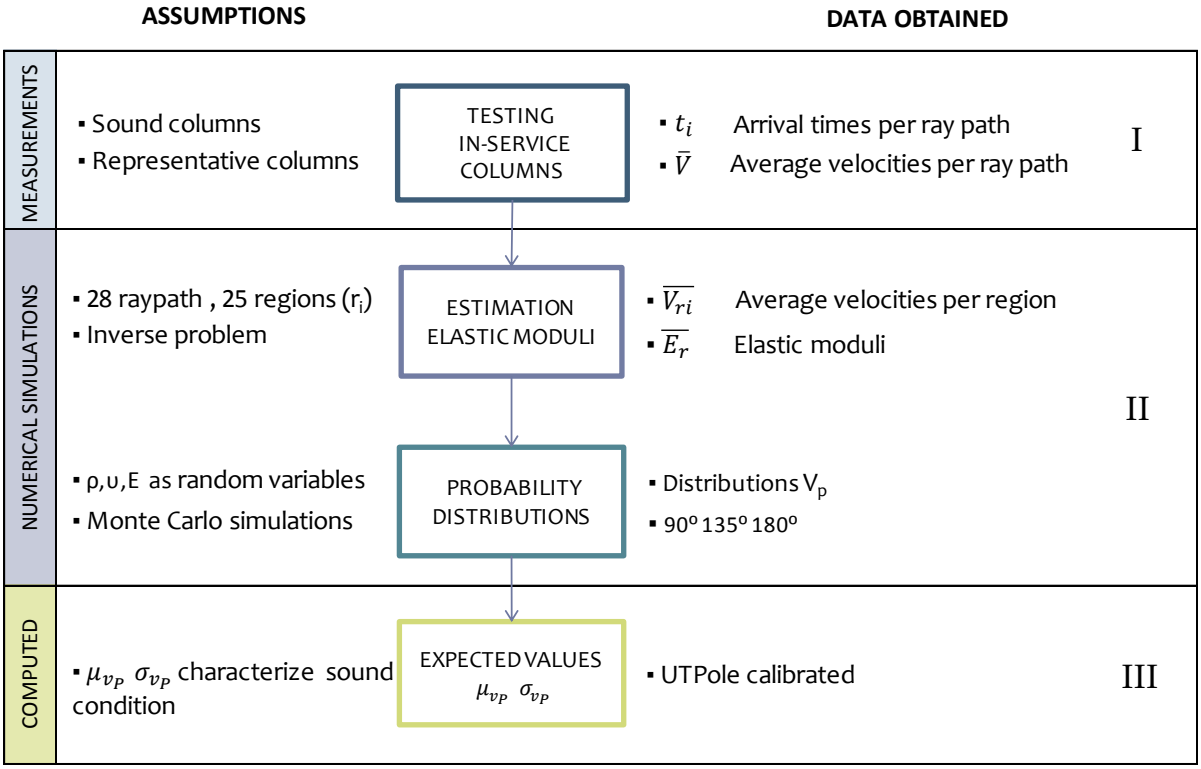

Figure 3-9: Calibration of the UTPole system to test reinforced concrete columns

3.4.4.1 Testing of in-service reference columns

In order to obtain an adequate assessment of the concrete, it is imperative to develop a sampling plan taking into consideration the standards and guidelines applicable for the evaluation of concrete elements. For example, the *Standard Practice for Examination and Sampling of Hardened Concrete in Constructions* (ASTM C823-12), *Code Requirements for Evaluation, Repair, and Rehabilitation of Concrete Buildings and Commentary* (ACI 562M-13) and the recommendations in the *Guide for Evaluation of Concrete Structures before Rehabilitation* (ACI 364.1R-07).

The sampling plan is the procedure used to select the samples for the evaluation. A sample in the context of NDT methods refers to the observations or test results, so the sampling plan should include the number of test locations and the number of tests that are going to be done at each location.

There is no unique sampling scheme for all NDT methods (ACI 228.2R-13), but there are suggested ranges for each method and the type of element inspected. For the ultrasonic pulse velocity method, the recommendation for individual columns is from five to eight locations and a minimum of two replicates at each location (ACI 228.1R-03).

Based on the instrumentation used in this experimental programme, each cross section tested had eight locations (position of the transducers) and two replicates (each transducer acts as transmitter and as receiver). At each receiver thirty-two signals were recorded (signal stacking) to reduce the noise in the measurements. The evaluation that is obtained is cross-sectional; therefore, the column should be tested at different heights to obtain data representational of the member.

Another consideration usually indicated for NDT procedures is the spacing between tests. ACI 228.2R-13 suggests that a test grid between 0.3 m to 0.6 m is ideal for the ultrasonic pulse velocity method but that a test grid between 1.0 m and 1.5 m is more practical. Given that, during a test, seven transducers act as receivers and one as transmitter, the separation between the sensors is 45°. For the largest diameter tested (0.60 m), the separation would be approximately 0.24 m, which is smaller than the ideal density. Hence, the recommendation of the separation between tests is satisfied. In the vertical direction, the maximum spacing between tests was less than one metre; the recommended spacing is also satisfied vertically.

There is also an important distinction about the sampling situations that could be found in a structure (ASTM C823-12 and ACI 228.2R-13):

i. The information and preliminary investigation indicates that the condition is similar throughout the structure.

ii. The preliminary information indicates that there are not similar conditions throughout the structure; therefore, different portions of similar conditions should be considered.

The columns selected for testing were part of groups of identical columns within the buildings. Thus, to determine which sampling situation should be considered, an initial visual inspection was performed. The visual inspection indicated that the concrete was in similar conditions

throughout the structure and the first sampling situation was assumed. In this case, "sampling locations should be distributed randomly or systematically over the region of interest" (ACI 228.2R-13). For each column tested, the height at which the device was installed was randomly selected and noted.

According to (ASTM C823-12), there are two types of samples that may be taken during an inspection:

a. The samples intended to be representative of the concrete in place.

b. The samples that present specific features of interest (unusual or extreme conditions).

With respect to the columns tested, both types of samples were taken. For every type of column, at least two sections were examined to obtain samples of the concrete in place. And for two columns where surface defects were evident, another sample was taken from the defective area.

In order to generate the baseline data for the system, three types of reinforced concrete columns with a circular cross section were tested. All the columns tested are located on the University of Waterloo main campus and the details for each column are included in Appendix A. Table 3-1 summarizes the main characteristics of the columns tested. The columns identified as RCH were originally designed using the Imperial system. For consistency, the parameters were approximated in the SI system and the original values are presented in parentheses.

Table 3-1: Properties of the columns tested

Column ID	Diameter (m)	f'c (MPa)	Concrete cover (m)	Longitudinal reinforcement	Reinforcement ratio (ρ)	Transverse reinforcement
STC-1	0.605	45	0.040	10-20M	1.0%	10M @ 300 mm
STC-2	0.605	45	0.040	10-20M	1.0%	10M @ 300 mm
STC-3	0.605	45	0.040	12-25M	2.1%	10M @ 300 mm
RCH-1	0.357	21	0.010 (3/8'')	6-15M (6 # 5)	1.2%	10M @ 44 mm (3/8'' @ 1 ¾'')
RCH-2	0.357	21	0.010 (3/8'')	6-15M (6 # 5)	1.2%	10M @ 44 mm (3/8'' @ 1 ¾'')
RCH-3	0.457	21	0.010 (3/8'')	6-30M (6 # 9)	2.4%	10M @ 64 mm (3/8'' @ 2 ½'')

The reinforcement details were obtained from the structural drawings provided by the Office of Plant Operations of the University of Waterloo. The columns identified as STC are new columns (built in 2016) and the ones identified as RCH were built in 1965.

3.4.4.2 Characterization of the parameters to obtain the wave velocity for reinforced concrete

The columns identified as STC (Table 3-1) are new and constitute the reference columns. For 120 UPV tests (24 ray paths at 180°, 48 ray paths at 90° and 48 ray paths at 135°) the expected velocity and the coefficient of variation were calculated. Thus, the measured field data provided the arrival times (t_i) needed for the application of the wave propagation model in UTPole. Then, with the values of the velocities computed for each region, and the equation of P-wave (V_p) given by the relation of the Young's modulus (E), Poisson's ratio (υ) and the density (ρ), the modulus of elasticity can be computed as:

$$E = \frac{V_p^2 \rho (1+\upsilon)(1-2\upsilon)}{(1-\upsilon)} \tag{3-5}$$

With estimates for the elastic moduli, it is then possible to describe every parameter as a random variable characterized by a probability distribution, which is needed by the software to obtain the probability density function for the velocity. Monte Carlo simulations (MCS) can be used to define the probability distribution for the velocity (V_P) generating random numbers for each statistical distribution and estimating the velocity by using the simplified method of analysis (Tallavó, 2011).

Modulus of Elasticity (E_d)

The typical values for the elastic modulus for concrete range between 21 GPa to 42 GPa and the modulus computed from the ultrasonic test can be up to 25% higher than the modulus of elasticity obtained from the static tests (Lamond & Pielert, 2006).

In the case of the estimates of the moduli computed from the test data, the mean moduli of elasticity in the radial and tangential direction have the same value of 54 GPa. As the values are equal in both directions, it follows that the cross section can be considered as isotropic. The value of 54 GPa is within the expected range for the moduli estimated from dynamic tests and also it is important to point out that the moduli computed corresponds to the section including the reinforcing steel. Figure 3-10 represents the probability density function for the elastic modulus using as mean value the estimates computed by the UTPole system.

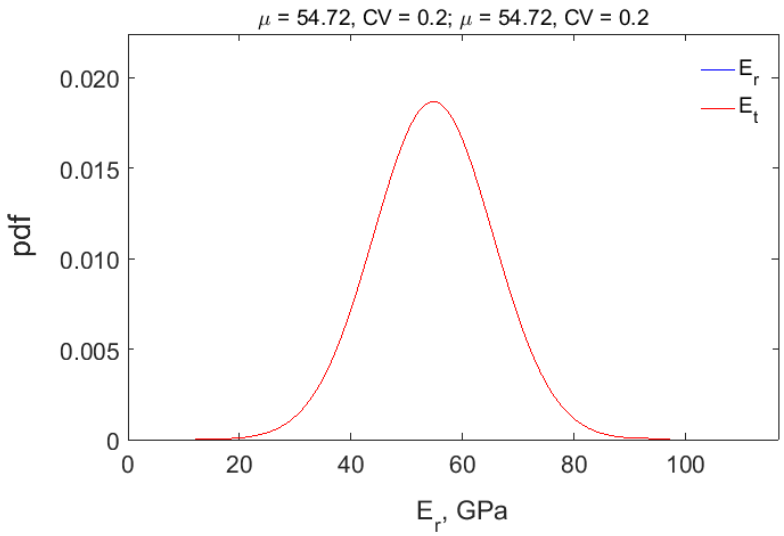

Figure 3-10: Probability distribution used for modelling the dynamic modulus of elasticity

Poisson's ratio (υ)

The Poisson's ratio was modelled by a uniform distribution with a mean value of 0.2 because it is a typical value for concrete (ACI 228.2R-13, 2013).

Density (ρ)

In the literature consulted were not found reference values for the density or for the coefficient of variation (COV) for the material density of concrete in place. However, there are reported values for the coefficient of variation for the compressive strength (f'_c) in columns. Also, the empirical equations included in (ACI 318-11M, 2011) to estimate the elastic modulus (E_c) relate it with the specified compressive strength and the density (ρ_c) :

$$E_c = 4700\sqrt{f'_c} \tag{3-6}$$

$$E_c = \rho_c^{1.5} 0.043\sqrt{f'_c} \tag{3-7}$$

Then, the expected value for the density and the COV were obtained using Monte Carlo simulations and the range considered for modelling the density is the one corresponding to normal density concrete in Table 3-2. The table summarizes the material density classification included in (A23.1-09/A23.2-09).

Table 3-2: Classification of concrete according to the dry air density (A23.1-09/A23.2-09)

Class	Range (kg/m³)
High-density concrete	> 2500
Normal-density concrete	2150-2500
Structural low-density concrete (f'c >20MPa)	< 1850

The compressive strength f'_c was modelled as a normal variable as suggested in ACI 214R-11. The coefficient of variation associated with the expected compressive strength in columns was obtained from (Nowak, Rakoczy, & Szeliga, 2005). This report recommends a COV that varies from 11 to 15.5% for columns. Both values were modelled and the values of the modulus of elasticity estimated from equation (3-6) were replaced in equation (3-7) to compute the density.

The average density obtained from ten thousand Monte Carlo simulations was 2290 kg/m³ and COV of 5.0%. Figure 3-11 shows the probability density function obtained for the material density for concrete.

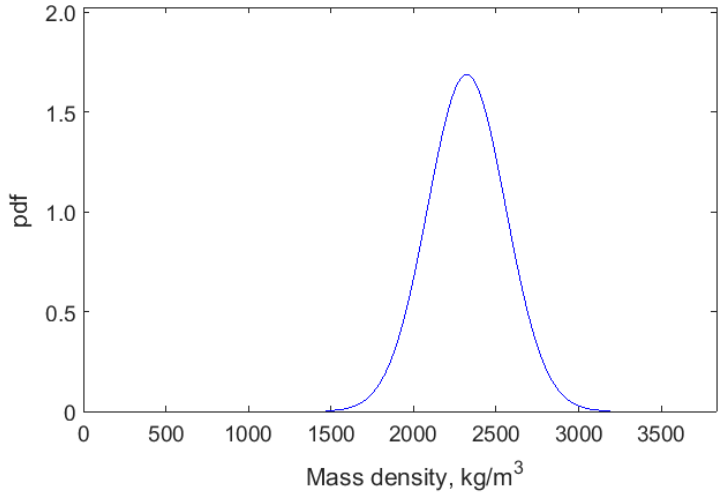

Figure 3-11: Probability density function for the concrete density

The probability distribution for the velocity using six thousand Monte Carlo simulations defined by UTPole software is shown in Figure 3-12 for the three positions of the receivers indicated before (90°, 135° and 180°).

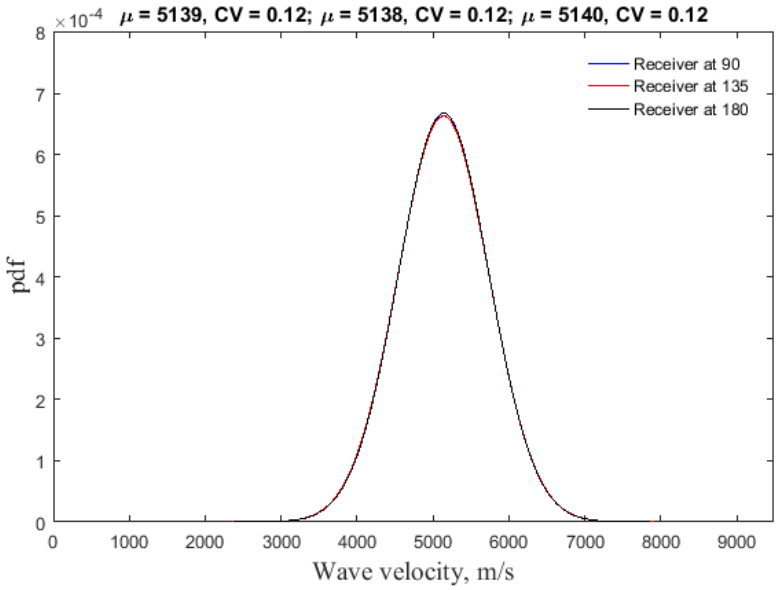

Figure 3-12: Probability distribution for the P-wave velocity obtained from UTPole

Figure 3-12 demonstrates that the distribution for the three positions considered (90°, 135° and 180°) are practically identical and the expected value is 5140 m/s for the mean (μ_{Vp}) and a standard deviation of 620 m/s.

3.4.4.3 Characterization of the attenuation for reinforced concrete

Generally, the variations in the amplitudes (voltages in the case of ultrasonic testing) are expressed in decibels dB (Blitz & Simpson, 1996):

$$\text{Increase in level} = 20\log\left(\frac{\text{A}}{\text{A}_0}\right) \text{ dB} \tag{3-8}$$

where the subscript 0 indicates the reference level. The attenuation may also be expressed in nepers (Np) per unit length. If the amplitude has been reduced by one neper, it means that the amplitude has fallen to 1/e of its initial value, where e is Euler's number. The relation between Neper and decibels is:

$$1\ Np \approx\ 8{,}686\ dB \tag{3-9}$$

Figure 3-13 represents the propagation of a plane wave in an attenuating medium and indicates the notation used for equation (3-10).

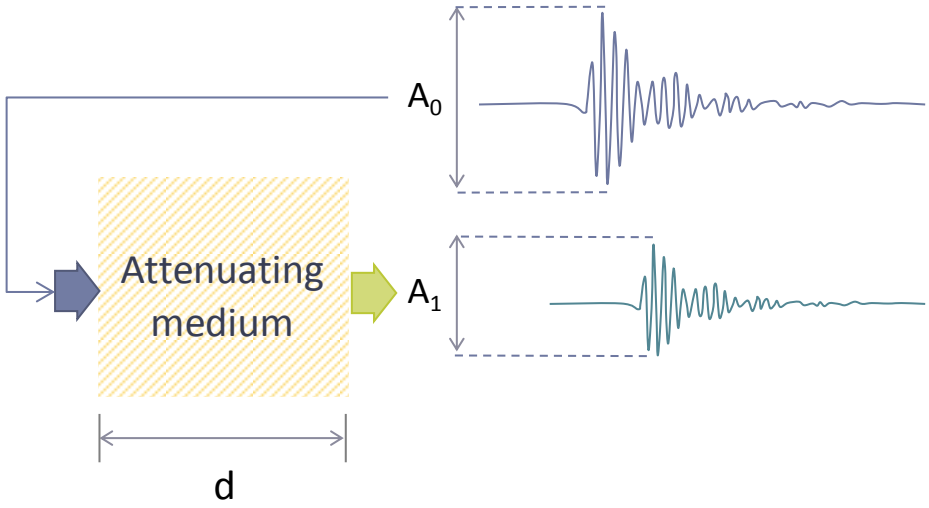

Figure 3-13: Propagation of a plane wave in an attenuating medium

The attenuation can be modeled in function of the distance travelled in the medium (d), the initial wave amplitude (A_0) and the magnitude recorded at the receiver (A_1) as follows:

$$\frac{A_1}{A_0} = e^{-\alpha(f)d} \tag{3-10}$$

The attenuation coefficient α depends on the frequency (f) and has units of Nepers/unit length. The distance considered in this case is the ray path or trajectory of the ultrasonic wave between the transmitter and the receiver. The frequency for the system is the frequency of the input signal applied to the transmitter.

Figure 3-14 presents box plots for the attenuation calculated for the columns used in the calibration process. The plot labelled as "All" includes the data from the 120 measurements from the reference columns. The other plots include the data for the ray paths that are located at the specific angle from the transmitter. For the ones at 180° there are 24 measurements, for 135° there are 48 measurements, and for 90° also there are 48 measurements. The dot indicates the mean value and the size of the rectangle (between the first and third quartile) gives an indication of the dispersion of the data. The horizontal lines indicate the minimum and the maximum values, thus they serve to point out the range for the attenuation coefficients. In opposition to the case of the velocity (where the values corresponding to all angles are very similar), the mean values and the dispersion obtained in the attenuation appear to be very distinct for each case (Figure 3-14).

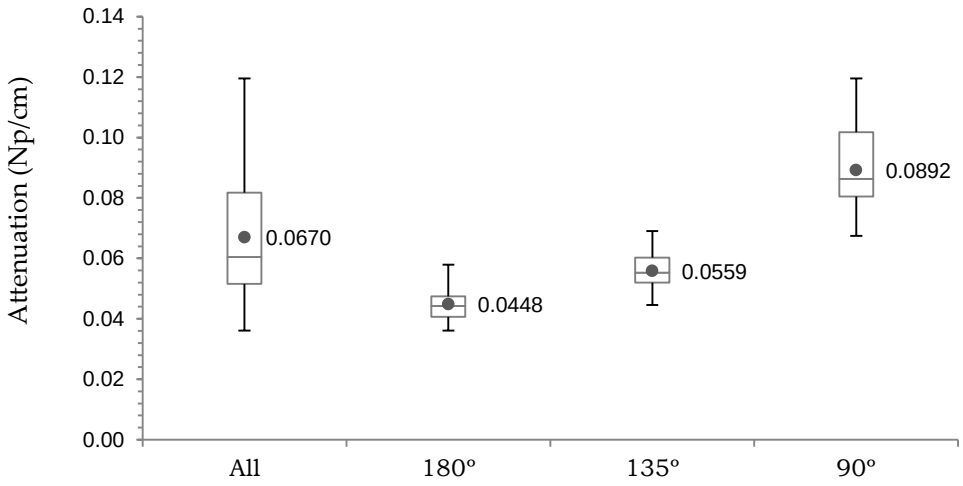

Figure 3-14: Attenuation computed from the measurements in the calibration columns

The average values computed for the attenuation are between the expected range for sound concrete (< 30 dB/m) and damaged concrete (> 90 dB/m) indicated by (Garnier, 2012) for P-wave attenuation at 100 kHz. This suggests that the attenuation results computed are reasonable.

To verify whether the difference between the average attenuation for the whole section and the mean value for each angle is significant, a hypothesis test of the difference of the means was done.

Null hypothesis *(H_0: $\mu_1 - \mu_2 = 0$)*

The null hypothesis is that there is no significant difference between the average for the whole section (μ_1) and the average for each angle.

Alternative hypothesis *(H_1: $\mu_1 - \mu_2 \neq 0$)*

The alternative hypothesis is that there is a significant difference between the means. The significance level was chosen as 5%.

Table 3-3 summarizes the parameters of the hypothesis tests. In the table, μ_1 stands for the average attenuation considering all measurements, μ_2 represents the average attenuation for each position of the receiver analyzed (90°, 135° and 180°), s_1 is the standard deviation for the case of all the measurements, s_2 corresponds to the standard deviation of the samples for each position, n_1 and n_2 represents the number of measurements, ν stands for the degrees of freedom,

t_e is the test statistic (3-11), s_d is the standard deviation of the difference of the means (3-12), $t_{v,0.025}$ represents the critic value to compare that corresponds to the t-distribution value for the specific number of degrees of freedom and the level of significance of 0.025 ($\alpha/2 = 0.025$, two-sided test), and s_c is the combined variance of the difference computed from equation (3-13) because this is the method to obtain a combined variance (Neville & Kennedy, 1966) for the mean difference.

$$t_e = \frac{\mu_1 - \mu_2}{s_d} \tag{3-11}$$

$$s_d = \sqrt{\frac{s_c^2}{n_1} + \frac{s_c^2}{n_2}} \tag{3-12}$$

$$s_c^2 = \frac{s_1^2(n_1 - 1) + s_2^2(n_2 - 1)}{(n_1 - 1) + (n_2 - 1)} \tag{3-13}$$

Table 3-3: Parameters considered in the hypothesis test to evaluate the difference in the mean attenuation

Angle	μ_1	μ_2	s_1	s_2	n_1	n_2	v	s_d	t_e		$t_{v,0.025}$	Result
180°	0.0670	0.0448	0.0207	0.0058	120	24	129	0.0043	5.21	>	0.0314	Reject null
135°	0.0670	0.0559	0.0207	0.0061	120	48	158	0.0030	3.66	>	0.0314	Reject null
90°	0.0670	0.0892	0.0207	0.0120	120	48	144	0.0032	-6.99	>	-0.0314	Reject null

For the three cases, the null hypothesis is rejected and the alternative hypothesis accepted, meaning that there is a significant difference between the means and it is appropriate to consider the average values for each position instead of an average for the whole section. These results indicate that the orientation of the transducer matters and should be taken into account when making any conclusions about your test results.

In addition to the difference in the average values, Figure 3-14 also highlights that the relative position of the receivers affects the magnitude of both the dispersion of the data and the mean value of the attenuation. The mean and dispersion are largest at 90° and smallest at 180°. There are two factors that could explain these observations, which are the directivity of the source and wave spreading.

The directivity pattern refers to the representation of the intensity of the radiated wave as a function of the position from the source. The directivity depends on the wavelength and the dimensions of the radiation surface (Ensminger & Bond, 2012) and can be represented in rectangular or polar coordinates. The representation in polar coordinates is convenient in this case to explain that the intensity of the radiated wave is larger opposite to the source (at 180°) than for the receivers located at 90° and 135°.

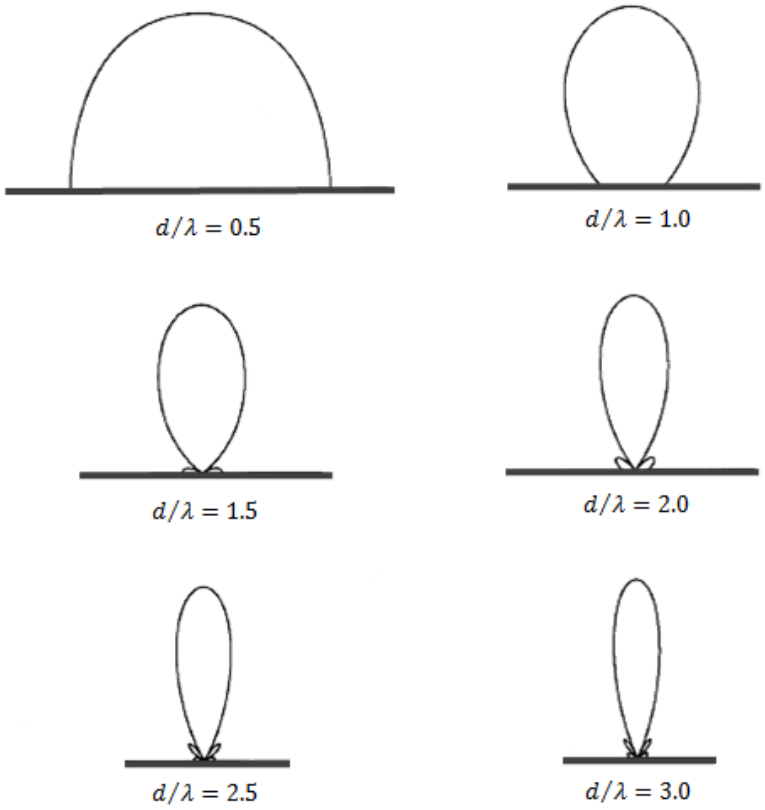

Figure 3-15: Polar coordinates representation of ultrasonic beam profiles for different ratios of the source diameter (d) and the wavelength (λ) (after Rose, 1999)

Figure 3-16 illustrates the beam spreading from a disc transducer (D represents the diameter). Because of the spreading of the ultrasonic beam, the receivers at 90° and 135° would get a more attenuated signal than those located at 180°. This explains the higher dispersion and the lower values recorded at these positions. If only the distance from the transmitter was considered, it would be expected that the attenuation was larger at 180° than at 135°, and larger than at 90°.

However, the attenuation computed includes both the effect of the distance from the source and the spreading of the ultrasonic beam.

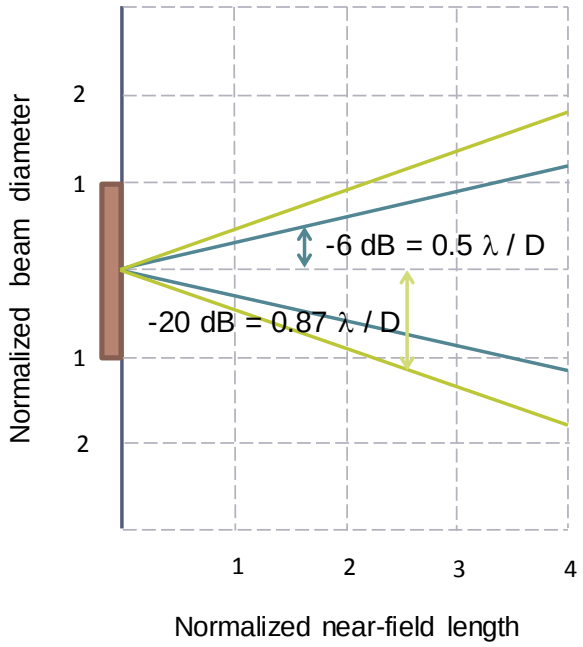

Figure 3-16: Ultrasonic field from a disc transducer showing beam spreading (after Ensminger & Bond 2012)

3.5 Summary

In this chapter, the methodology followed in the research project was described. The methodology was divided in three components: the literature review, the laboratory testing and the field testing. The main outcomes from each methodology component are presented. Since one of the main contributions of the research is the improvement of a new ultrasonic field testing device, a detailed description of the modifications done is also included in this chapter. Finally, it is explained the calibration procedure of the testing device to evaluate reinforced concrete columns.

Chapter 4 Calibration of the ultrasonic transducers

4.1 Introduction

In order to obtain reliable measurements, any instrument needs to be calibrated, that is, compared to or adjusted to a known reference (ASTM E1316-11b). The calibration procedure depends on the type of instrument. In the case of the ultrasonic transducers for the pulse velocity test, the common calibration consists on the measurement of the arrival time using a reference bar. This calibration determines the adjustment in the time, so that the transit time represents the propagation in the specimen, and (ASTM C597-16) only requires it for manual zero-time adjustment systems. However, the transducers are not characterized by this test and they are the most important parts of the ultrasonic measuring system (Schmer & Song, 2007).

Any signal obtained with piezoelectric transducers includes a combined response of the transducer, the couplant and the sample. Therefore, the response has to be normalized by the frequency response of the transducers to reflect the response of the specimen (Kirlangic, 2013). Generally, it is assumed that the frequency response of the transducer is represented by the nominal frequency indicated by the manufacturer. Yet, the technical characteristics of the transducers can change due to ageing and use (Chevalier & Vinh, 2010).

The coupling between the transducer and the surface is another essential aspect for the repeatability of the tests. The study of the coupling agent is very important because one of the main limitations to employ attenuation measurements is the difficulty of obtaining consistent coupling in the field.

The coupling refers to the transmission of the sound waves from the transducers to the specimen. To eliminate the air between the surfaces and to ensure an adequate transmission, generally the transducers are placed with a viscous material like oil, petroleum jelly, mouldable rubber or grease (ASTM C597-16). In the laboratory, vacuum grease can be used because provides good coupling in rough surfaces; but it cannot be used for testing in-service columns because it stains the surface. For this reason other coupling materials were evaluated in the laboratory and in the field.

This chapter describes the calibration performed of the piezoelectric transducers and the study of different couplants. These two tasks were needed to define the adequate test configuration.

4.2 Ultrasonic transducers

There are diverse methods to generate ultrasonic waves: piezoelectric transducers, lasers, electromagnetic and mechanical transmitters (Ensminger & Bond, 2012); however, the piezoelectric transducers are the most commonly used in ultrasonic testing and are devices that converts electrical energy in ultrasonic energy and vice versa (Blitz & Simpson, 1996).

As any other testing device, the transducers have to be calibrated to obtain reliable results. Two calibration procedures were implemented: the determination of the frequency response using a laser vibrometer and the determination of the time delay caused by the electronic equipment.

4.2.1 Determination of the time delay

As explained in section 2.5.2.1, the time delay caused by the electronics can be measured following the same principle of the UPV method, but placing the transducers face-to-face. The delay is the time from the trigger of the input signal to the detection of the arrival of the P-waves. Figure 4-1 present the experimental setup employed.

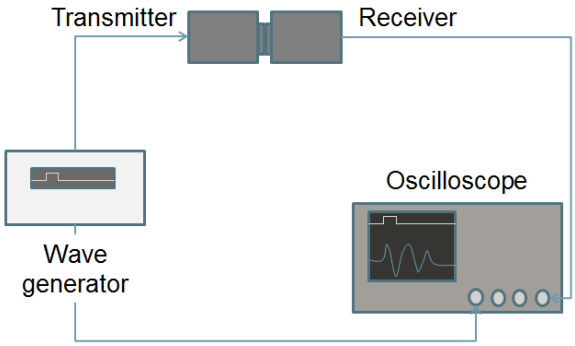

Figure 4-1: Experimental setup to determine the delay of the electronic equipment for UPV test and calibration face-to-face

The average measured delay was 4.2 μs, and this value was subtracted from all the transit times so the time considered in the velocity computation corresponds to the propagation within the specimen.

4.2.2 Direct measurement of the system function

The same configuration can be used to determine the system function $s(\omega)$ (Schmer & Song, 2007). The system function allows determining and separating the effect of the electronics from

the response corresponding to the specimen. It can be expressed in terms of the transfer functions as follows:

$$s(\omega) = t_G(\omega)t_R(\omega)V_i(\omega) \tag{4-1}$$

where $t_G(\omega)$ is the transfer function for the sound generating process, $t_R(\omega)$ is the reception transfer function, and is $V_i(\omega)$ the pulser source voltage. All terms are expressed as a function of ω because the computation is done in the frequency domain. From a calibration setup is possible to characterize all the components because if the received voltage $V_R(\omega)$ is measured, and the transfer function $t_A(\omega)$ is known, the system function can be calculated by deconvolution:

$$s(\omega) = \frac{V_R(\omega)}{t_A(\omega)} \tag{4-2}$$

According to (Schmer & Song, 2007), to reduce the sensitivity of the deconvolution to noise the system function is computed using a Wiener filter:

$$s(\omega) = \frac{V_R(\omega)t_A^*(\omega)}{|t_A(\omega)|^2 + \varepsilon^2 max\{|t_A(\omega)|^2\}} \tag{4-3}$$

()* denotes the complex conjugate of $t_A(\omega)$ and ε represents the noise level present. For ultrasonic problems ε could take values from 0.01 to 0.05.

The system function was needed to normalize the frequency responses computed from the time signals from the UPV tests. For the attenuation calculation (5.2.4) the frequency response considered is the deconvolution of the frequency spectrum of the output signal and the system function.

4.2.3 Calibration using laser vibrometer

The selection of the transducers for ultrasonic testing is based mainly on the element being tested, and in the size of the defect or feature under investigation. These characteristics define the range of usable frequencies.

For testing concrete, the standard ASTM C597-16 establishes that the transducers should have a resonant frequency in the range of 20 kHz to 100 kHz. Even though the manufacturers usually indicate a nominal frequency, this frequency does not necessarily represent the frequency with

more participation in the spectrum. To characterize the frequency response of the transducers it is needed to measure its response to a known input and this can be done using a laser vibrometer.

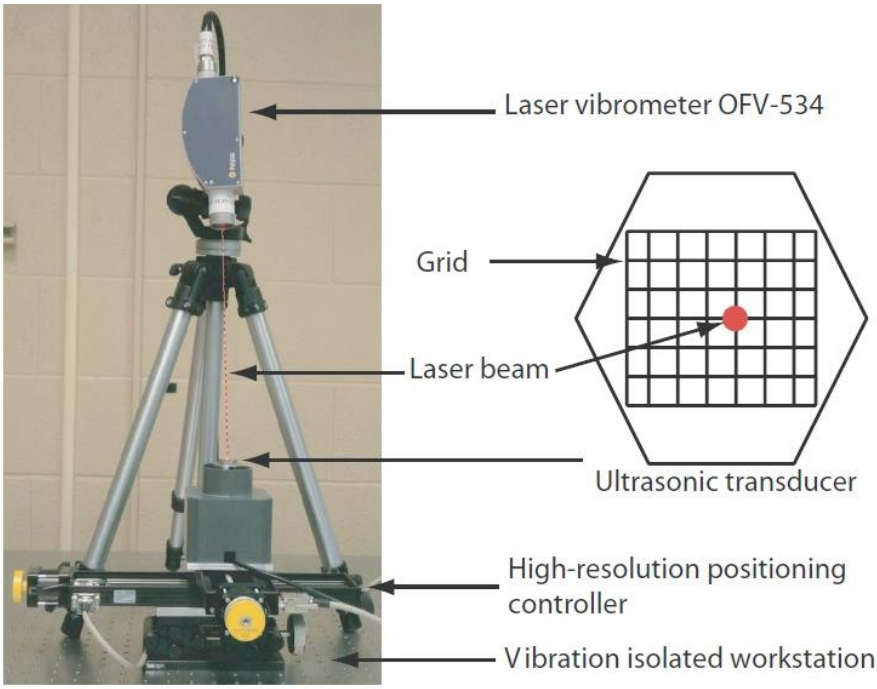

Figure 4-2: Setup to measure the frequency response of the ultrasonic transducers with a laser vibrometer (Tallavó & Kalyan, 2014)

Figure 4-2 shows the setup used to measure the response of the piezoelectric transducers. The frequency spectra of the transducers was computed from the displacements histories recorded with the laser vibrometer in fifty-six points defined in an area of 1.2 × 1.4 cm^2 on the wear plate of the transducer. The input signal was a one cycle sinusoidal pulse with a frequency of 68.6 kHz and amplitude of 10 volts.

Figure 4-3 illustrates the typical frequency response for the displacement histories measured in the face of the transducer. The resonance frequency (frequency with larger amplitude) is closer to 58 kHz than to 82 kHz, which is the nominal frequency indicated by the manufacturer. The assumption of a flat response at a frequency equal to the nominal frequency does not represent the actual response of the transducers.

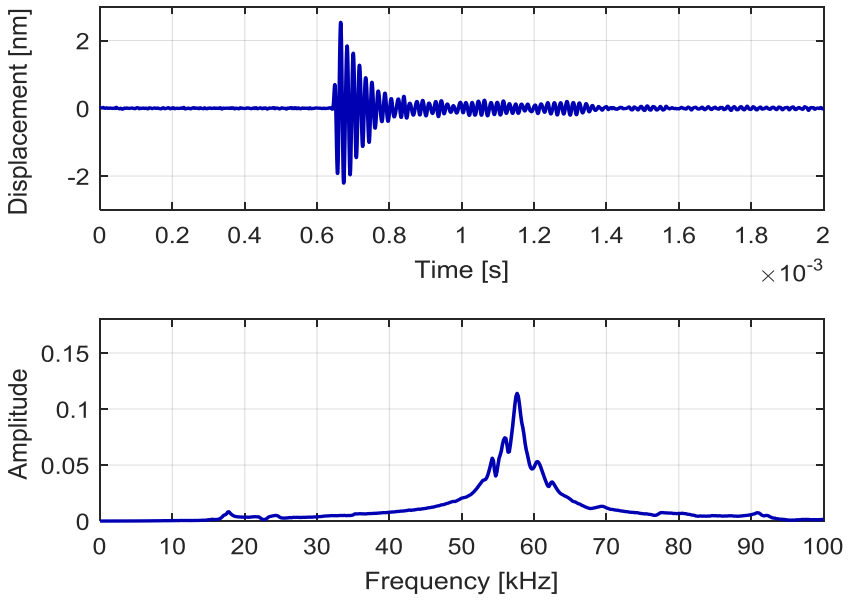

Figure 4-3: Example of the time signal and spectrum for the ultrasonic transducers

The vibration modes of the transducers can be determined from the displacement time histories recorded for each of the points measured with the laser vibrometer. As an example, Figure 4-4 presents a vibration mode and it is evident that the assumption of the flat response of the transducer is inadequate.

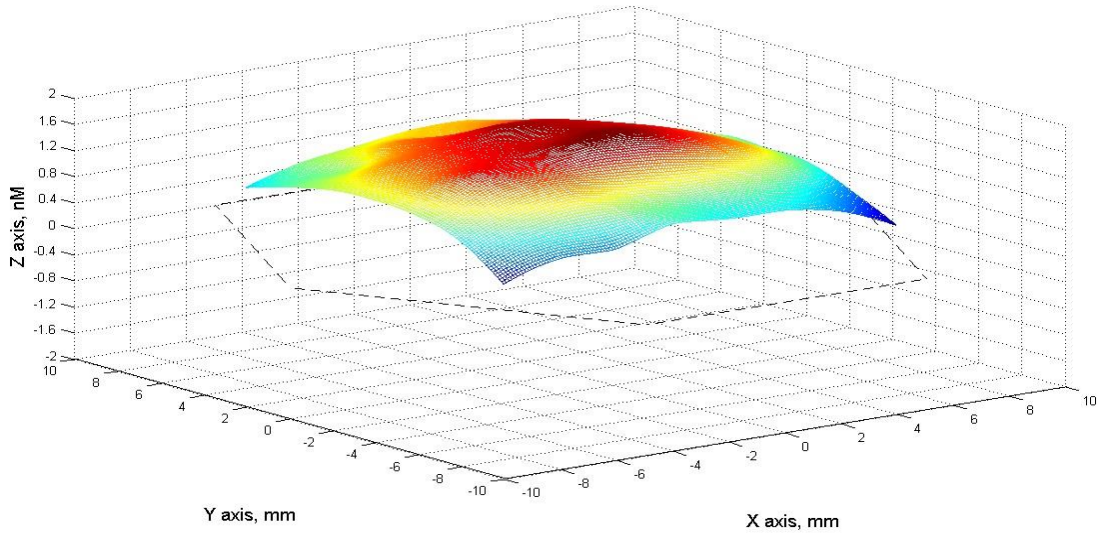

Figure 4-4: Example of the vibration modes of the transducers measured with the laser vibrometer (Tallavó & Kalyan, 2014)

The characterization of the frequency response is also needed to identify the frequency range where the vibration energy is a maximum; and then employ these frequencies for testing. According to the results obtained from the laser vibrometer measurements, the resonance frequency of the transducers used for the testing is around 58 kHz and this was the frequency employed in the subsequent tests.

Another step in the calibration is the linearity verification, which means that the response of the transducer is linear for the range of interest (Dalimar Instruments, 2014). It is demonstrated when, for an increment in the input voltage, there is a corresponding linear increase in the measured displacement amplitude. The linearity provides a physical meaning to the electrical output measured.

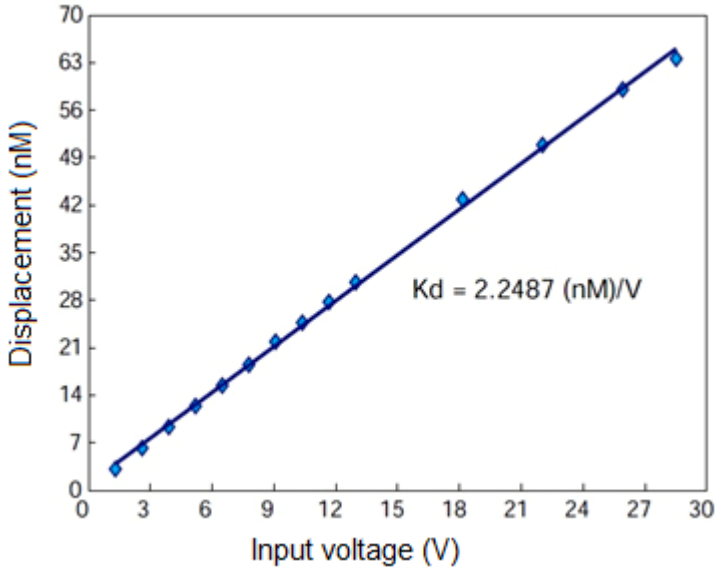

Figure 4-5: Verification of the linearity of the ultrasonic transducer (Tallavó & Kalyan, 2014)

For every increase in the input voltage, the measured displacement augments proportionally; therefore, the linearity of the transducer is verified (Figure 4-5). Given that the test results are based on the measured voltage, the verification of the linearity of the transducers is the physical verification of the relation between the output voltage and the displacement in the element. For piezoelectric transducers this verification is essential because the functioning principle is the conversion between voltage and deformation. To transmit an ultrasonic signal, a voltage is applied and it is converted into deformation of the piezo crystal which produces vibration. For the reception, the vibration sensed is converted into an output voltage recorded in the data acquisition system.

4.3 Study of coupling agents for the ultrasonic transducers

The couplants are the materials that facilitate the transmission of the mechanical waves in the element being studied. The standard (ASTM C597-16) enumerates as common coupling materials for concrete: oil, petroleum jelly, grease, mouldable rubber or water soluble jelly. Nevertheless, these materials shall not be used for testing in-service elements, because they stain the elements. Even though the stains are only external and do not affect the elements performance, this could be aesthetically inacceptable. Accordingly, four different couplings were studied for the application in the field:

a. Duct tape,
b. Duct tape and vacuum grease,
c. Tegaderm™ (transparent medical film material used for the ultrasonic tests when there are unhealed wounds) and
d. Tegaderm™ and vacuum grease.

The coupling materials were selected taking into consideration the easiness to use them in the field, the cost and the quickness to remove them after testing.

The tests consisted on the measurement of the first arrival of P-waves using the same input signal (5 cycles sinusoidal signal of 50 kHz and 5.0 Volts) but changing the coupling agent between the transducers and the unreinforced concrete sample. Figure 4-6 shows the testing setup for the study of the different couplants.

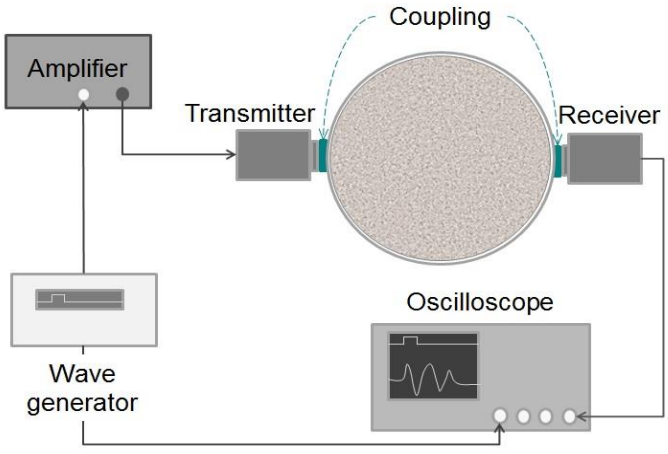

Figure 4-6: Testing configuration for the coupling study

The time signals recorded for each of the coupling materials signals differ significantly in shape and maximum amplitude (Figure 4-7). These results confirm the importance of evaluating the coupling and ensuring consistent coupling to obtain reliable measurements.

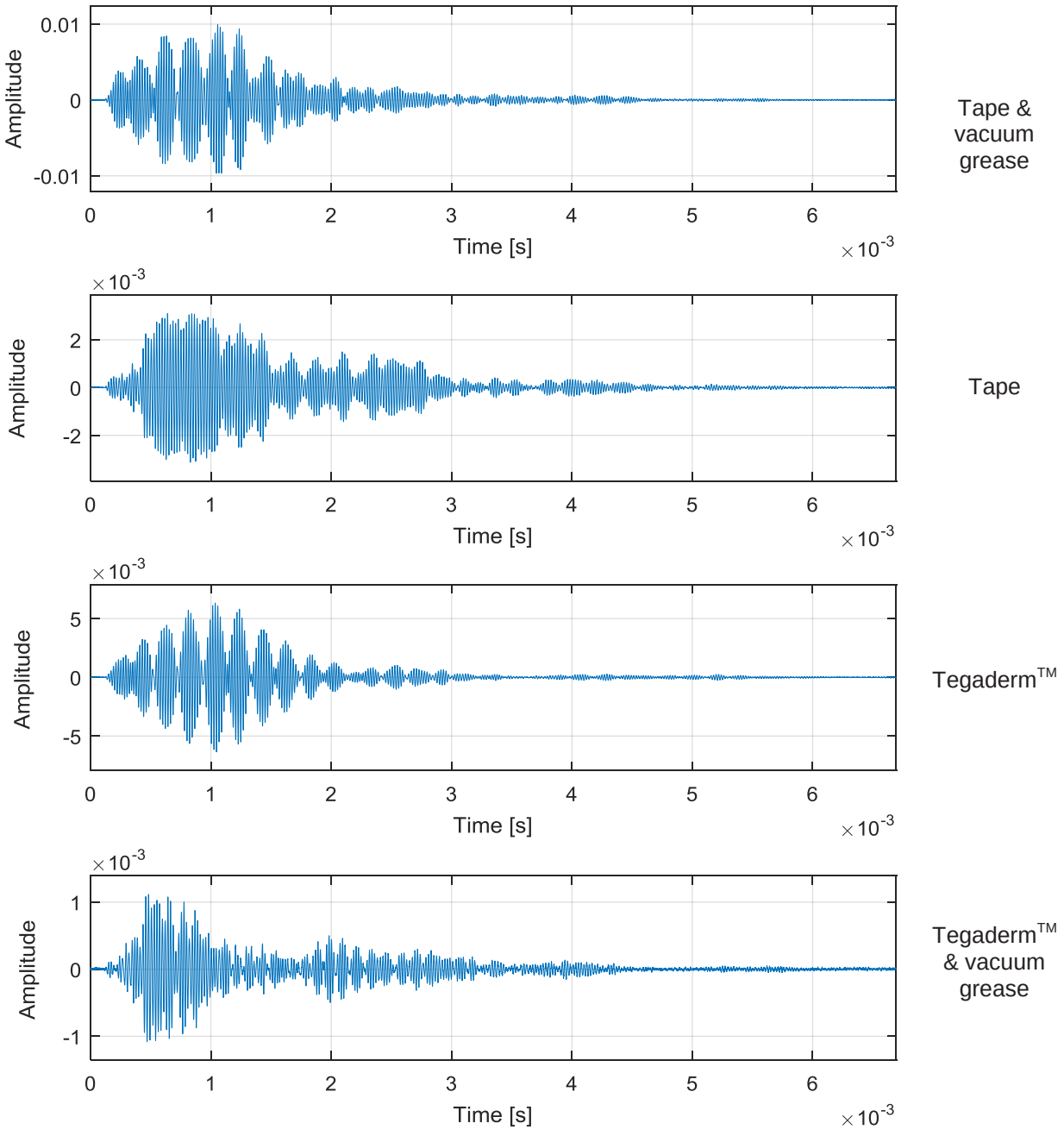

Figure 4-7: Comparison of the time signals for the different coupling materials

In Figure 4-8 below are presented the frequency spectra obtained for the different cases and it is evident that the coupling material affects the transmitted signal, the frequencies that are present in the spectra and that the assumption of a nominal frequency is not appropriate.

According to the results, the coupling agent that provides better transmission is the duct tape with vacuum grease, because results in the largest amplitude, and it is more than double the value for the other coupling materials. Then, the selected couplant to use in the field is the combination of duct tape and vacuum grease because provides a higher response and does not stain the elements.

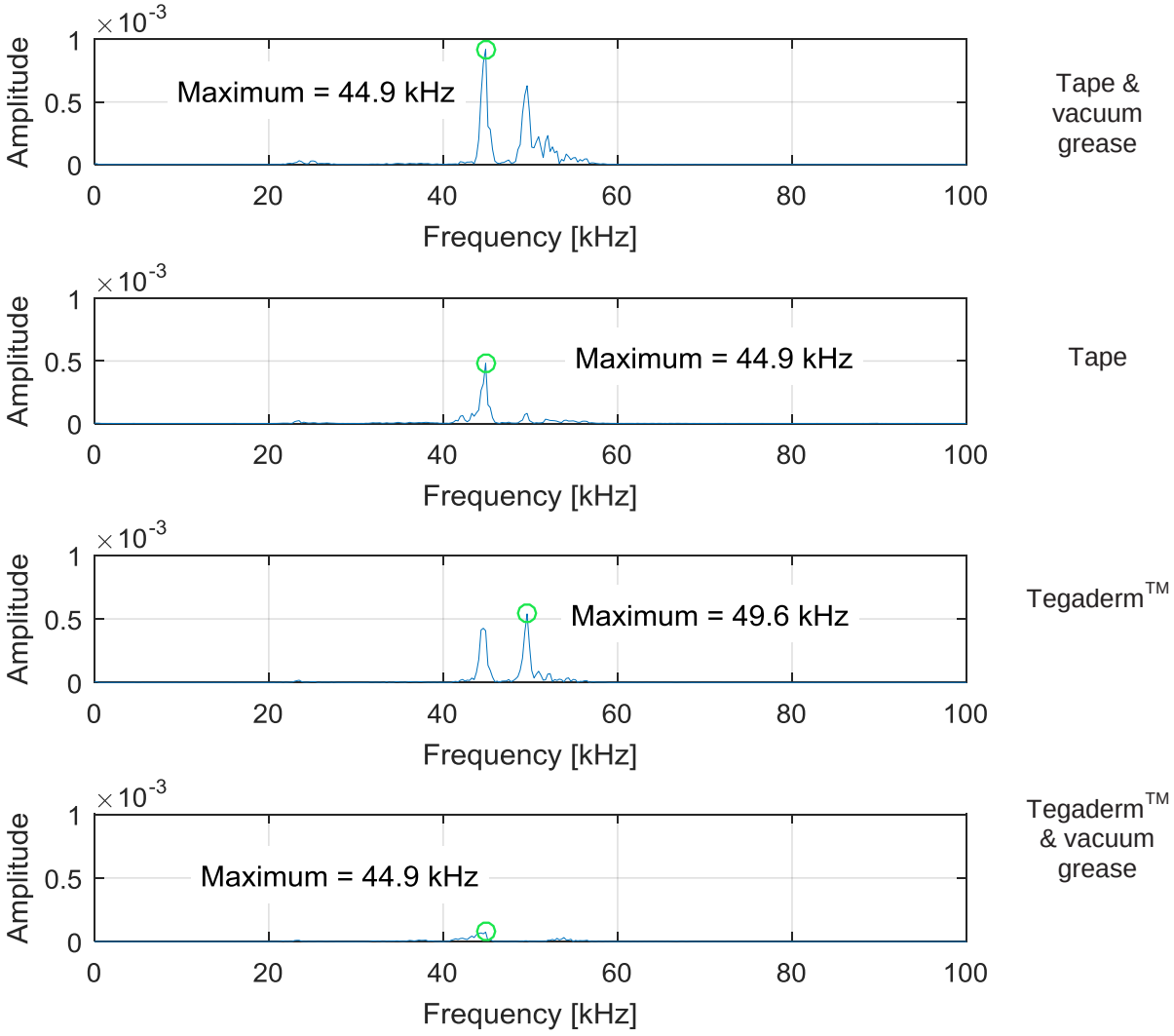

Figure 4-8: Comparison of the frequency spectra for the different coupling materials

4.4 Summary

In this chapter the calibration performed of the ultrasonic transducers and the selection of the couplant for the field testing was described. Both procedures are required to obtain reliable measurements from the ultrasonic test.

The calibration included the verification of the linearity of the transducers, the determination of the time delay, the derivation of the frequency response of the transducers and the computation of the system function.

It was confirmed that the assumption of a flat response with the nominal frequency given by the manufacturer is not adequate to characterize the response of the transducers. Also the results exposed that the resonance frequency of the transducers is closer to 58 kHz than the nominal frequency of 82 kHz reported by the manufacturer.

Since the results of the NDT methods under study depend on the signals recorded, the coupling has a key role in the testing. Four types of coupling were tested and it was decided that the coupling to use for the field test is the combination of duct tape and vacuum grease. From the couplings studied, this combination results in the larger amplitude (which is convenient for the attenuation calculation) and does not stain the elements.

Chapter 5 Study of the sensitivity of UPV to internal damage[1]

5.1 Introduction

In this chapter the tests done to samples of unreinforced concrete in the laboratory are described. The purpose of these tests was to verify the adequacy of UPV to detect internal damage in concrete samples. Two types of damage were studied: freeze/thaw damage and compression.

5.2 Prisms subjected to freeze/thaw damage

The study of frost damage in concrete is one of the major problems in cold climates (Molero et al., 2012). Nine prisms of unreinforced concrete were tested following the ultrasonic pulse velocity method established in the standard (ASTM C597-16) during nine weeks and 324 cycles of freezing and thawing. The testing of the prisms was performed with two purposes. First, to compare the results of ultrasonic pulse velocity tests with the results obtained through the resonant frequency tests (ASTM C215-08). These two methods are the recommended methods to determine the frost resistance of concrete (RILEM TC 176-IDC, 2004). The second purpose was to evaluate whether the UPV method is capable of detecting changes in the internal condition in concrete elements. In this case, the change in the internal condition is induced by cycles of freeze and thawing, which generate internal fracturing of the concrete.

5.2.1 Materials and sample conditioning

The specimens used for the study were nine prisms (405 mm x 70.5 mm x 100 mm) with three different percentages of nanosilica: three specimens without nanosilica (0.0%), three samples with 1.0% of nanosilica and three samples with 2.0% nanosilica. The nanosilica was included to the concrete mixtures in different proportions with the purpose of evaluating the effect of noise production and friction in concrete pavements. For a detailed description of the study refer to (González, Safiuddin, Cao, & Tighe, 2013) and (González, 2014).

The concrete mixture design was developed according to the Canadian Standards Association requirements for concrete (A23.1-09/A23.2-09) and the proportions were weight based. The parameters considered in the experimental design are presented in Table 5-1. The concrete class

[1] The contents of this chapter have been incorporated within a paper that has been submitted for publication: Rodríguez-Roblero, González, Cascante, Pandey, & Tighe. "Evaluation of Freeze/Thaw Damage in Nanoconcrete through Ultrasonic Wave Velocity and Attenuation" Submitted to the Journal of Materials in Civil Engineering. Submission date: April 11th, 2017.

selected is C-2, which applies for plain concrete exposed to chlorides and freezing and thawing. This is the applicable class because the concrete mixtures studied were intended to be used in pavements subjected to freezing and thawing.

Table 5-1: Parameters for concrete mixture design

Parameter	Range
Slump	75 mm - 100 mm
Air content	5% - 8% (tolerance: ±1.5%)
Water/cement ratio	0.39
Concrete class	C-2
Nominal coarse aggregate size	20 mm
Specified compressive strength at 28 days	32.5 MPa
Design strength	43.5 MPa

The weight-based proportions of the control mixture were: 7.3% water, 21.2% cement, 44.8% coarse aggregate and 26.7% fine aggregate. The cement used was General Use portland cement.

The admixtures added were: nanosilica, polycarboxylate-based high range water reducer (HRWR) and air-entraining admixture (AEA). The nanosilica used was white, amorphous, with an apparent density of 0.370 g/cm^3, a dry basis silica content of 99.8% and a particle size between 10 to 20 nanometers. The nanosilica was used as a partial replacement for cement by weight and Figure 5-1 shows a Transmission Electron Microscopy (TEM) image of the nanosilica employed.

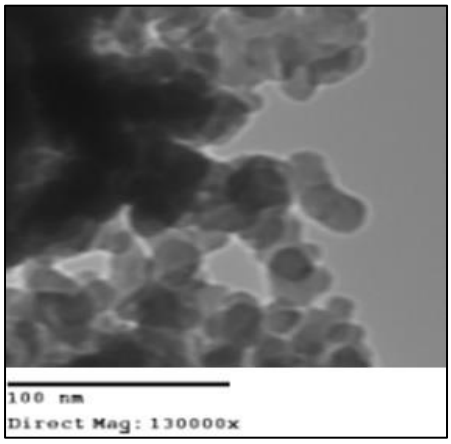

Figure 5-1: Transmission Electron Microscopy (TEM) image of the nanosilica used in the mixtures (image by Marcelo González)

The reference standards for testing the fresh concrete were: ASTM C143/C143M-10a (slump), ASTM C231/C231M-10 (air content) and ASTM C138/C138M-12 (wet density). Table 5-2 summarizes the properties of the fresh concrete mixtures.

Table 5-2: Fresh concrete properties of the mixtures tested

Property	**Nanosilica content**		
	0.0%	1.0%	2.0%
Density (kg/m^3)	2379	2387	2379
Air Content (%)	5.0	5.0	5.1
Slump (mm)	90	75	90

Three cylinders from each concrete mixture were tested at seven and twenty-eight days to verify the compliance with the specified compressive strength, and the results are presented in Table 5-3. The compressive strengths for all cylinders exceeded the specified compressive strength of 32.5 MPa.

Table 5-3: Compressive strength results

Property	**Age**	**Nanosilica content**		
		0.0%	1.0%	2.0%
Compressive strength (MPa)	7 days	45	47	53
Standard deviation (MPa)	7 days	0.5	0.7	1.1
Compressive strength (MPa)	28 days	53	55	59
Standard deviation (MPa)	28 days	1.1	1.8	1.1

The prisms were placed in a moisture room for 14 days after casting. Then, the specimens were positioned in a freezing and thawing chamber surrounded by water as required in ASTM C666-08. The temperature and the cycles were automatically controlled by the apparatus. The specimens were tested every 36 cycles (maximum number of cycles allowed in the standard), which corresponded to once per week for nine weeks. The surface of the specimens was dried to eliminate the excess of water before testing, and the specimens were tested after the thawing cycle.

5.2.2 Pulse velocity results

Figure 5-2 illustrates the variation of the average ultrasonic pulse velocities computed for the three mixtures studied during the testing period.

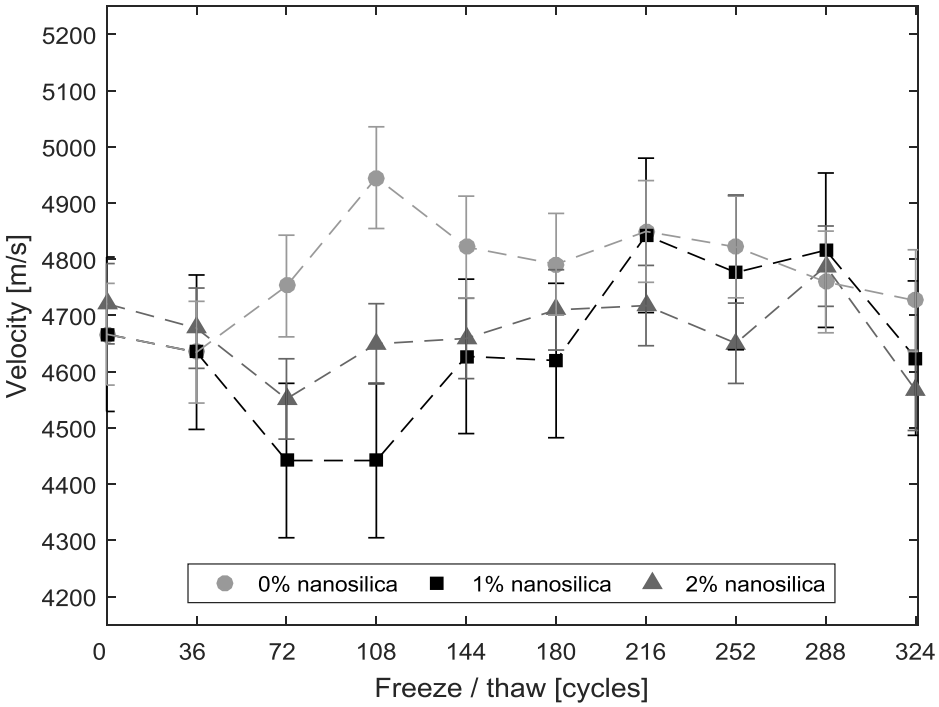

Figure 5-2: Variation of the ultrasonic velocity for samples with and without nanosilica

In both cases (with and without nanosilica), the velocities of the specimens do not present a clear trend during the complete period of study. The first two weeks (up to 72 cycles) the velocity is reduced (maximum reduction of 2.0% from initial condition for the samples with 1.0% of nanosilica), but in the third week (108 cycles) the velocities increased. The maximum increase in the velocity corresponds to the samples without nanosilica and it is of 1.9%. After the third week, the velocity values start reducing again for the case without nanosilica and 1.0%. For the 2.0% mixture, the velocities present an increasing trend. The velocities measured after the sixth week (216 cycles), present a decreasing trend. However, the maximum reduction with respect to the baseline condition is for the specimens with 1.0% of nanosilica and is only 0.85%.

The velocities computed from the specimens that contain nanosilica are lower than the ones without nanosilica, except for one case (288 cycles). Nevertheless, the difference between the values tends to reduce after the fourth week (144 cycles) and the error bars show that the

difference is within the variability of the test. The maximum difference for the velocities measured between the specimens with nanosilica (in this case for the mix with 1.0%) and without nanosilica was obtained the third week, and it has a value of 3.08%.

To analyze whether the initial increase in the velocities (until the third week) may be related with the increase of the strength expected with the aging of concrete, the results of the compression tests for each mixture were plotted and are shown in Figure 5-3. The figure illustrates how the measured strengths for all mixtures are above the specified and the design strength. The slope of the lines joining the measurements at seven and twenty-eight days indicate an increasing trend in the strength (0.38 for the mixtures without nanosilica and 1.0%, and 0.29 for the mixture with 2.0% nanosilica content). According to these results, for an increase of more than 30% in the compressive strength, there is a slight increase (maximum 1.9%) in the pulse velocity. Therefore, the change in the velocities should be related with another phenomenon other than the gain of strength of the concrete.

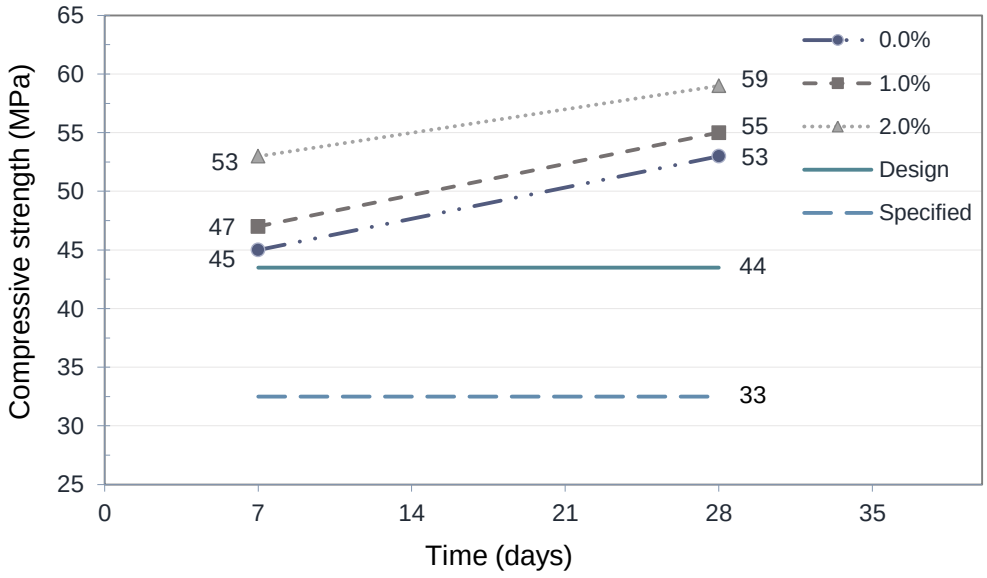

Figure 5-3: Results from the compression tests for the three concrete mixtures evaluated

Figure 5-4 presents the variation of the velocity and the density as the ratio between the values corresponding to the specific number of freeze/thaw cycles, divided by the values calculated at the baseline condition. The variation observed in the velocity is significantly larger than that of the density, which points out that the variability observed in the velocity cannot be due only to variations in the density. Therefore, the measured variation of the mass density of the

specimens cannot explain the corresponding variation in wave velocity. This result suggests that the change in the velocity may be produced by other factor different from the density.

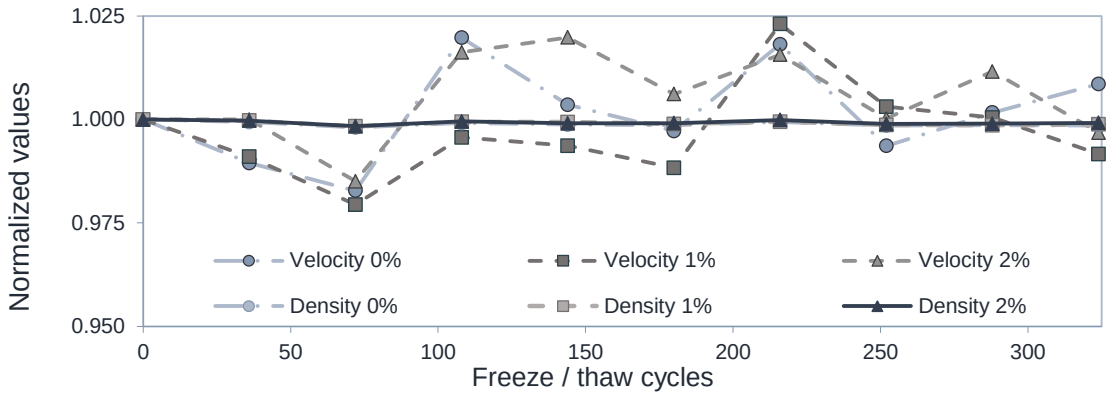

Figure 5-4: Comparison of the variation of the velocity and the density of the specimens normalized with respect to the baseline condition measurements

Another possible cause for the increase in the velocities is the saturation of the samples. ASTM C597-16 states that the velocity for a saturated sample of concrete could be 5% larger than in dry concrete. The saturation of the samples may have improved because the specimens are submerged in water in the freeze/thaw chamber. To verify the changes in the degree of saturation in the samples the information about the density of the samples is presented in Figure 5-5. The density corresponds to the average of three specimens per mix calculated every 36 freeze/thaw cycles (after each resonance test the weight was determined). The initial value included is the wet density measured for the specific mixture. The subsequent values of density were computed dividing the mass measured every week by the nominal volume of the samples. The variation in the density for the three mixtures presents a similar trend, and the three mixtures classify as high-density concrete because the densities vary between 2665 kg/m^3 and 2690 kg/m^3. According to (A23.1-09/A23.2-09), the concrete mixtures above 2500 kg/m^3 are considered high-density mixtures. Since the increase in the density of the samples could only arise from the absorption of water, the change observed between week one and two may be attributed to the increase in the saturation. However, the same figure shows that after the fourth week the variation in the density is minimal which would indicate that the saturation of the samples is reached. Therefore, the effect of the change in the saturation of the samples could only be present during the first three weeks of testing. Since the maximum increase in the

velocity is of 3.0%, and the maximum expected effect on the ultrasonic pulse velocity caused by the saturation of the samples could be from 4.0% to 5.0% (Malhotra & Carino, 2004), it is likely that the initial increment in the velocity is related to the increase in the saturation of the prisms.

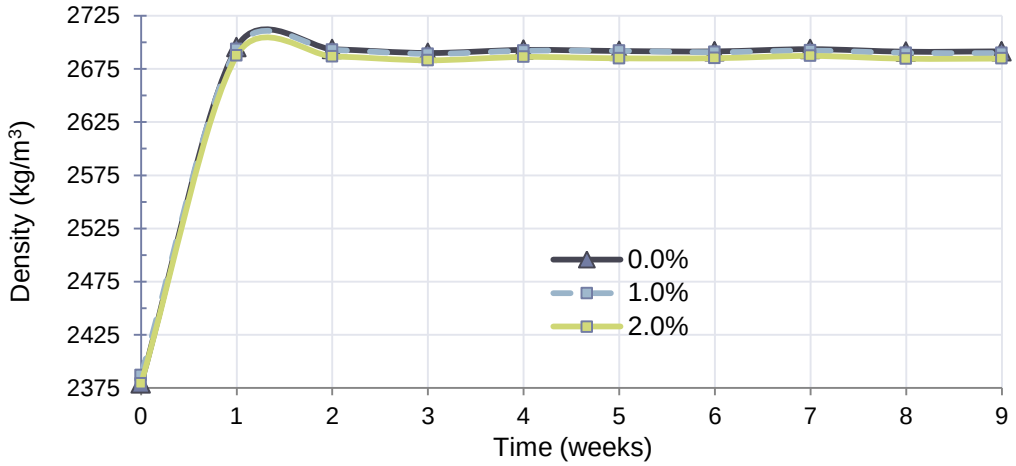

Figure 5-5: Variation of the density of the samples

To investigate further the variability in the measurements, Figure 5-6 includes the box plots for each specimen tested. The circle indicates the median value for the ultrasonic pulse velocity; the lower horizontal line indicates the minimum value computed and the highest horizontal line the maximum. The vertical lines extending from the box (whiskers) indicate the variability between the lower and upper quartile. The results indicate that the variability is different for each sample, being the largest for sample B4 (prism with 1.0% of nanosilica) and the velocities for all cases are within the range of 4450 m/s and 4950 m/s. The median and the maximum values for the velocity of the samples without nanosilica are larger than those for the prisms with nanosilica. The lower velocities correspond to the samples with 1.0% of nanosilica and the crosses for sample B8 indicate outliers (values that are more than ± 2.7σ which is the standard setting for the boxplots in Matlab™ version R2016a that was the software used for the box plots).

A first evaluation of the concrete quality commonly done based on the pulse velocity is to compare the measured value with a reference value (Krautkrämer & Krautkrämer, 1990; Ensminger & Bond, 2012; Lamond & Pielert, 2006). The quality of the concrete is considered as good if the computed velocity is between 3600 m/s and 4600 m/s, and very good above 4600 m/s. The minimum value computed from the specimens was 4442 m/s and the maximum was 4945 m/s. Therefore, according to the reference values, the concrete of all specimens may be considered of good quality during the whole period of study.

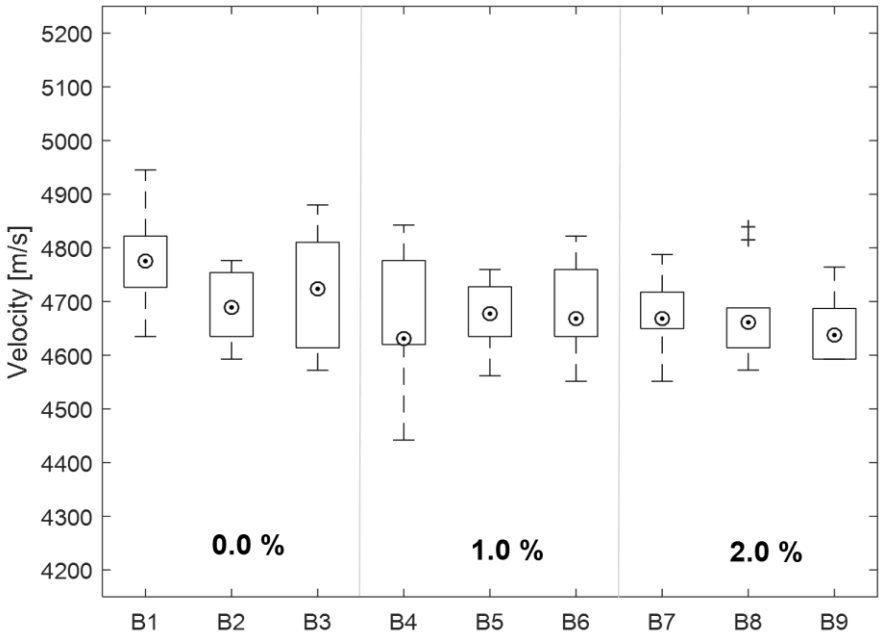

Figure 5-6: Variability of the velocity measurements for each specimen

Other factors that are indicated in the literature that could have an effect on the ultrasonic velocity are the proportion of aggregates, the water/cement ratio and the porosity (Malhotra & Carino, 2004). Since the measurements that are compared correspond to the same specimen, the proportion of aggregates and the water/cement ratio do not change, and the only parameter that could vary during the period of study would be the porosity. The porosity is an important property for the durability of the concrete because it affects the strength, permeability and transport properties (Meng, Müller, & Rübner, 2010). In the literature is indicated that for larger porosity the ultrasonic velocity is expected to be lower (Vergara, Miralles, Gonzálbez, Juanes, Ullate, Anaya, Hernández, & Izquierdo, 2001; Hernández, Izquierdo, Ibáñez, Anaya, & Ullate, 2000). However, it is not included a discussion on the effect of the porosity because it was not measured in this study.

5.2.3 Other parameters investigated to detect freeze and thawing damage

Since the ultrasonic pulse velocity results do not reflect that there is a significant change produced by freezing and thawing, other parameters were investigated. The evaluation of the frost resistance following ASTM C666-08 is through the durability factor DF (5-1) and the dynamic modulus of elasticity $\tau_n{}^2$ (2-15) is the parameter suggested in (RILEM, 2004). Table 5-4 presents the results for the durability factor DF, the relative transit time τ_n and dynamic modulus of elasticity ($\tau_n{}^2$) calculated for each specimen.

Table 5-4: Evaluation of the frost resistance according to ASTM C666 and RILEM TC 176-IDC

REFERENCE	(ASTM C666-08)	(RILEM TC 176-IDC)	
Specimen ID	Durability factor (DF)	Relative transit time (τ_n)	Dynamic modulus of elasticity (τ_n^2)
B1	93.1	1.013	1.026
B2	93.1	0.979	0.959
B3	93.1	1.034	1.068
B4	93.1	0.991	0.982
B5	92.3	1.020	1.040
B6	93.1	0.964	0.930
B7	92.3	0.967	0.936
B8	94.0	1.016	1.033
B9	93.1	1.007	1.014

The evaluation of the frost resistance following ASTM C666-08 is through the durability factor DF, which is calculated as:

$$DF = \frac{\left(\frac{f_x^2}{f^2}\right) \cdot x}{y} \tag{5-1}$$

where the relative dynamic modulus of elasticity at x cycles (as percentage) is multiplied by the specified number of cycles at which the exposure is determined (x), and divided by the specified number of cycles at which the exposure is to be terminated (y). The relative dynamic modulus of elasticity is the ratio between the fundamental transverse frequency after x freeze/thaw cycles (f_x) squared, and the fundamental transverse frequency at the initial condition (f). The relative dynamic modulus of elasticity is adequate to make comparisons between the relative dynamic moduli of specimens or different concrete formulations (ASTM C666-08) and to evaluate mix designs that include innovative materials (Kosmatka, Kerkhoff & Panarese, 2008), as in the case of nanosilica. In the case of the durability factor, it is expected that the concrete has an adequate frost resistance if the DF is above 80% (Cordon & Merril, 1963; Lamond & Pielert, 2006). The lowest durability factors obtained were for the specimen B5 (prism with 1.0% of nanosilica) and B7 (specimen with 2.0%) at 92.3%. Since all the specimens present a DF above 80%, they are considered not deteriorated by freezing and thawing.

The damage criterion in (RILEM, 2004) establishes that the concrete presents frost damage when the dynamic modulus of elasticity τ_n^2 has a value below 0.8. The results in Table 5-4 suggest

that none of the prisms have experienced frost damage, because the dynamic modulus of elasticity for all specimens is above 0.8. This observation is consistent with the results from the UPV and with the DF results.

Another parameter studied to evaluate whether the samples presented frost damage was the dynamic modulus of elasticity, since it can be obtained from both, the resonance test (ASTM C215-08) and the UPV (ASTM C597-09). Thus, the elastic moduli computed from the resonance, UPV and static methods were compared. For the static method, the tests were performed following ASTM C469-10, and the results correspond to the average of three cylinders for each mixture. As an example of the typical results from the static modulus test, Figure 5-7 presents the stresses and strains measured experimentally for a cylinder with 0.0% of nanosilica. The dots indicate the date recorded during the test, and the rhombus point out the strains and stresses specified in the standard ASTM C469-10 to compute the modulus.

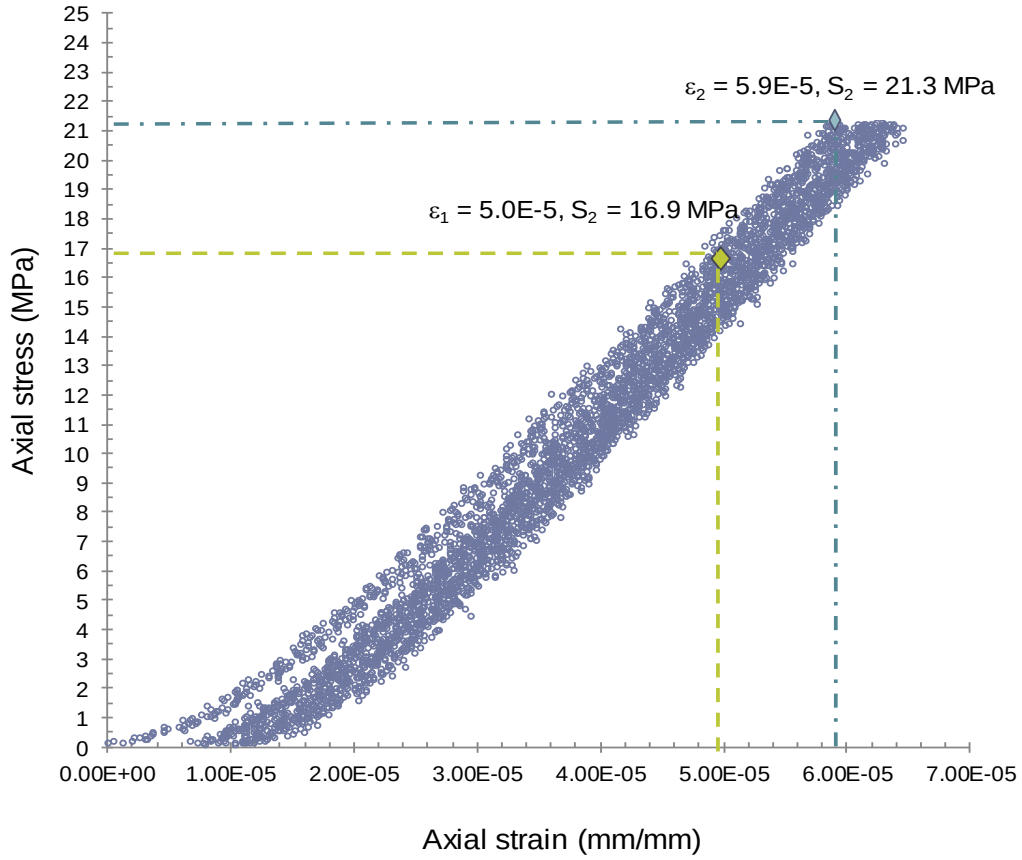

Figure 5-7: Example of the results from the static modulus of elasticity test (ASTM C469-10)

Figure 5-8 presents the comparison of the elastic moduli computed from the resonance, UPV and the static tests. The Poisson's ratio considered was 0.2 because it is a typical value for concrete (ACI 228.2R-13). In the figure, the circular marker indicates UPV results; the square marker the resonance test results and the triangular marker the static test results. The percentage of nanosilica (NS) is indicated in the plot.

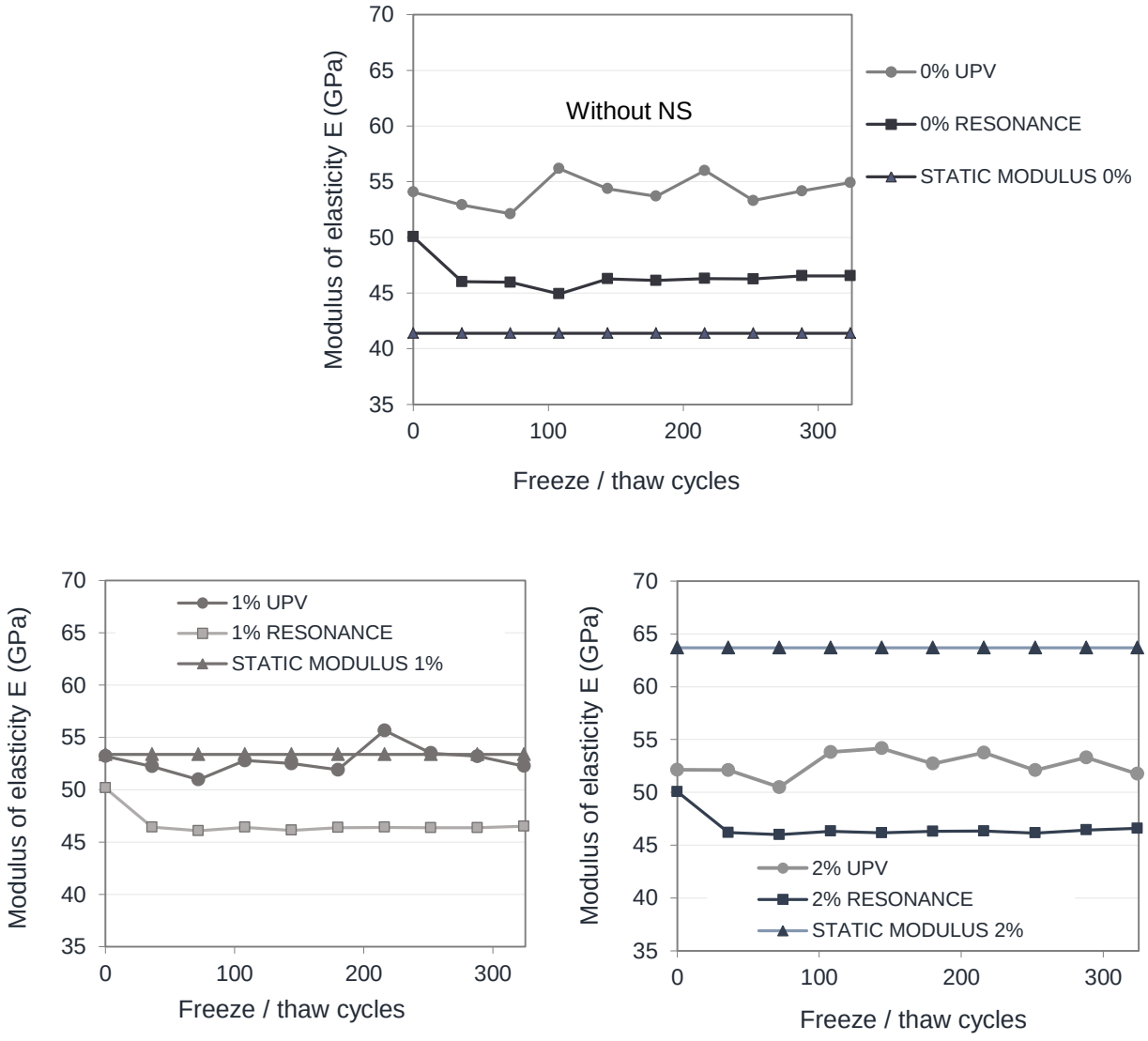

Figure 5-8: Comparison of the modulus of elasticity obtained from different laboratory testing methods (circular marker for UPV, square marker for resonance test, and triangular marker for static test)

The results from the resonance test demonstrate that there is a reduction in the dynamic modulus with respect to the initial condition. Nevertheless, the change is evident only in the first measurement (between the first and the second week), and the maximum change is of 8%. It was noticed that the change in the saturation of the samples (see Figure 5-5) occurred during the same period. This suggests that the reduction in the dynamic modulus is likely to be caused by the moisture gradient produced in the samples until the saturation is reached, and in literature it is reported that the gradients in moisture affect the vibration modes (Malhotra & Carino, 2004).

For the case of the dynamic moduli computed from UPV, all the moduli are larger than those obtained from the resonant method, and they present more variability. This behaviour is consistent with the findings of a study of more than two hundred specimens with compressive strengths between 24 MPa and 161 MPa, elastic modulus from 25.3 GPa and 61.7 GPa and testing ages between 4 and 730 days by (Popovics, Zemajtis, & Shkilnik, 2008). This study evaluated the relation between the different elastic moduli and different empirical equations suggested in the literature. The authors indicated that the values of the dynamic moduli depend on the testing method, and that the UPV results were higher.

With respect to the comparison between the static and the dynamic moduli, the published literature reports that the dynamic moduli are generally found to be greater than those obtained from the static test (Lamond & Pielert, 2006; Popovics et al., 2008; ASTM C469-10, 2010) and the modulus obtained from the UPV could be higher up to 25% with respect to the static modulus. The difference between the dynamic and the static methods are attribute to the different stress levels at which the tests are performed (the ultrasonic test is performed at lower stress levels), and that the elastic modulus is dependent on the load rate (Weiss, 2006).

To quantify the differences between the different methods evaluated, Table 5-5 summarizes the percentage of difference with respect to the static test. The differences were computed with respect to the static test because it is the reference test to estimate the elastic modulus of hardened concrete (ASTM C469-10). The comparison was done for the moduli at the base line condition (zero freeze/thaw cycles).

For the samples of concrete without nanosilica the dynamic methods provide higher estimates than the static test (around 30% for the UPV and 20% for the resonance method), as it is expected (section 3.3 of ASTM C469-10). However, in the mixtures with nanosilica the dynamic moduli are all below the estimate from the static test. For the specimens with 1.0% of nanosilica,

the dynamic moduli are lower than the static (around 0.3% for UPV and 6.0% for the resonance test). For the mix with 2.0% of nanosilica the static modulus is higher than the UPV by 18.1% and 21.4% with respect to the resonance test. The results indicate that there is not a constant relation between the methods evaluated, and suggest that it is not convenient to assume that the dynamic methods would always provide a conservative estimation of the elastic modulus.

Table 5-5: Percentage of error with respect to the static modulus determined according to ASTM C469-10

Testing method	Elastic moduli (MPa)			Difference with respect static (%)		
	0.0%	**1.0%**	**2.0%**	**0.0%**	**1.0%**	**2.0%**
Static	41.4	53.4	63.7	0.0	0.0	0.0
UPV	54.1	53.2	52.1	30.6	-0.3	-18.1
Resonance	50.1	50.2	50.1	20.9	-6.0	-21.4

The relationship between the dynamic and static moduli for the samples including nanosilica is contrary to the expected behaviour (greater dynamic values). The reported results correspond to a limited number of samples and mixture design. Therefore, the results about the relationship between the nanosilica content and the elastic modulus should not be generalized and more research is warranted. From the tests performed for the specific mixtures, it is only possible to suggest that the nanosilica has an effect on the strength of the concrete which is reflected in the elastic moduli determined. This observation is consistent with the reported effect on the strength of concrete including admixtures. As indicated by (Kosmatka et al., 2002)., the strength of concrete with admixtures can be higher or lower than that with only portland cement as cementing material.

5.2.4 Attenuation results

The first result needed to calculate the attenuation is the identification of the frequencies corresponding to the vibrations induced in the specimen. The identification of these frequencies was done by normalizing the frequency spectra by the transfer function of the system (relation between the magnitude of the Fourier transform of the output signal and the Fourier transform of the input signal). From the analysis of the responses for all specimens, three bandwidths were identified of interest: from 0 to 30 kHz, from 30 kHz to 60 kHz and from 60 to 90 kHz. The spectrum of the transducers presented in Figure 4-3 indicates that the frequencies related to the

vibration of the transducers are mainly in the bandwidths from 30 kHz to 90 kHz. Therefore, the vibrations in the bandwidths from 0 kHz to 30 kHz may be the ones related with the vibrations induced in the specimens, so the results of the attenuation are presented for this bandwidth.

Figure 5-9 presents the average normalized frequency spectra (three specimens per mixture). To show the variation over time, the results for the baseline condition, for 180 cycles (half of the testing time) and the 324 cycles (end of the tests) are included. The figure points out that the amplitude of the spectra is decreasing when the number of freeze/thaw cycles increase.

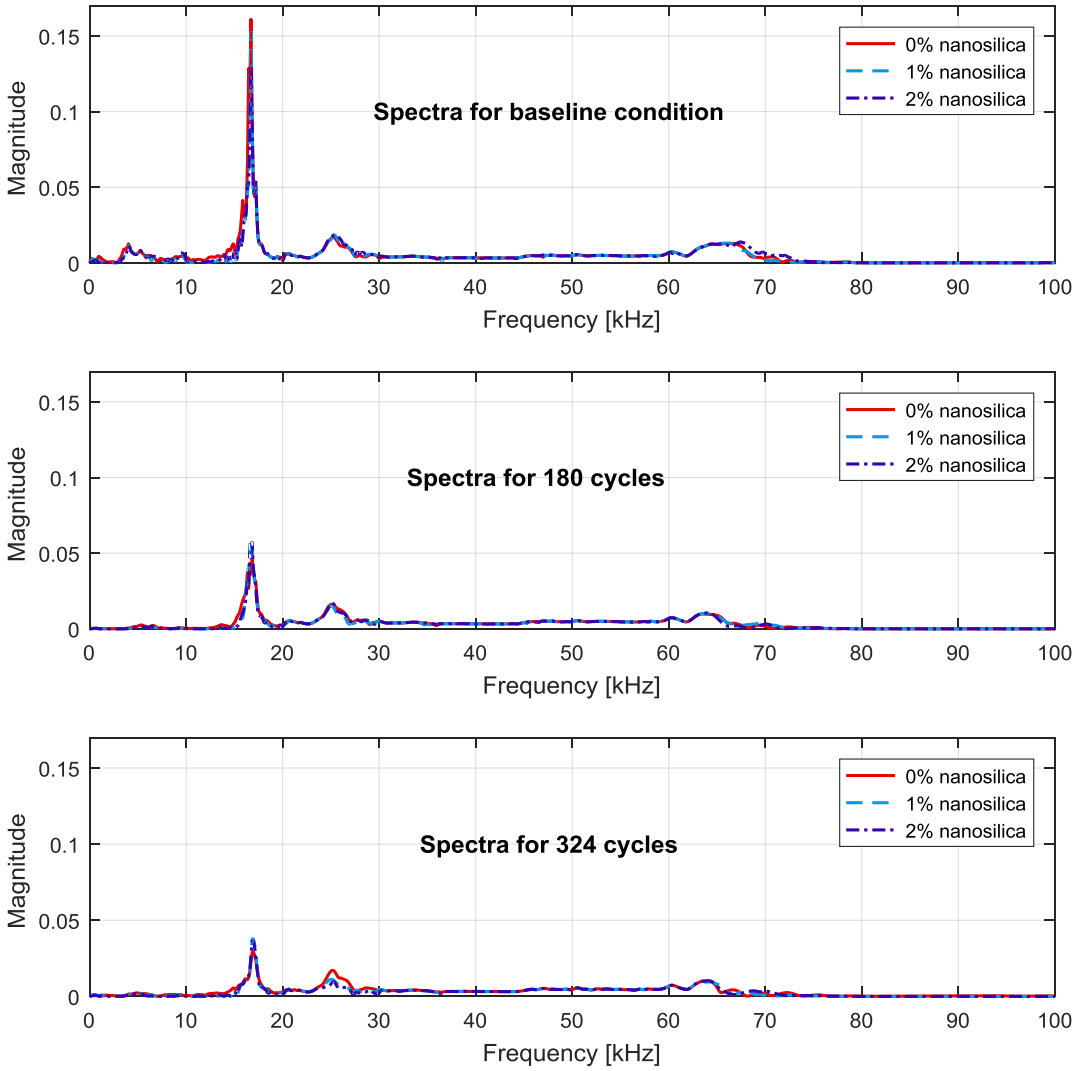

Figure 5-9: Frequency spectra computed from the signals recorded in the UPV tests normalized by the transfer function of the system

Figure 5-10 displays the results of the ratio between the areas below the frequency spectra for a specific number of cycles, with respect to the area below the spectra in the baseline condition. The results expose a similar behaviour for the samples without and with nanosilica. With the exception of the results for 72 cycles and 252 cycles, the ratios of the areas exhibit a decreasing trend. The reduction in the ratio between the areas relates with a larger attenuation, because a reduction in the ratio indicates that the area below the spectrum (for the frequencies of interest) is smaller than the area corresponding to the baseline condition. If the area is smaller, the ultrasonic signal has experienced more attenuation. The maximum reduction at the end of the tests is above 50% for the three mixtures. It was expected an increase in the material attenuation would occur because freezing and thawing induces microcracking in the concrete. The existence of more cracks in the specimen would produce more scattering of the ultrasonic wave. Scattering refers to the dispersion, deflection, or redirection of the energy in an ultrasonic beam caused by small reflectors (ASTM E1316-11b). In this case, the development of the microcracks would cause an increase in the reflectors of the wave, and therefore, a larger material attenuation.

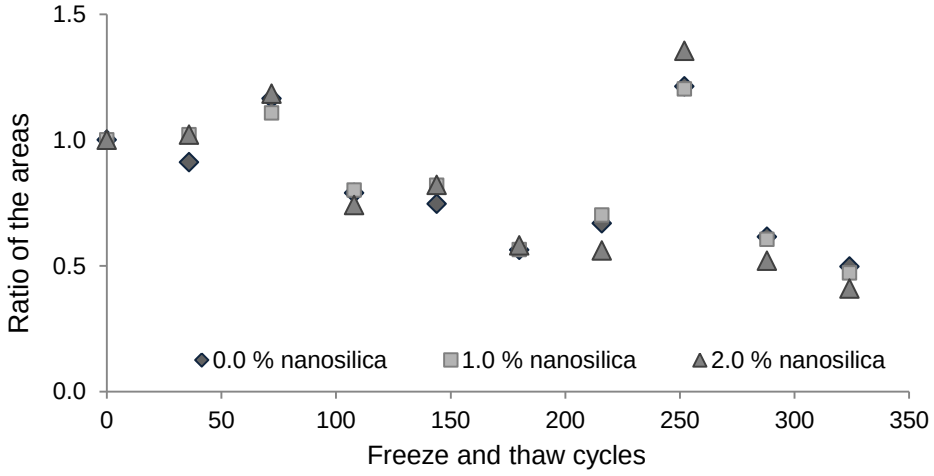

Figure 5-10: Ratio of the area below the frequency spectrum (bandwidth 0-30 kHz) as a quantification of wave attenuation

To verify whether the increase in attenuation is related with damage in the samples, nine cores were extracted from the prisms (three cores for each mixture: 0.0%, 1.0% and 2.0%). The purpose was to evaluate whether the decreasing trend obtained in the attenuation results is reflecting a reduction in the compressive strength due to freeze/thaw damage. The evaluation of

the strength of the concrete is an indirect measure of damage because "deterioration results in a strength reduction" (ACI 437R-03).

The geometric properties of the cores and the compression test results are presented in Table 5-6. According to ASTM C42-13, the diameter of the core should be the larger of 94 mm or twice the maximum nominal size of the coarse aggregate. The standard allows the use of cores of a diameter smaller than 94 mm if it is not possible to obtain cores with a larger diameter. Nevertheless, it is indicated that samples with smaller diameter are known to provide lower compressive strengths with larger variability. In this study the cores had a diameter of approximately 44 mm, which satisfies the requirement of twice the aggregate size, since it was 20 mm. It was not possible to extract cores of larger diameter because of the width of the specimens was 70.5 mm.

Table 5-6: Geometric properties and experimental compressive strengths for the core samples

Sample	% Nanosilica	Average height (mm)	Average diameter (mm)	Test σ (MPa)	Average σ (MPa)
FT0#1	0.0	97.01	43.92	52.85	
FT0#2	0.0	97.01	43.82	60.94	
FT0#3	0.0	95.34	43.68	57.22	
				Average for 0.0%	57.00 ± 4.05
FT1#1	1.0	95.00	43.90	58.61	
FT1#2	1.0	96.02	43.71	56.34	
FT1#3	1.0	95.17	44.04	61.92	
				Average for 1.0%	58.96 ± 2.81
FT2#1	2.0	97.68	44.02	58.67	
FT2#2	2.0	96.01	44.08	66.51	
FT2#3	2.0	96.01	43.84	65.62	
				Average for 2.0%	63.60 ± 4.29

ACI 562M-13 provides the following equation to compute the equivalent strength of the cores extracted according to ASTM C42-13 and ASTM C823-12:

$$f_{ceq} = 0.9\overline{f_c}\left[1 - 1.28\sqrt{\frac{(k_c COV)^2}{n} + 0.0015}\right] \quad (5\text{-}2)$$

Where $\overline{f_c}$ is the average core strength (accounting for the diameter and moisture condition of the cores); COV is the coefficient of variation of the core strengths; n the number of cores taken and k_c is the coefficient of variation modification factor. Since for each case three cores were extracted, k_c is 1.47. Table 5-7 summarizes the parameters considered and the average equivalent strength obtained for each mixture. Comparing the equivalent core strengths to the specified design strength in Table 5-1, it is verified that all the mixtures have a higher strength than the specified.

Table 5-7: Equivalent strength of the core samples

Nanosilica content	Average σ_{test} (MPa)	Standard deviation (MPa)	Coefficient of variation COV	f_{ceq} (MPa)
0.0%	57.00	4.05	0.07	46.60
1.0%	58.96	2.81	0.05	49.26
2.0%	63.60	4.29	0.07	52.17

To evaluate if the difference between the strength estimated from the cylinders (before freezing and thawing) and the cores (after freezing and thawing) is significant, hypothesis test of the difference of the mean values of the compressive strengths is postulated.

Null hypothesis H_o: $\mu_{before} - \mu_{after} = 0$

The null hypothesis is that there is no difference between the mean strengths of the cylinders and the equivalent strength from the cores.

Alternative hypothesis H_1: $\mu_{before} - \mu_{after} > 0$

The alternative hypothesis is that there is a significant difference between the strength before and after freezing and thawing.

The significance level chosen is 90%, based on section 3.1 of ACI 228.1R-03, which establishes that it is reasonable to verify that the tenth-percentile in-place compressive strength is at least 0.85 of the required compressive strength. It was considered that if the significance level to evaluate the compliance with the strength requirement is 90%, the same significance level

would be adequate to evaluate the difference of the strengths in this case. Therefore, the hypothesis test is done using the t-student distribution with a significance level of 10%.

The degrees of freedom for the case where the standard deviations are unequal and unknown are given by the Satterthwaite's approximation presented in the following expression (Gaylor & Hopper, 1969):

$$\nu = \frac{\left(\frac{s_1^2}{n_1} + \frac{s_2^2}{n_2}\right)^2}{\left[\left(\frac{s_1^2}{n_1}\right)^2 \frac{1}{n_1 - 1}\right] + \left[\left(\frac{s_2^2}{n_2}\right)^2 \frac{1}{n_2 - 1}\right]} \tag{5-3}$$

where s_1 and n_1 are the standard deviation and the number of samples for the cylinders, and s_2 and n_2 are the standard deviation and number of samples for the cores. The t value in this case is given as:

$$t = \frac{\mu_1 - \mu_2}{\sqrt{\frac{s_1}{n_1} + \frac{s_2}{n_2}}} \tag{5-4}$$

Table 5-8 summarizes the information from the hypothesis test. For the three mixtures, the null hypothesis is rejected and the alternative hypothesis accepted, which means that the resistance from the cores is smaller than the strength of the cylinders measured at 28 days. The reduction in the strength is of 12.4% for the control mix (0.0%), 11.1% for the mix with 1.0% of nanosilica and 11.5% for the 2.0% mix.

Table 5-8: Hypothesis test parameters

Nanosilica content	μ_{before} **(MPa)**	μ_{after} **(MPa)**	s_1	s_2	n_1	n_2	ν	t		$t_{2,0.10}$	Result
0.0%	53.21	46.60	1.137	4.05	3	3	2	5.02	>	1.89	Reject null
1.0%	55.39	49.26	1.786	2.81	3	3	3	4.95	>	1.64	Reject null
2.0%	58.96	52.17	1.118	4.29	3	3	2	5.05	>	1.89	Reject null

5.2.5 Conclusions from the study of freeze/thaw damaged samples

The results from UPV and resonant frequency consistently reflect that none of the specimens presented significant frost damage after more than 300 freeze/thaw cycles. The maximum change is 8.0% change in the resonance frequency method and less than 5.0% for velocity.

According to the reference velocity values indicated by (Krautkrämer & Krautkrämer, 1990), all the velocities calculated denote a concrete in very good condition. Therefore, from the ultrasonic pulse velocity is not possible to assess whether there is internal deterioration in the samples. The velocities computed from the specimens that contain nanosilica are lower than the ones without nanosilica (at maximum 3%); thus, there is no significant evidence of different behaviour between the specimens that contain nanosilica and the ones that do not. Similarly, the results obtained from the resonant frequency test (ASTM C666-08) do not show a significant variation during the period of study (less than 8%). However, the results from the attenuation estimations manifest an increase that could be related to internal damage resulting from freezing and thawing. The comparison of the strengths of the cores extracted from the prisms and the strength of the cylinders of the same mixtures affirm that there is a reduction in the strengths of the specimens. However, to confirm that the change is due to frost damage it would be necessary to conduct a petrographic investigation of the samples.

The analysis of the variation of the density indicates that it varies throughout the study period, but the variation on the density cannot explain the variation in the velocity measurements. From the accepted relationship between the pulse velocity, the density and the elastic constants (equation 2-1), it may be concluded that there should be a change in the elastic modulus of the specimens. Thus, the elastic moduli computed from the resonance test, the UPV, the static test were analyzed. For the specimens without nanosilica, the dynamic methods provide larger estimations of the elastic modulus, as expected. However, for the specimens with nanosilica the static modulus is the largest. This result suggests that it is not convenient to assume that the dynamic methods would always provide a conservative estimation of the static elastic modulus.

5.3 Cylinders under axial load

The second set of tests done to assess the ability of UPV to detect internal damage consisted in the measurement of the arrival time and the calculation of the pulse velocity for four concrete cylinders of the control mixture (without nanosilica). The cylinders were tested before and after the uniaxial compression test and the results in terms of the velocity and the attenuation are presented in the following sections. The purpose of these tests was to investigate if from the

results of the pulse velocity is possible to recognize internal damage. In this case the internal damage consisted in the micro-cracks that resulted from the compression tests. The compressive load was applied until the failure and the cracking pattern observed in all specimens was longitudinal cracking. The UPV measurements were taken parallel to the direction of application of the compressive load.

5.3.1 Ultrasonic pulse velocity results for the specimens tested in compression

Figure 5-11 shows the box plot of the ultrasonic pulse velocity data before and after the compression test. The whiskers indicate the minimum and the maximum value, and the circular markers represent the average velocities.

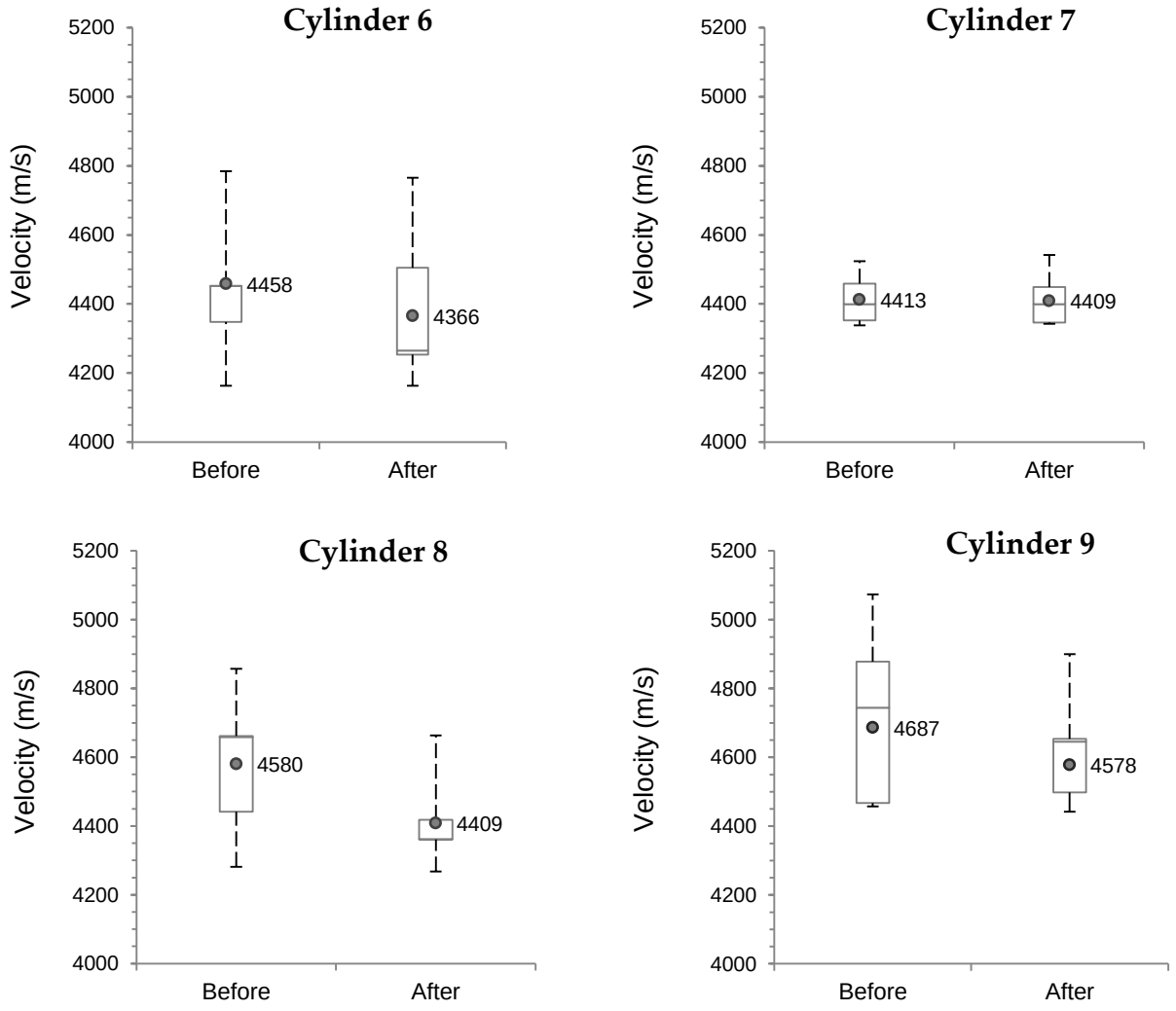

Figure 5-11: Comparison of the variation of the ultrasonic pulse velocity for four cylinders tested before and after the compression test

For all cylinders, the average velocities are comparable, and except for cylinder 7, the average velocity after the compression test is reduced.

The minimum velocities are above 4000 m/s and comparing the velocities with the reference ranges suggested by (Krautkrämer & Krautkrämer, 1990), none of the cylinders is damaged because the velocity is above 3600 m/s. Nevertheless, the four cylinders are damaged after the compression test, because the compressive load was applied until the failure of the cylinder occurred. This inconsistency demonstrates that comparing the pulse velocity with a reference value is not sufficient to ensure that the concrete is sound.

Table 5-9: Comparison of the pulse velocity for the cylinders tested in compression

Specimen ID	μ_{before} (m/s)	s_{before} (m/s)	μ_{after} (m/s)	s_{after} (m/s)	Ratio of UPV (μ_{after} /μ_{before})
Cylinder 6	4458	200	4403	218	0.99
Cylinder 7	4425	77	4448	71	1.01
Cylinder 8	4580	222	4418	150	0.96
Cylinder 9	4687	213	4590	90	0.98

The ratios in Table 5-9 indicate that there is no significant reduction in the values of the velocity, since the maximum reduction is 4%. In the same table is included also the standard deviation computed for each sample with the intention of showing that the difference obtained between the velocity before and after compression is smaller than the standard deviation.

5.3.2 Attenuation results for the specimens tested in compression

Figure 5-12 presents the normalized frequency spectra for the four cylinders evaluated. The normalized spectra refers to the frequency spectra of the output signal convolved with the system function using a Wiener filter, as it was explained in section 4.2.2. For all cases, the plots indicate a reduction in the area below the frequency spectrum after the specimens were subjected to uniaxial compression until failure. The attenuation in this case was quantified as ratio between the area below the normalized frequency spectrum after the compression test and the area below the spectrum before the test.

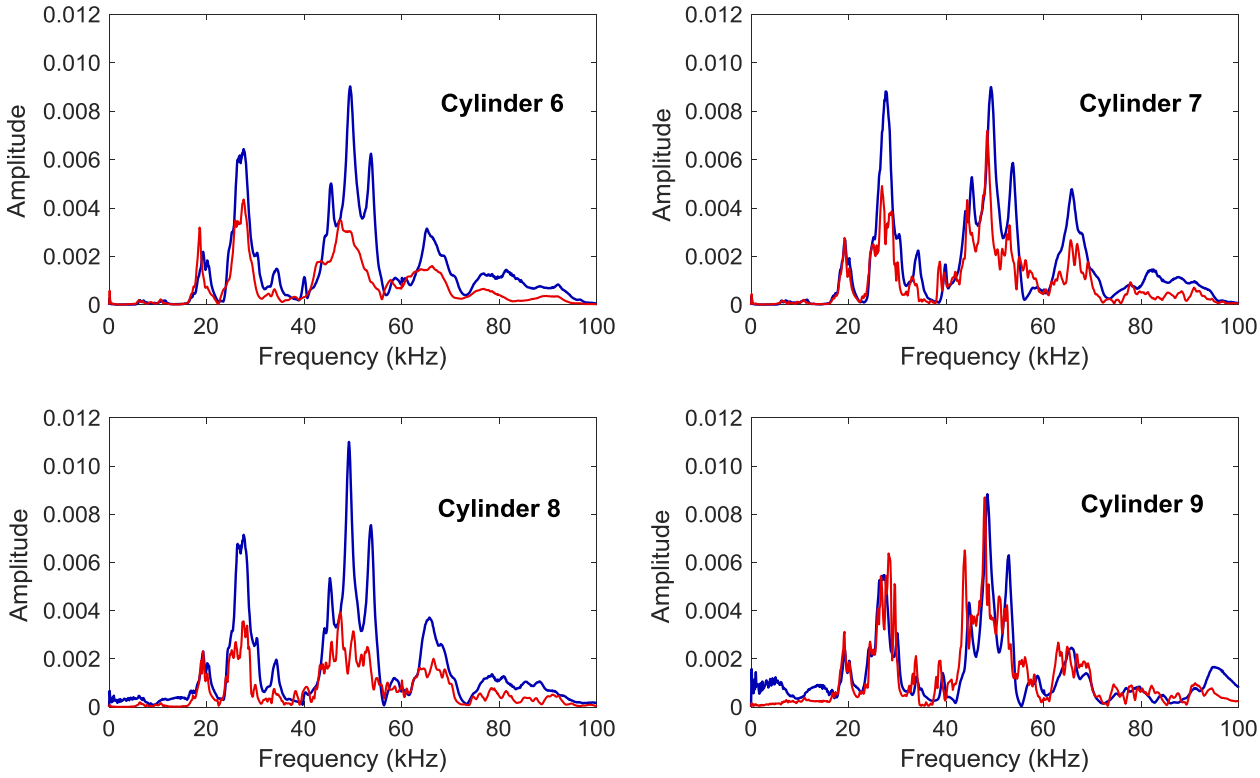

Figure 5-12: Comparison of the spectra before and after the compression tests

Table 5-10 presents the results of the areas computed for each cylinder (A stands for after and B before the compression test). The reduction in the area was calculated assuming the initial condition as the unity, and subtracting the ratio between the areas and multiplied by 100 to present the results as percentage.

Table 5-10: Quantification of the attenuation for the cylinders tested under uniaxial compression

Case	Area below spectrum	Ratio (After / Before)	Reduction
Cylinder 6B	1.28E-06	0.536	46.4
Cylinder 6A	6.87E-07		
Cylinder 7B	1.38E-06	0.653	34.7
Cylinder 7A	9.00E-07		
Cylinder 8B	1.51E-06	0.456	54.4
Cylinder 8A	6.88E-07		
Cylinder 9B	2.21E-06	0.654	34.6
Cylinder 9A	1.44E-06		

For the cylinders tested in compression, the attenuation results show a change between 30% and 50%, while the change in the velocity is only 4%.

The test results demonstrate that the attenuation indicates the existence of damage in the specimens, while the velocity does not indicate a significant change in the condition. This can be explained because the velocity depends only on the arrival time. Therefore, if there is no significant change in the time, there would not be any change in the velocity. However, the attenuation can show the damage, since there is a reduction in the magnitude. The interaction of the sound waves with the micro fractures results in scattering, which produces magnitude reduction and redirection of the waves.

The reduction of the areas below the spectra indicates an increase in attenuation because there is a reduction in the energy of the received signal for the same input. While for the velocities the maximum change was about 4%, for the attenuation the changes are 35% for cylinders 7 and 9, 46% for cylinder 6 and 54% for cylinder 8. In this case it is known that the specimens are damaged because the compression load was applied until the failure of the specimen.

5.4 Summary

This chapter included the results of two sets of tests intended to evaluate the sensitivity of pulse velocity to internal damage. The two types of damage studied were freeze/thaw and fracturing by compression.

For the evaluation of freeze/thaw damage, three methods were compared: ultrasonic pulse velocity, resonance method and attenuation. Even though UPV and resonance are the testing methods suggested in the standards to evaluate freeze/thaw damage, both methods showed limited sensitivity. In contrast, attenuation results indicated deterioration and the results from the cores extracted from the specimens show a consistent trend.

In the case of the damage induced by compression, UPV results do not indicate a significant change between the values before or after the test. Also when the estimated velocities were compared with reference values the results did not indicate damage. These findings confirm that it is not adequate to base the assessment of the condition of a concrete element on individual measurements of pulse velocity, because the velocity does not appear to be sensitive to internal damage. In addition, the results demonstrated that an evaluation based on a reference value of pulse velocity may mislead the evaluator.

Chapter 6 Surface waves evaluation

6.1 Introduction

The main objective of this research project was the study of the possible combination of two stress wave nondestructive methods (ultrasonic pulse velocity and surface waves) to assess the condition of reinforced concrete elements. In this chapter are included the results related with the surface waves tests done.

Surface wave analysis is evaluated as an initial global assessment because this type of analysis is convenient for large concrete surfaces where is aimed a quick evaluation (Aggelis 2009). In addition, the use of surface waves to assess the condition of concrete elements presents several advantages:

a) It is needed access only from one surface

b) The penetration depth of the waves can be controlled by changing the testing frequency

c) Surface waves can be easily generated by an impact or with a transducer

d) Most of the energy recorded at the surface of an element is transported by surface waves.

Two types of structural elements were tested using surface waves: five beams tested in the laboratory and a reinforced concrete dome in the field. The purpose of these tests was to analyze the limitations of the equipment available, to improve the testing setup and to verify the effect of the coupling in the measurements. Also, to experiment different techniques to process the experimental data recorded.

6.2 NDT of reinforced concrete beams under fatigue loading

This study was performed as a collaborative project for the PhD thesis of Rayed Alyousef (Alyousef, 2016) and had two objectives. First, it was of interest to verify if through surface wave analysis it is possible to obtain some indication of the imminence of failure of the beams that were tested under fatigue loading. The second objective was to experiment different setups of the NDT system to identify the best testing configuration to perform surface wave tests of reinforced concrete elements. The parameters that were modified were the spacing between the sensors (accelerometers), the mounting of the transducers acting as source, and the mounting between the accelerometers and the surface of the beams.

6.2.1 Generalities about fatigue evaluation using NDT

Fatigue of a material is the weakening by repeated loading (ACI CT-16), and it results in a brittle failure. The analysis of concrete elements under fatigue is an important aspect because it can cause cracking at lower than expected loads, and the cracking of a member can affect the static loading characteristics (ACI 215R 1997). Brittle failures are undesirable because their occurrence is sudden, they do not provide signs of distress and they can result in significant losses, especially in the case of structural elements. As there are no signs or indicators of distress, different studies have aimed to measure other properties that may be used as indicators of the imminence of failure.

To evaluate the actual condition of concrete elements different methods can be used, being the most common visual inspection. Also nondestructive techniques (NDT) are valuable tools for fatigue assessment. In the case of damage assessment of beams, NDT methods such as acoustic emission (Zarate, 2012), modal analysis (Kessler, 2002) or surface wave analysis have being reported (Kalinski, 1992).

In this study, the purpose was to evaluate if the data recorded using surface wave testing may provide an indication of the progression of the damage induced by fatigue loading.

6.2.2 Specimens tested

The test specimens were five reinforced concrete beams part of an experimental program of 55 beams tested under fatigue loading. For a detailed description of the testing program see (Alyousef, 2016).

From the five beams tested, three were wrapped with fibres polymer (FRP) sheets and two of the beams did not have any type of external reinforcement. The beams were simply supported, and the cyclic load was applied at two points located at 600 mm from each support.

All the beams tested had a rectangular cross section of 250 mm width and 350 mm of depth. The beams had 2200 mm of length and the longitudinal reinforcement consisted of two bars diameter 10 mm as compressive reinforcement, and two bars of 20 mm diameter as the tensile reinforcement. The reinforcement bars in the compressive zone extend from the supports to the points of application of the load. The transverse reinforcement consisted of stirrups diameter 10 mm spaced 100 mm. The transverse reinforcement was located only from the supports to the points of application of the load. In the case of the tensile reinforcement, the bars are spliced in the center of the beam 150 mm to each side. The failure of the specimen was expected to start at

the location of these splices, and therefore, the accelerometers were placed in this section. Figure 6-1 shows the geometry of the beams.

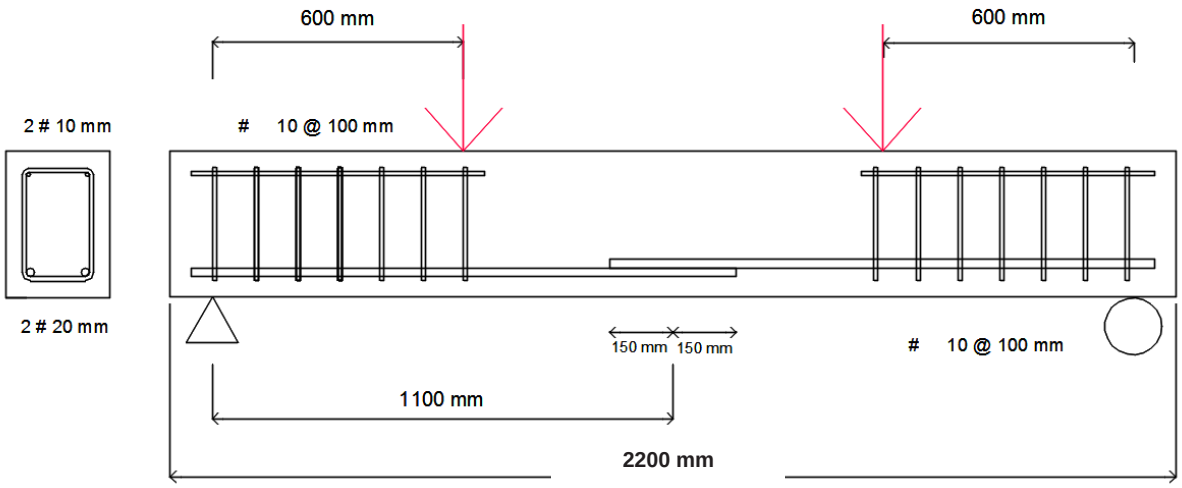

Figure 6-1: Geometry of the reinforced concrete beams tested

6.2.3 NDT testing instrumentation

Figure 6-2 presents an example of the NDT testing setup. The sensors used in these tests were nineteen piezoelectric accelerometers (PCB Piezotronics model 3055B3) with a nominal frequency of 35 kHz. Accelerometers or acceleration transducers are devices that convert vibratory motion into an electrical signal. For field applications, the accelerometers have to be attached to the element under study and the resonance frequency obtained for this condition is called mounted resonance frequency. This frequency is important because the upper frequency limit of an accelerometer is usually considered to be one-third of its mounted resonance frequency (Miller, 1973).

Two ultrasonic transducers with a nominal resonant frequency of 50 kHz were employed as the source and were located at 40 mm from the first accelerometer (indicated as A) and the last accelerometer (B). Two types of mounting of the source transducers were evaluated: manual pressure and using metallic frame (Figure 6-3). The manual pressure was only used for the first beam tested because it is the usual way of using an ultrasonic transducer as source. For the other beams the metallic frames were employed because they allowed maintaining a constant pressure, which is needed to ensure consistency of the tests.

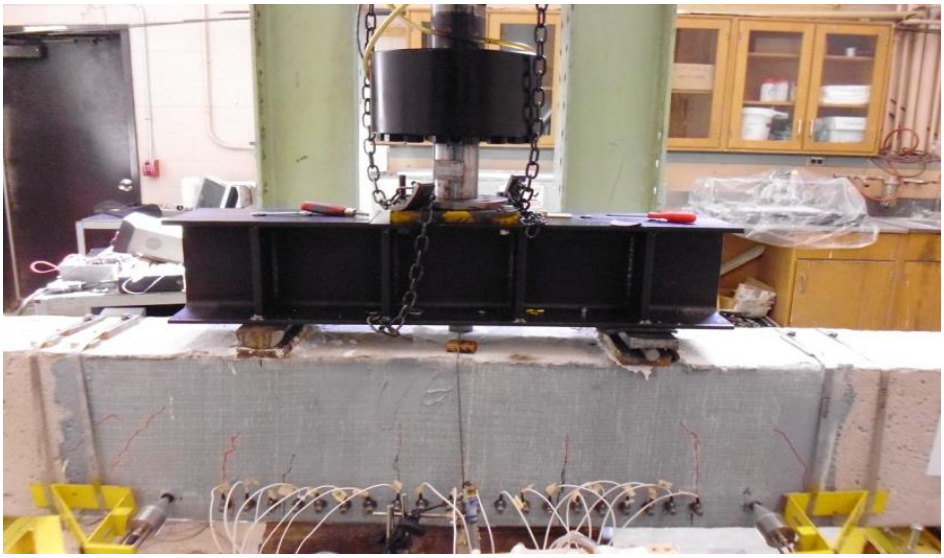

Figure 6-2: Setup for the surface wave analysis test of a reinforced concrete beam with GFRP reinforcement

Figure 6-3: Mounting of the source transducers (left: manually, right: rigid frame)

The excitation of the ultrasonic transducer (input signal) was a one-cycle sinusoidal pulse with a frequency of 50 kHz. The input signal and the accelerations were recorded with a data acquisition system of 24 channels and sampling frequency of 1.0 MHz (LDS Nicolet Genesis). The ultrasonic transducer was preferred as the source over a hammer because the frequencies generated are in a narrow band and there is better control and consistency in the waves induced.

Figure 6-4 shows the wave field generated by a point source as it could be idealized a piezoelectric transducer.

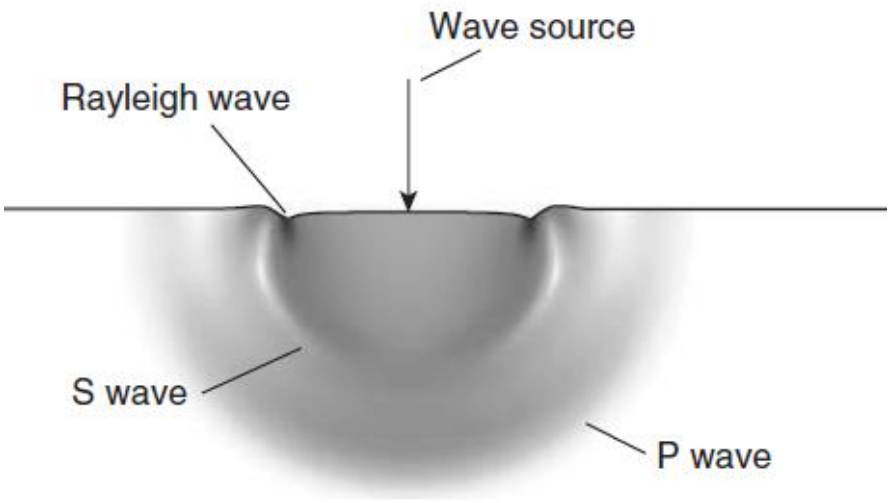

Figure 6-4: Waves generated by a wave source applied to a free surface (Popovics & Abraham, 2010)

To ensure the accuracy and repeatability of the measurements the mounting is essential, and for the accelerometers two types of systems were tested: adhesive and magnetic mounted. The accelerometers were mounted in studs that were screwed in metallic washers. The washers were adhered to the surface of the beams using epoxy resin (Figure 6-5) or magnets (Figure 6-6).

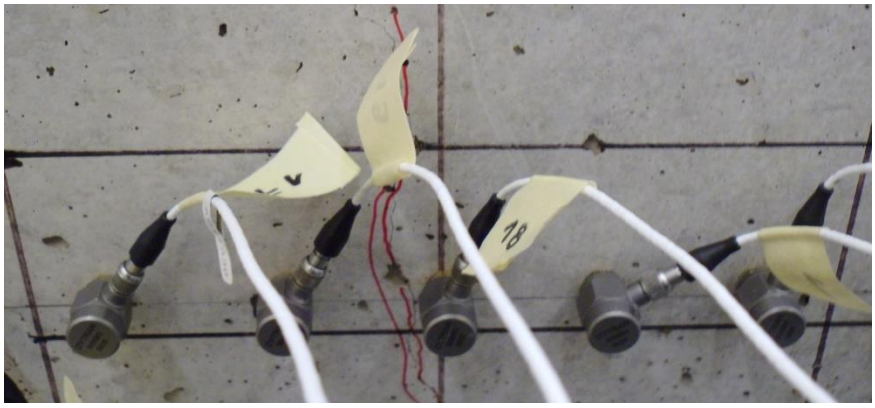

Figure 6-5: Accelerometers mounted with epoxy resin

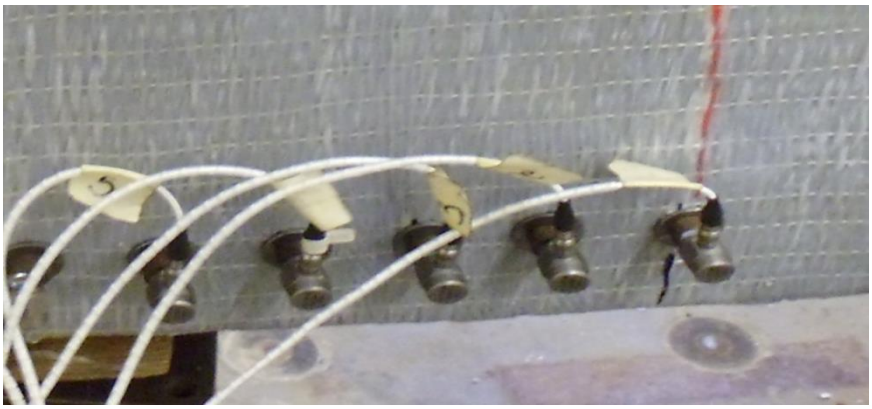

Figure 6-6: Magnetic mounting of the accelerometers

Initially it was used the adhesive system, but as several accelerometers were detached during the testing of the first beam, for the other beams it was used the magnetic mounting. In acoustic testing is common to employ magnetic clamps when drilling is not permitted, and most piezoelectric transducers are relatively insensitive to magnetic fields. The disadvantage of the magnetic clamp method is that the addition of element in series with the accelerometer may reduce the useful upper frequency (Miller, 1973).

6.2.4 Surface wave tests results

For the five beams studied, the testing procedure was similar. The base line condition was recorded before the fatigue load was applied to the beam. Then, the test was repeated at different stages of the loading cycle, stopping temporarily the cyclic loading to record the ultrasonic signals. Each record consisted of 30 signals (30 repetitions) for each accelometer and the measurements were done for two positions of the source.

Figure 6-7 is an example of the time signals recorded for one of the beams (beam B1 which is unwrapped) and Figure 6-8 presents the corresponding frequency spectra. In this case the spacing between the accelerometers was 40 mm and the results shown correspond to the baseline condition.

The surface wave test results can be analyzed both in the time and the frequency domain. In the time domain, a common way of analyzing the data is obtaining the surface wave velocity. For example, Figure 6-9 is the representation of the multiple time signals for equally spaced sensors. The arrival of the surface waves can be defined as the maximum that precedes a drop in signal value (Popovics & Abraham, 2010). Then, the slope of the line joining the peaks (largest amplitude) would give an approximation of the surface wave velocity.

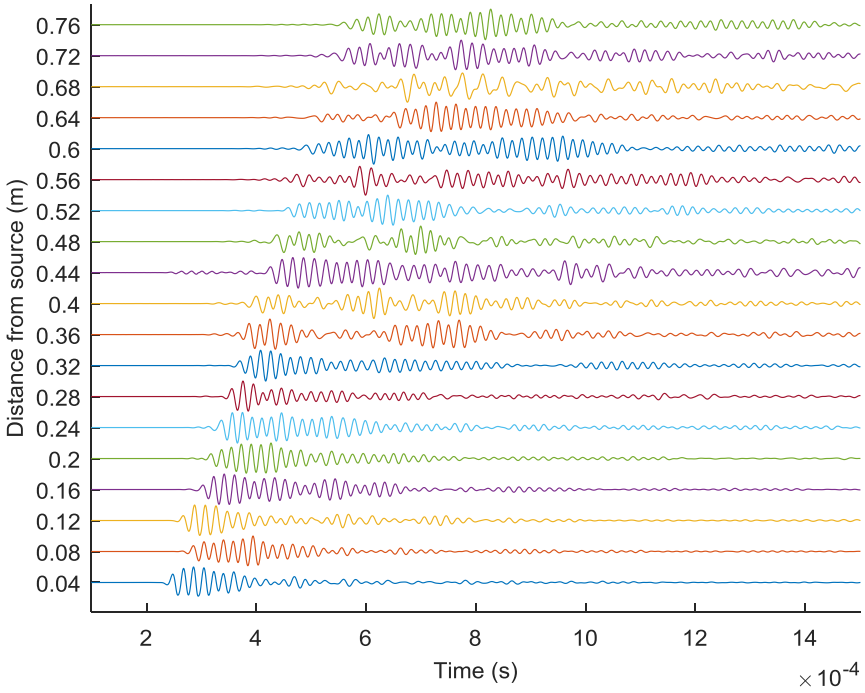

Figure 6-7: Example of the time signals recorded for the baseline condition (beam B1, source at A)

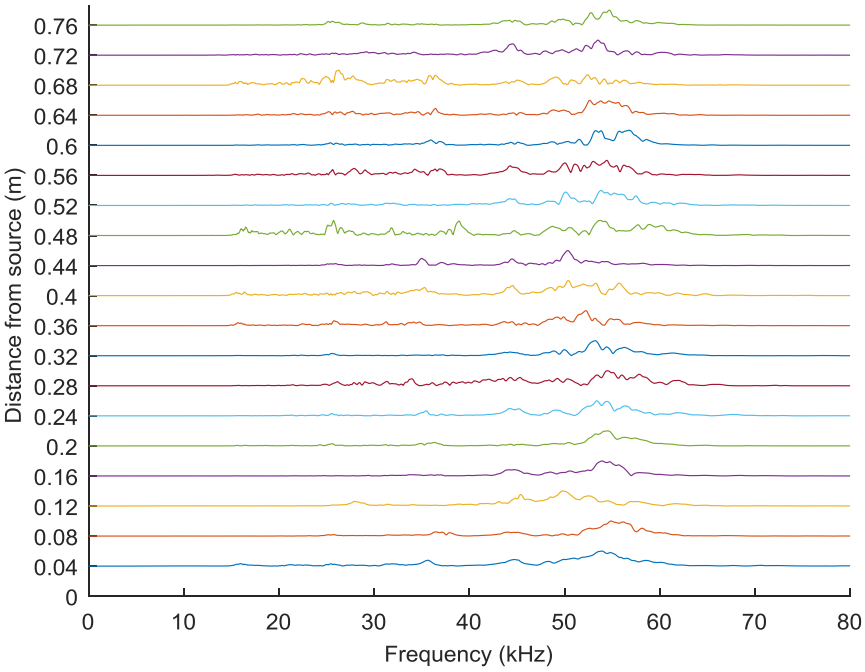

Figure 6-8: Frequency spectra of the time signals for the base line condition (beam B1, source at A)

Since in the surface wave tests the accelerometers are spaced a constant distance (Δx), the surface wave velocity (V_R) can be calculated as follows:

$$V_R = \frac{\Delta x}{\Delta_{t_R}} \tag{6-1}$$

where Δ_{t_R} is the difference in the arrival times of the different signals. Figure 6-9 is a graphical representation of the method. In this case, the time signals presented correspond to the baseline condition for the second beam tested (B2, source at A) which was also unwrapped.

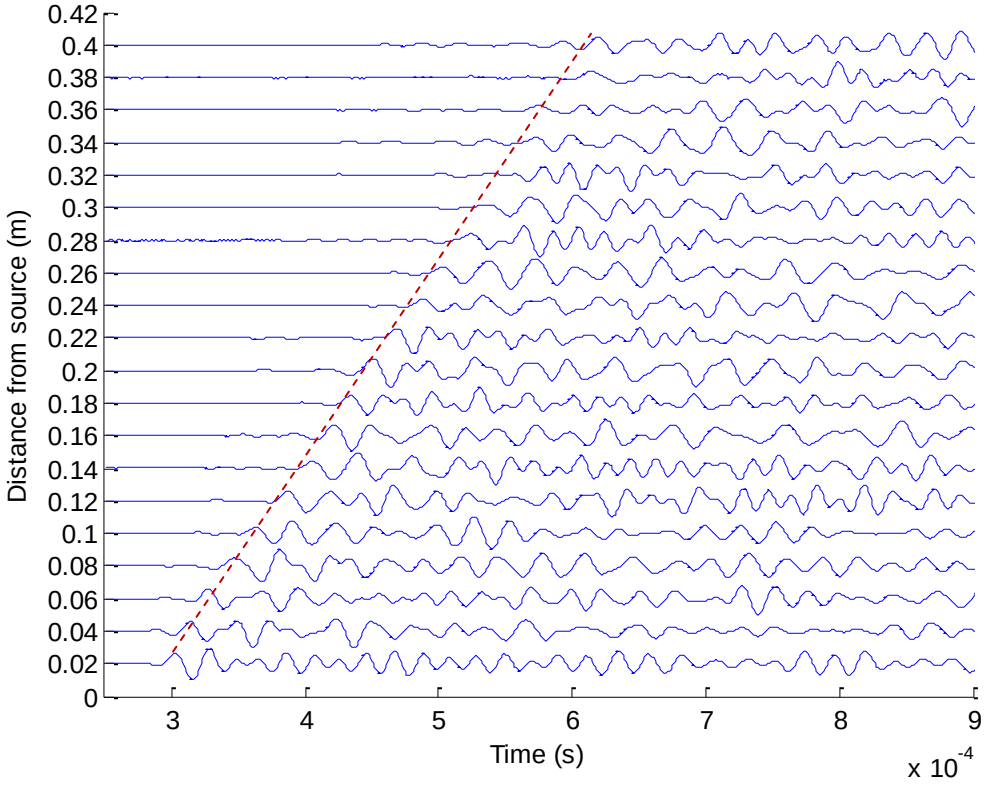

Figure 6-9: Example of the time signals for the initial condition (beam B2, source at A)

The previous procedure was not applicable for the later stages of the testing because after few cycles of fatigue loading there is no recognizable trend in the time signals (Figure 6-10). For all the beams tested, only for the baseline condition is possible to apply the aforementioned method, so it was considered that for the testing conditions the time domain analysis was not convenient.

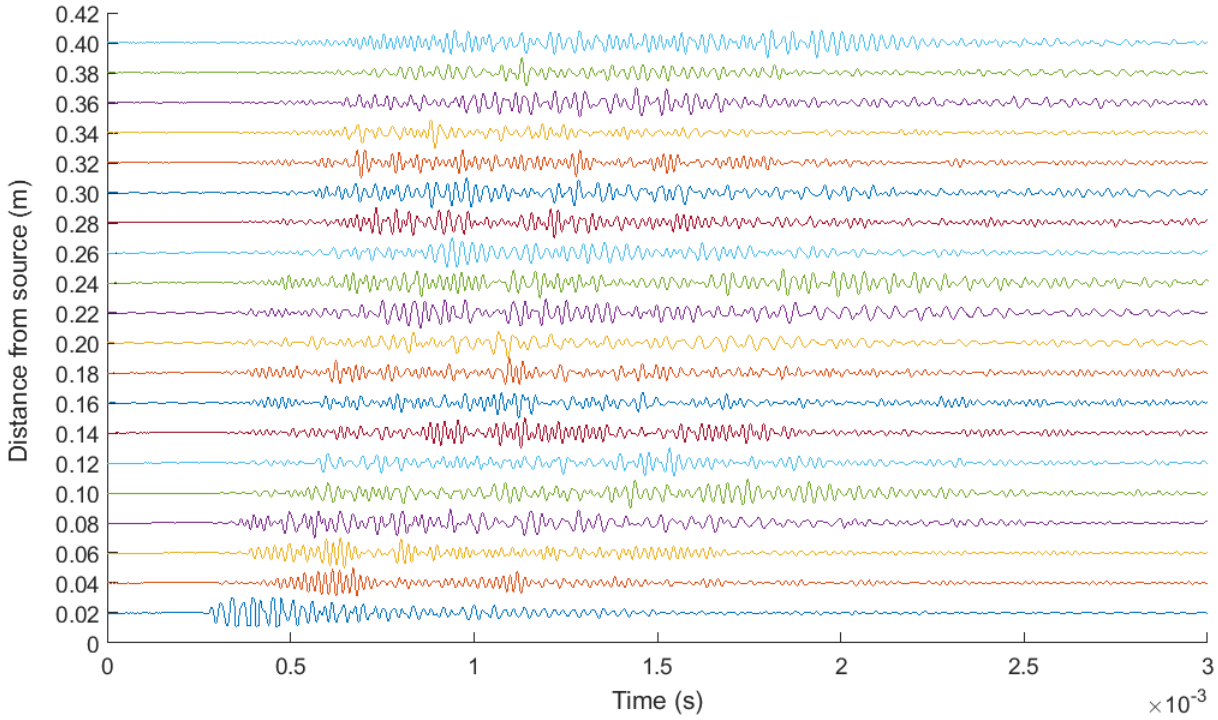

Figure 6-10: Time signals after 32000 fatigue cycles (beam B2)

Additionally, when the thickness of the layer is of the same order than the wavelength, the frequency domain methods are suitable (Popovics & Abraham, 2010). To determine the dominant wavelengths in the signals, windowing of the time signals was evaluated using a Tukey window defined as follows:

$$W(x) = \begin{cases} \frac{1}{2}\left\{1 + \cos\left(\frac{2\pi}{r}\left[x - \frac{r}{2}\right]\right)\right\}, & 0 \le x \le \frac{r}{2} \\ 1, & \frac{r}{2} \le x \le 1 - \frac{r}{2} \\ \frac{1}{2}\left\{1 + \cos\left(\frac{2\pi}{r}\left[x - 1 + \frac{r}{2}\right]\right)\right\}, & 1 - \frac{r}{2} \le x \le 1 \end{cases} \quad (6\text{-}2)$$

where r is the ratio of the cosine-tapered section length to the entire window length with $0 \le r \le 1$.

Two types of windowing were analyzed. First, a window with the same characteristics (same width, taper) but with a proportional starting point was applied to all the signals. Figure 6-11 shows an example of the application of a Tukey window to the signals measured in beam B2. The other type of windowing evaluated was the application of several windows to each individual signal. Figure 6-12 illustrates the consideration of different windows for a time signal

and Figure 6-13 presents the frequency spectra of the windowed signals. The dominant frequencies observed were 36 kHz and 53 kHz.

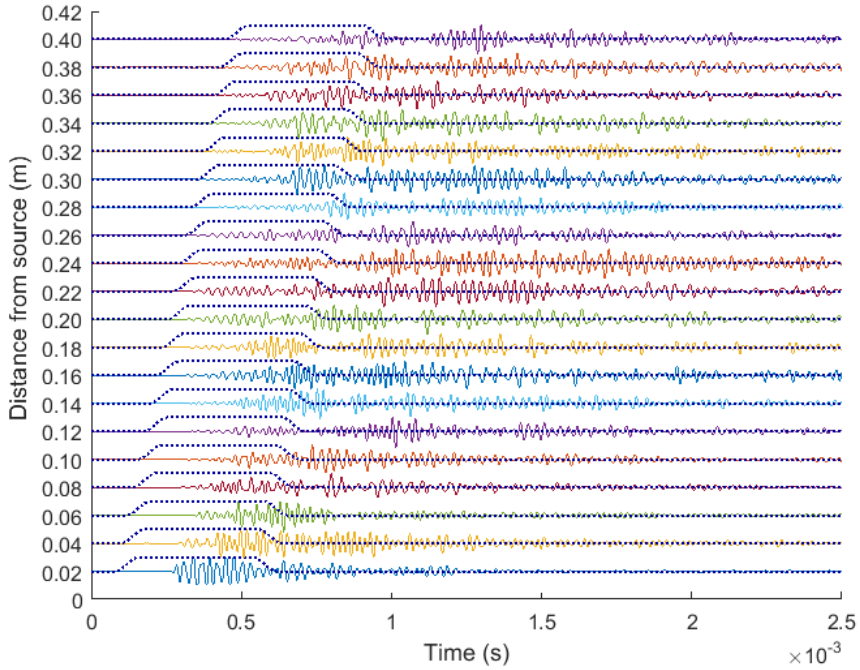

Figure 6-11: Example of the application of windowing in one of the records to determine the dominant frequencies

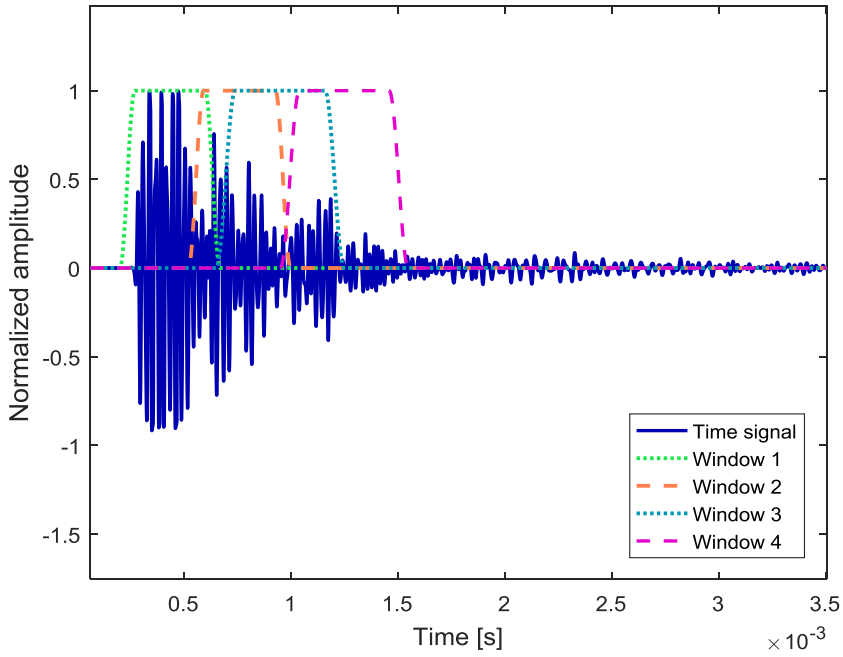

Figure 6-12: Example of the application of different windows in the time signals

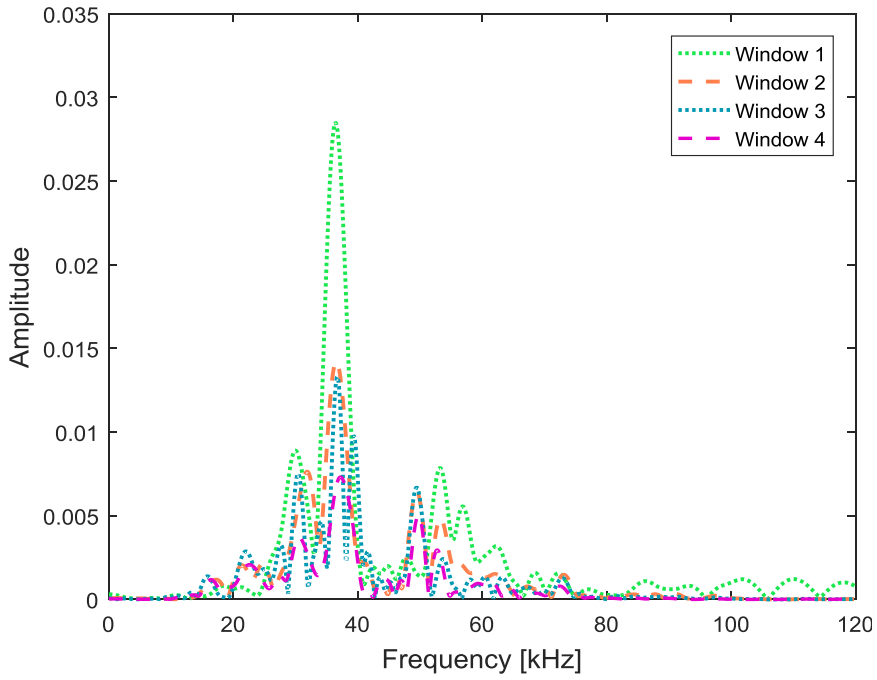

Figure 6-13: Example of the frequency spectra for the windowed signals

For the location of the accelerometers selected, the beams can be visualized as a layered media, where the first layer corresponds to the concrete cover; the second layer is the longitudinal reinforcement, and the third layer the core concrete. The surface wave propagation is generally limited to a wavelength, so in this case for a frequency of 53 kHz and a reference R-wave velocity of 2200 m/s, the effective depth is around 40 mm, which corresponds to the concrete cover. Therefore, the thickness of the layer evaluated is of the same order as the wavelength of the ultrasonic waves and the analysis in the frequency domain is preferable.

In the frequency domain, the usual representation of the surface wave test results is through the dispersion curves, where the phase velocity is presented as a function of the frequency. Phase velocities are calculated by determining the travel times for each frequency (or wavelength) component between the two receivers. Figure 6-14 illustrates the variation of the phase velocity in the frequency range from 40 kHz to 60 kHz for the first beam tested. For this case, the phase velocity presented a clear reduction as the number of fatigue cycles increased so the phase velocity was studied as a potential indicator of the progression of damage.

For all the beams tested, the phase velocity as a function of the frequency was determined. However, the phase velocity did not present a clear trend with the increasing number of fatigue

loading cycles. For this reason, the phase velocity was discarded as the parameter that would allow monitoring the progression of the fatigue damage.

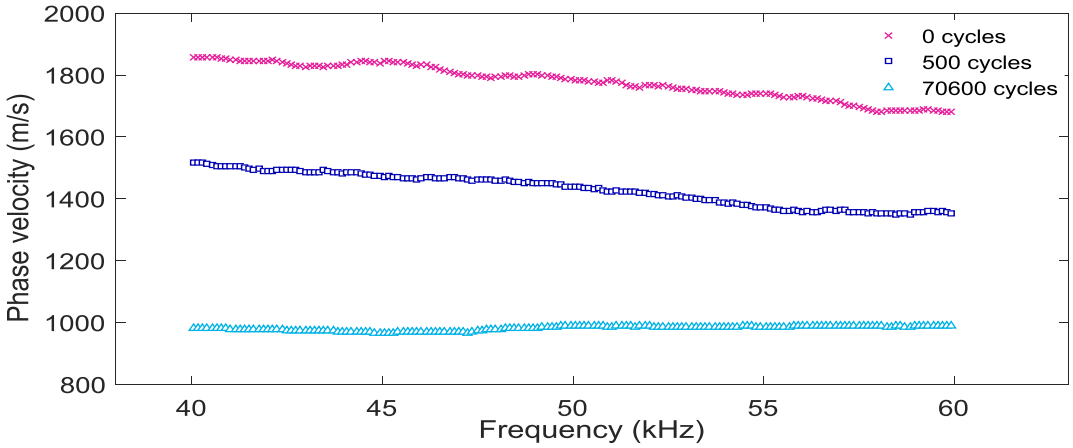

Figure 6-14: Dispersion curve for the phase velocity for beam B1

Even though the dispersion curves are the usual representation of surface waves tests, the computation of the dispersion curves could be a numerically intensive method and requires an experienced investigator (ACI 228.2R-13; Chai, Aggelis, Momoki, Kobayashi, & Shiotani, 2010). Since the purpose of using the surface wave method was to obtain an indirect indication of the progression of fatigue damage, a simpler procedure that could facilitate the interpretation of the data was necessary and three signal processing techniques were investigated.

6.2.5 Alternative processing procedure for the surface waves tests

The alternative methods studied were the Pearson correlation, the Power Spectral Correlation Index and the Coherence Spectrum, which are briefly described below. The three methods evaluated were based on the study by (Nuño Ayón, 2011). Dr. Nuño Ayón facilitated the algorithm (called MEICE in his work) to analyze the data and the references related to it.

For the three methods, the reference signal is indicated as $\mathbf{x}_i = [x_i(1) \quad \cdots \quad x_i(n) \quad \cdots \quad x_i(N)]$ and $\mathbf{x}_j = [x_j(1) \quad \cdots \quad x_j(n) \quad \cdots \quad x_j(N)]$ is the compared signal. For all signals, n is the n-th sample and N denotes the number of samples.

Pearson Correlation

The Pearson correlation is a time domain technique that gives a measure of the linear dependence of the signals, and the values are between -1 and +1. If the Pearson correlation is +1, the two signals are linearly related; and if it gives −1, the two signals have an inverse linear relationship. The correlation between two signals $\mathbf{x}_i = [x_i(1) \quad \cdots \quad x_i(n) \quad \cdots \quad x_i(N)]$ and $\mathbf{x}_j = [x_j(1) \quad \cdots \quad x_j(n) \quad \cdots \quad x_j(N)]$, is computed as follows:

$$\rho_{\mathbf{x}_i\mathbf{x}_j} = \frac{cov(\mathbf{x}_i\mathbf{x}_j)}{\sigma_{\mathbf{x}_i}\sigma_{\mathbf{x}_j}} = \frac{E\left[\left(\mathbf{x}_i - \mu_{\mathbf{x}_i}\right)\left(\mathbf{x}_j - \mu_{\mathbf{x}_j}\right)\right]}{\sigma_{\mathbf{x}_i}\sigma_{\mathbf{x}_j}} \tag{6-3}$$

where n is the n-th sample, N denotes the number of samples, $cov(\mathbf{x}_i\mathbf{x}_j)$ is the covariance between $\mathbf{x}_i$ and $\mathbf{x}_j$, $\sigma_{\mathbf{x}_i}$ and $\sigma_{\mathbf{x}_j}$ are the standard deviations of the signals, $\mu_{\mathbf{x}_i}$ and $\mu_{\mathbf{x}_j}$ the average of the signals and E[ ] stands for the expectation.

Power spectral correlation index

The Power spectra correlation index (PSCI) gives the correlation between the power spectra of two different time signals (measurements). This index provides a measure of the commonness of oscillatory frequencies, and takes a real value between 0 and 1. If two measurements have similar frequencies, then the PSCI value is close to unity. When the value of PSCI is close to zero the two time signals have different frequencies.

The PSCI computation is carried out in two steps. In the first step, the means of the time signals $\mathbf{x}_i$ and $\mathbf{x}_j$ are removed, and the Fast Fourier Transform (FFT) is applied to estimate their power spectra. In the second step, the power spectra are used to estimate PSCI:

$$\text{PSCI} = \frac{\sum_{f_k}|X_i(f_k)|^2\left|X_j(f_k)\right|^2}{\sqrt{\sum_{f_k}|X_i(f_k)|^4\left|X_j(f_k)\right|^4}} \tag{6-4}$$

where f_k denotes the *k-th* frequency, $X_i(f_k)$ is the power spectrum of the reference signal $\mathbf{x}_i$ and $X_j(f_k)$ represents the power spectra of the signal compared $\mathbf{x}_j$ (Tangirala, Shah, & Thornhill, 2005).

Coherence spectrum

In this research, the Welch algorithm was used to obtain the self- and cross-power spectral density estimation from the recorded measurements. Welch algorithm differs from the averaged periodogram in two ways. First, the data is windowed and secondly, data blocks are overlapped. The data window reduces spectral leakage and by overlapping blocks of data, typically by 50 or 75%, some extra variance reduction is achieved. Those relevant characteristics make it attractive to extract the spectral information and to identify the similar or different frequencies that onset during the oscillatory process.

The collected measurements can be described as follows:

$$\mathbf{x}_i = [x_i(1) \quad x_i(2) \quad \cdots \quad x_i(n) \quad \cdots \quad x_i(N)], \qquad i = 1,2,\dots,m \tag{6-5}$$

where $\mathbf{x}_i$ is the vector that represents the signals collected by the accelerometer, sampled at time $n = 1, 2, \dots, N$ and m is the number of measurements.

Each signal, $\mathbf{x}_i$ is divided in *K* segments with overlapping data D:

$$x_j^l(n) = x_j(n + lD) \tag{6-6}$$

where the intervals are:

$$0 \le l \le K - 1 \text{ and } 0 \le n \le N - 1 \tag{6-7}$$

The Welch estimator uses the Discrete Fourier Transform (DFT). However, the procedure of overlapping samples often provides better results than those obtained with the DFT. In practice, the overlap of signal segments is often chosen as 50%, i.e $D = N/2$, while the number K of the intervals is chosen as a compromise between spectral resolution and precision (Welch, 1967). The segments of the selected signals are multiplied by a window function $w(n)$ and their spectra are then estimated as:

$$\mathbf{P}_{\mathbf{x}_i\mathbf{x}_i}^l(f) = \frac{1}{E_w}\left|\sum_{n=0}^{N-1} x_i^l(n)x_i^l(n)w(n)e^{-j2\pi f_k n}\right|^2 \qquad \begin{matrix} k = 0, 1, \dots, N-1 \\ l = 0, 1, \dots, K-1 \end{matrix} \tag{6-8}$$

where $f_k = k/N$ denotes the *k-th* frequency. Here, E_w is defined by the following:

$$E_w = \sum_{n=0}^{N-1} w(n)^2 \tag{6-9}$$

in which $w(\mathrm{n})$ represents a window function. In this research, the Hanning function was selected for its accuracy and easy implementation and it is defined as:

$$w(n) = \frac{1}{2} - \frac{1}{2}\cos\left(\frac{2\pi n}{N}\right) \tag{6-10}$$

where $n = 0, 1, 2, \ldots, N-1$.

The averaged periodogram for the self-power spectral density is then estimated as follows:

$$\mathbf{P}_{\mathbf{x}_i\mathbf{x}_i}(f) = \frac{1}{K}\sum_{l=0}^{K-1} \mathbf{P}^{l}_{\mathbf{x}_i\mathbf{x}_i}(f) \tag{6-11}$$

Following the same procedure, the cross-power spectral density is estimated. Assume that $\mathbf{x}_j = \begin{bmatrix} x_j(1) & x_j(2) & \cdots & x_j(n) & \cdots & x_j(N) \end{bmatrix}$ represents the signal that contains the frequency of interest, which is correlated in the frequency domain with the spectral decomposition of $\mathbf{x}_i$ as follows:

$$\mathbf{P}_{\mathbf{x}_i\mathbf{x}_j}(f) = \frac{1}{K}\sum_{l=0}^{K-1} \mathbf{P}^{l}_{\mathbf{x}_i\mathbf{x}_j}(f) \tag{6-12}$$

where $\mathbf{P}_{\mathbf{x}_i\mathbf{x}_j}(f)$ is a vector that contains complex values for every frequency f_k. From the self- and cross-power spectral densities, the magnitude of the spectral coherence $\mathbf{C}_{\mathbf{x}_i\mathbf{x}_j}(f)$ can be computed from (6-13) and the phase $\boldsymbol{\varphi}_{\mathbf{x}_i\mathbf{x}_j}(f)$ from (6-14) :

$$\mathbf{C}_{\mathbf{x}_i\mathbf{x}_j}(f) = \frac{\left|\mathbf{P}_{\mathbf{x}_i\mathbf{x}_j}(f)\right|^2}{\mathbf{P}_{\mathbf{x}_i\mathbf{x}_i}(f)\mathbf{P}_{\mathbf{x}_j\mathbf{x}_j}(f)} \tag{6-13}$$

$$\boldsymbol{\varphi}_{\mathbf{x}_i\mathbf{x}_j}(f) = \tan^{-1}\left(\frac{\mathrm{Im}\left(\mathbf{P}_{\mathbf{x}_i\mathbf{x}_j}(f)\right)}{\mathrm{Re}\left(\mathbf{P}_{\mathbf{x}_i\mathbf{x}_j}(f)\right)}\right) \tag{6-14}$$

The magnitude of the coherence is a real value between 0 and 1 that represents how two signals are linearly correlated in the frequency. In the range of 0.8 to 1, both signals show significant

similarity, meanwhile, a rate in the range from 0 to 0.79 indicates no similarity on their behavior (Zang, Halliday, Jiang, Liu, & Feng, 2006; Lesniak, A. & Nitsuma, H., 1998). The phase coherence is usually interpreted as a phase lead of one signal over the other and it can range between -180° ($-\pi$) to 180° (π) for every frequency.

In practice, this coherence has been used to evaluate the linear association between two stationary time series in the long-term and for all spectra. The coherence spectrum is a function of frequency, which is an advantage compared with the PSCI value. Therefore, it allows detecting oscillatory behaviours and identifying similar frequencies of a set of measurements.

Figure 6-15 is a schematic representation of the coherence spectrum method.

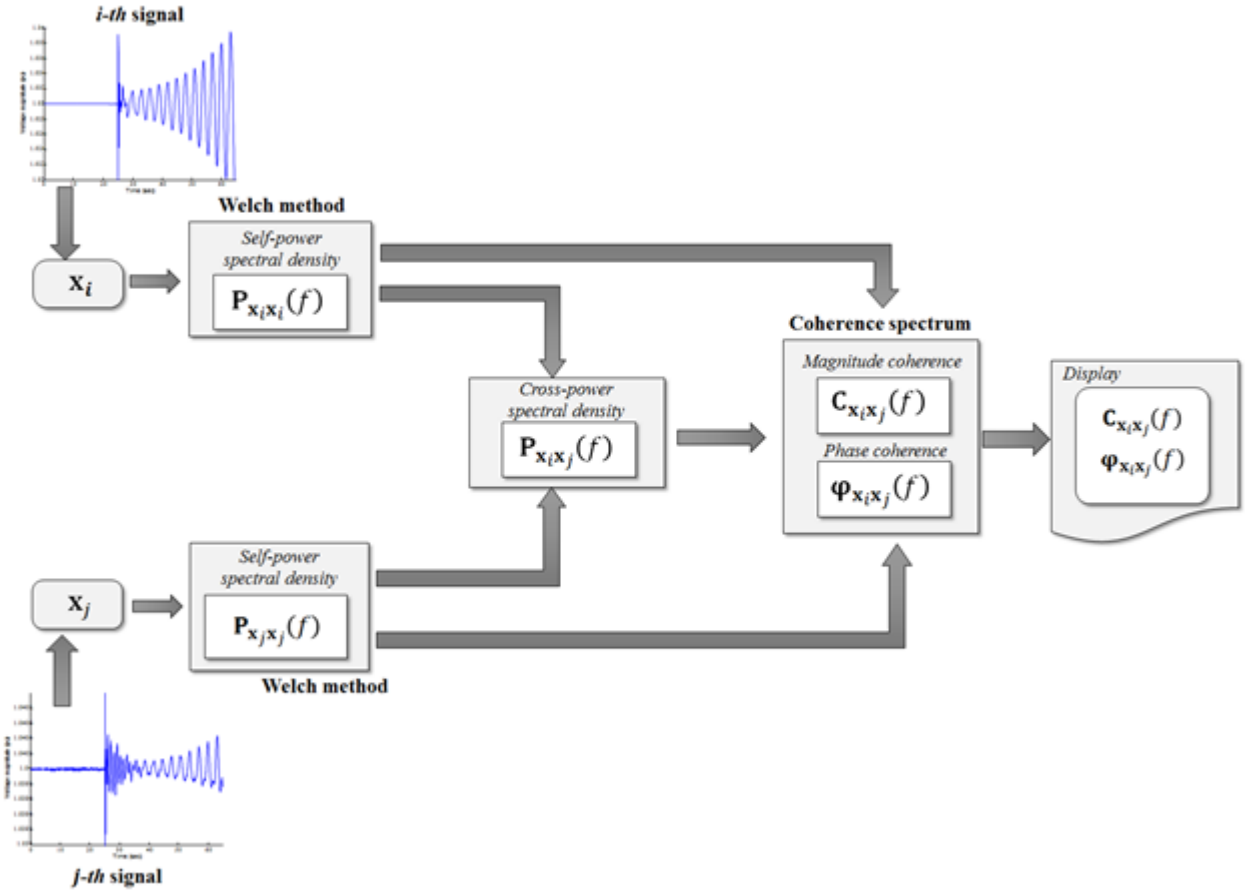

Figure 6-15: Coherence spectrum method (figure by Jesús Nuño)

Given that in this study the purpose was to obtain an indicator of the imminence of failure under fatigue loading, the comparison is done between the signals recorded in each accelerometer and not between neighbouring accelerometers. If the signals are from the same accelerometer, the changes in the signals could be an indication of a change in the condition of the element because the measurements are taken a fixed point. Therefore, all the recorded signals at an accelerometer were compared using the three correlation procedures and some examples of possible applications of the methods are presented below.

Figure 6-16 presents the Pearson correlation results computed for all the thirty-nine measurements (different number of fatigue cycles, from 100 to 156500 cycles) for beam B3 at the accelerometer closer to the source. The representation used facilitates identifying that there is a good correlation in the time domain (above 0.7) between the measurements up to the 24th measurement and that after the 30th until 39th measurement the correlation is below 0.4, which indicates little correlation. The last three measurements have no correlation and indicate the failure of the element.

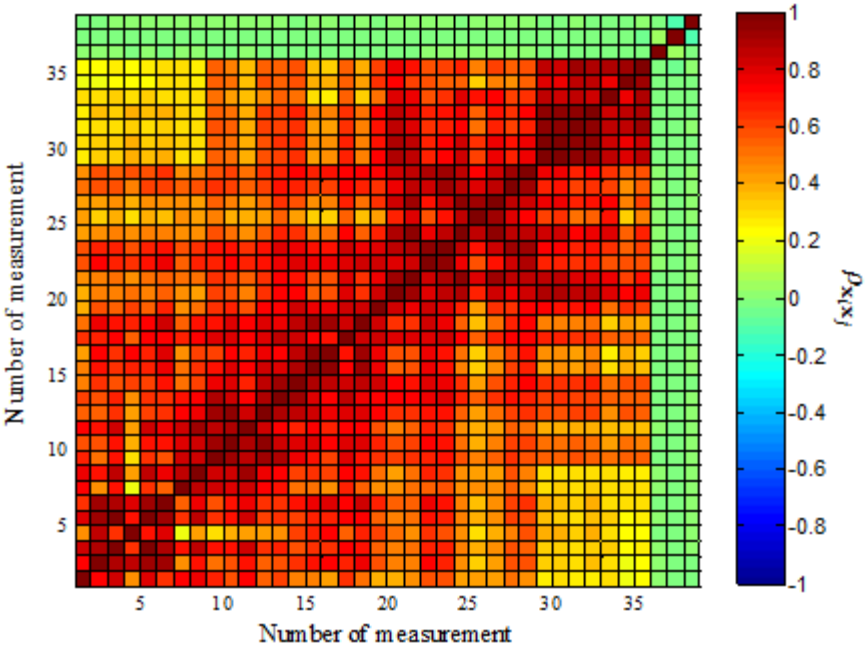

Figure 6-16: Pearson correlation for accelerometer 1 (beam B3)

Another potential application of the Pearson correlation results is illustrated in Figure 6-17 In this case, the plot indicates there is no correlation between none of the signals which may be due to inadequate mounting of the accelerometer and these measurements are discarded. Thus, the results of the Pearson correlation could be considered to categorize the recorded signals.

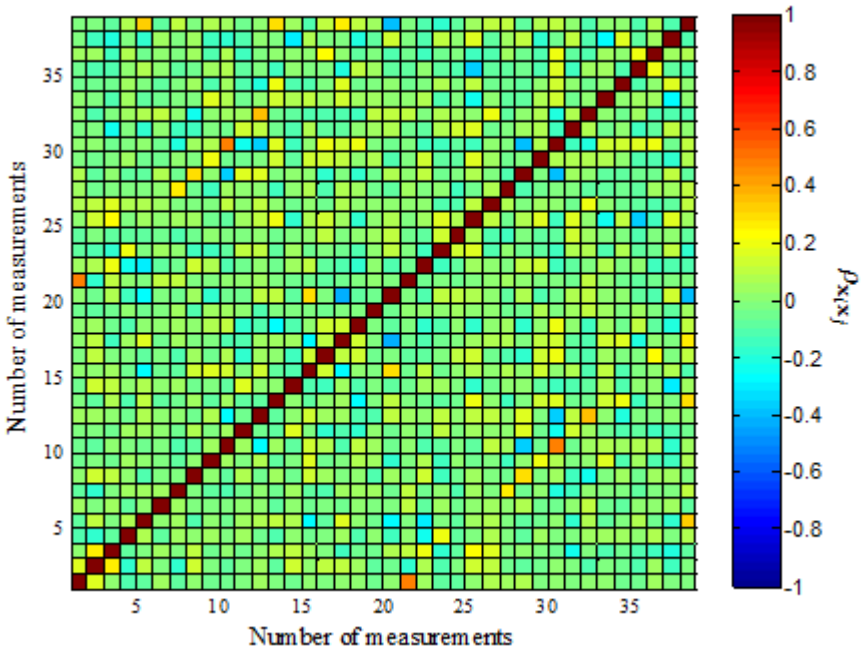

Figure 6-17: Pearson correlation for the accelerometer 19 (beam B3)

The results presented in Figure 6-18 for the spectral correlation correspond to the same set of measurements shown in Figure 6-16. Both figures indicate that the last three measurements are no correlated with the base line condition. It may also be observed that the correlation in the frequency domain is close to one up to the 19th measurement. It is observed that the correlation is above 0.7 from the 20th until the 24th measurement, which highlights that for the type of vibratory phenomenon under study (ultrasonic waves induced by the transducer in the beam) the frequency correlation is valid in a longer range. Therefore, is better suited to monitor the changes in the beam than the Pearson correlation. Also, the figure may be employed to identify stages in the testing. For example, the results that indicate a change for the spectral correlation are stages where there is a change in the condition of the beam. In Figure 6-18 for example, the changes in the correlation in 19, 24 and 29 draw attention to these measurements. As each measurement corresponds to a specific number of fatigue cycles, it is possible to relate the change in the condition with the number of fatigue cycles.

Figure 6-19 shows an example of the coherence spectrum results obtained for the accelerometer closer to the source for the same set of measurements. In addition to confirm the stages identified by the power spectral correlation, the coherence spectrum displays the information about the specific frequencies. For this analysis the reference signal selected corresponds to 100 fatigue loading cycles. The coherence representation allows also recognizing the frequencies that are significant. For example, the measurements from the 1st until 19th and 22th until 24th show a coherence magnitude close to 0.8 for the frequency of 40 kHz (approximately). This value indicates that these measurements have very similar oscillatory components. Finally, the analyzed data have frequencies with higher coherence magnitude, which are between 35 kHz and 70 kHz. On the other hand, the last three measurements have a coherence magnitude equal to zero for all frequencies. Therefore, these time signals have different oscillatory behaviours, which may be associated a strong damage in the study beam and are consistent with the results from Pearson correlation and PSCI.

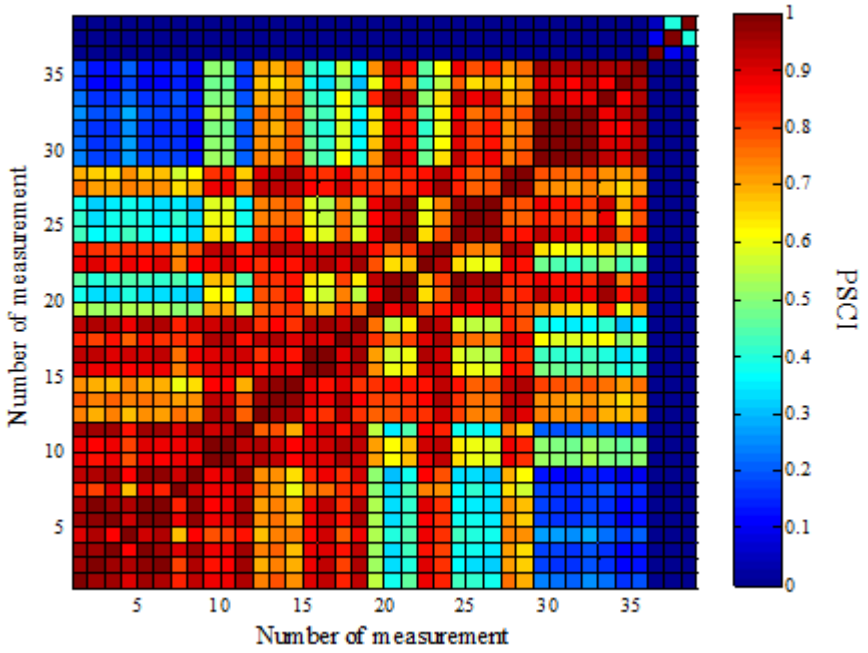

Figure 6-18: Power spectral correlation (accelerometer 1, beam B3)

Taking into consideration the relation between the wavelength, the velocity and the frequency it follows that for a given wavelength, the vanishing of a specific frequency would be related to a change in the velocity:

$$V = \lambda \cdot f \tag{6-15}$$

If the testing conditions are the same, this change in velocity may be related with the alteration in the specimen. In the testing procedure under study, the frequencies around 50 kHz are related with the ultrasonic waves produced by the source transducer. Therefore, the monitoring of these frequencies and the changes observed suggest changes in the medium. The medium in this case is a layered system of concrete and steel. The propagation of the waves initially is through a composite medium and the resulting velocity includes the propagation through the concrete and steel. The beams tested failed because of debonding of the reinforcing bars, which is a sudden change in the medium. When the debonding occurs, the waves are propagating only through concrete, because the low acoustic impedance in air would produce the complete reflection of the ultrasonic waves. To verify the previous statement it would be needed additional experimentation with materials of known properties or numerical simulations.

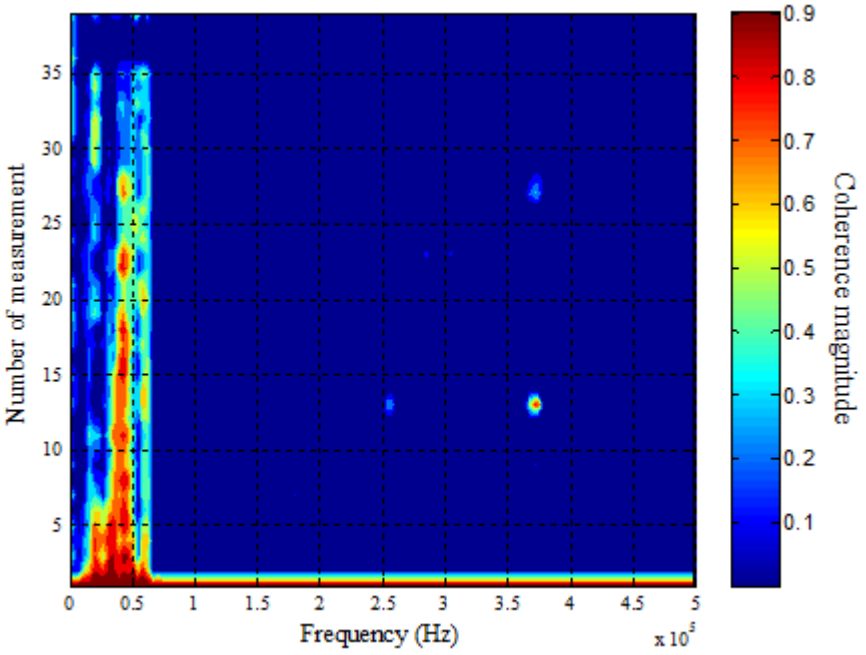

Figure 6-19: Example of coherence spectrum (accelerometer 1, beam B3)

As an example of the possible use of tracking specific frequencies to monitor the condition of the structural elements, Figure 6-20 includes the results for 40 kHz, 50 kHz and 60 kHz for two of the beams tested.

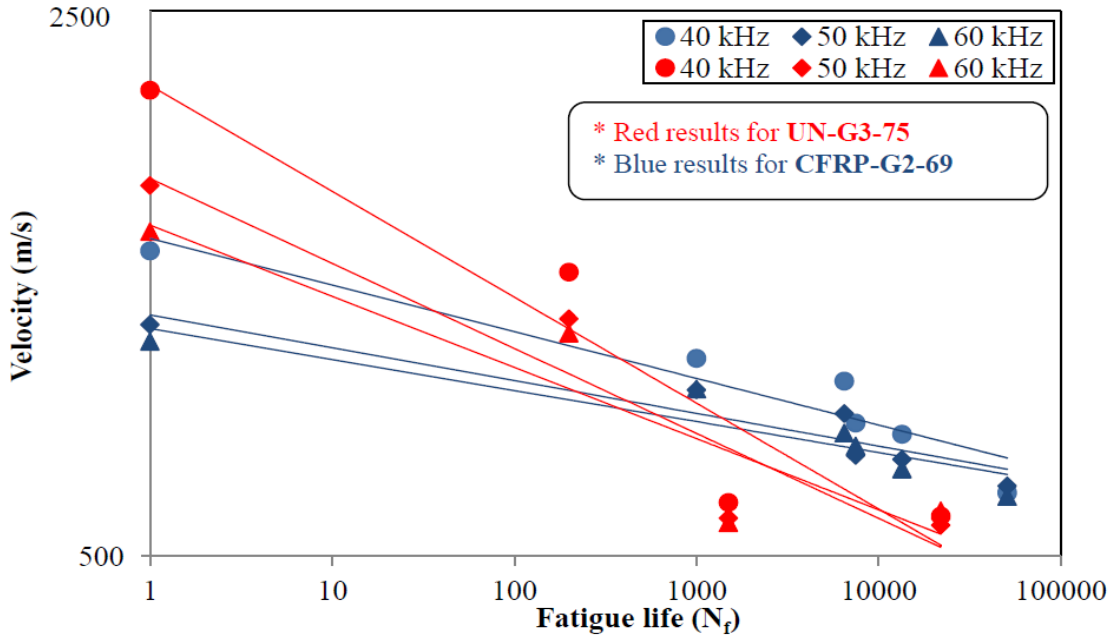

Figure 6-20: Variation of the velocity determined from the surface wave testing and the number of cycles of fatigue loading (Alyousef, 2016)

Figure 6-20 evidences the reduction of the velocity for an increasing number of fatigue cycles. In this example the blue markers correspond to a beam that was retrofitted with carbon fibres sheets (CFRP) and the red markers relate to a beam that was not retrofitted. The steeper slope observed for the unwrapped beam relates with more abrupt changes in the specimen and lower fatigue resistance. The results for the beam with CFRP sheets demonstrate the suitability of the retrofit to increase the fatigue life of the beams with the fatigue prone details studied.

6.3 Summary

In this chapter were presented the results of a study where the surface wave testing was employed to monitor the progression of fatigue damage in reinforced concrete beams. The testing of five beams allowed evaluating different setups; assessing two types of mounting of the sensors and the ultrasonic source, and studying alternative processing procedures of the data.

From the setups evaluated it was found that for the consistency of the tests it is necessary to maintain a constant pressure on the source transducers. It is suggested to use a clamp or similar

device to attach the transducer that is working as source. It was verified that the compression transducers work adequately as source, and that the vacuum grease is an adequate couplant for unwrapped beams but not for the beams that were retrofitted with FRP sheets.

To mount the accelerometers the adhesive and the magnetic mounting were evaluated. The use of epoxy to place the accelerometers is unfavourable because damages the surface of the elements and some of the accelerometers fell off during the fatigue loading test. The magnetic coupling ensures an uninterrupted mounting. However, for the application of the surface waves testing in the field, it would be convenient to build an array with the accelerometers to facilitate the installation. Another option is to utilize different sensors, for example air-coupled sensors. Air-coupled sensors may be an adequate solution because they do not require contact with the element tested so they allow faster scanning and are adequate for NDT methods using surface waves (Popovics & Abraham, 2010).

For the beams evaluated, the layer thickness was of the same order of the wavelength of the propagating wave from the source. Therefore, the frequency domain methods provided better results than the time domain ones. The typical way of presenting the results of the surface wave test in the frequency domain is through the dispersion curves of phase velocity as a function of frequency. Initially it was considered the variation of the phase velocity as a potential indicator of the progression of damage. Nevertheless, it was not possible to identify a clear behaviour of the phase velocity as a function of the number of cycles of fatigue loading. Hence, three alternative methods to compare the signals were evaluated: Pearson correlation of the time signals, Power spectral correlation and Coherence spectrum. From the methods studied, the Coherence spectrum is the one that provides more information and additional investigation (experimental and numerical) is recommended.

Chapter 7 Field testing results

7.1 Introduction

The main objective of the research project was to construct a field testing tool for the assessment of concrete columns. This chapter describes the testing of several in-service concrete columns of different characteristics (diameter, compressive strength, reinforcement) using the UTPole system. The experiments were done with the following purposes:

a. To verify that the UTPole system (initially developed for testing wood poles) can be used to test in-service concrete columns;

b. To corroborate the efficacy of the proposed coupling or the method used to secure the sensors to the column;

c. To explore the effect of different properties of the concrete elements (vertical and transverse reinforcement, diameter) on the results obtained with the testing device; and,

d. To evaluate the practicality of the system to test reinforced concrete columns with a circular cross section.

Section 7.2 summarizes the verification of the UTPole system in the laboratory using a mortar sample of known characteristics. Section 7.3 presents the results of the evaluation of a sample of in-service columns using the field testing device. The results of the evaluation of a column with honeycombing are summarized in 7.4, and the results of the evaluation of a damaged column are included in section 7.5. Finally, section 7.6 is the summary of the main findings of the field testing.

7.2 Testing of a mortar sample with UTPole system

The verification of the functioning of the system and the proposed coupling was done by testing a cylindrical mortar sample (Figure 7-1). This specimen can be used as verification because the properties of the sample are known (

Table 7-1). The mortar cylinder was constructed by Simon Berubé as part of his Master thesis (Berubé, 2008) and the values for the parameters were verified by numerical simulations. The selection of the sample of mortar instead of a sample of other material was based on the consideration that the properties of mortar are closer to those of concrete.

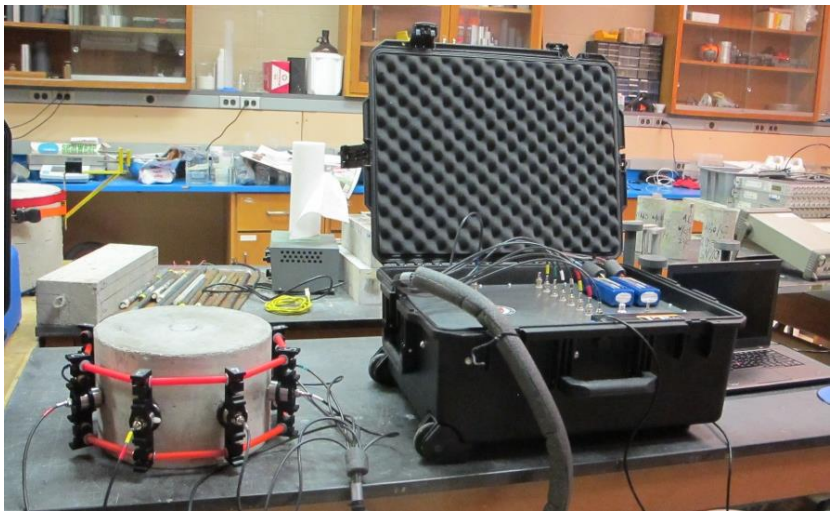

Figure 7-1: Setup for the verification of the equipment and testing of the coupling system proposed

Table 7-1: Properties of the mortar sample tested in the laboratory

Parameter	Value
Density	2102 kg/m^3
Modulus of elasticity	29.6 GPa
Poisson's ration	0.33
Diameter	0.29 m

The evaluation of the proposed coupling was done by comparing the velocity and the attenuation measurements using the typical coupling employed in the laboratory tests (vacuum grease) and the results when duct tape and vacuum grease were used (coupling proposed for the field testing, as explained in Chapter 4). The first case is called M1 (only vacuum grease) and the second case M2 (duct tape plus vacuum grease).

A first evaluation performed consisted in the comparison of the velocity and attenuation profiles obtained from the UTPole software. The velocity and attenuation profiles are the plots corresponding to the values of velocity and attenuation computed by the software for each ray path. The first letter indicates the position of the transmitter, and the second letter identifies the receiver (

Figure **7-2**).

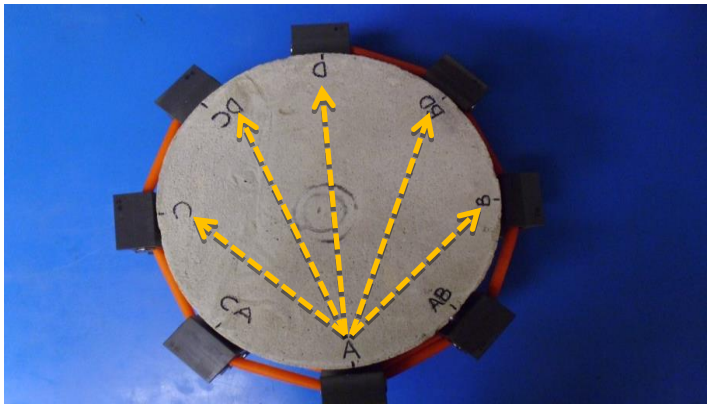

Figure 7-2: Nomenclature used for the ray paths

As an example, Figure 7-3 shows the velocity profile for the case M1 (only vacuum grease) and Figure 7-4 for case M2 (duct tape and vacuum grease). The representation of the profiles allows the comparison of the general trend of the measurements. The figures demonstrate that the velocity profiles present the same pattern and the same behaviour was observed for the attenuation. Also from the velocity and attenuation profiles it is possible to read the values for each ray path, and that is how the values for each case were obtained.

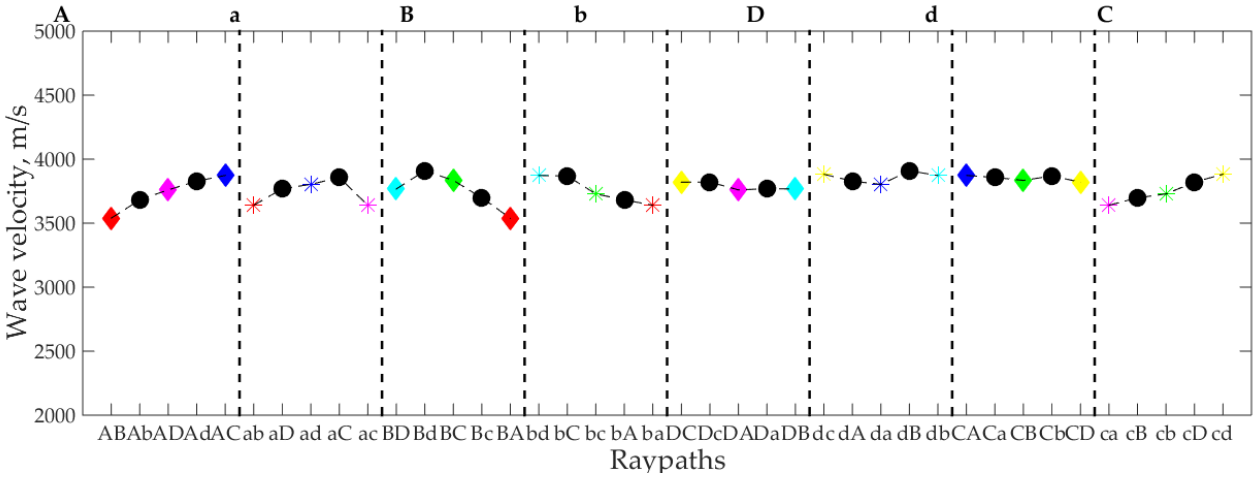

Figure 7-3: Velocities computed for each ray path for case M1(UTPole results)

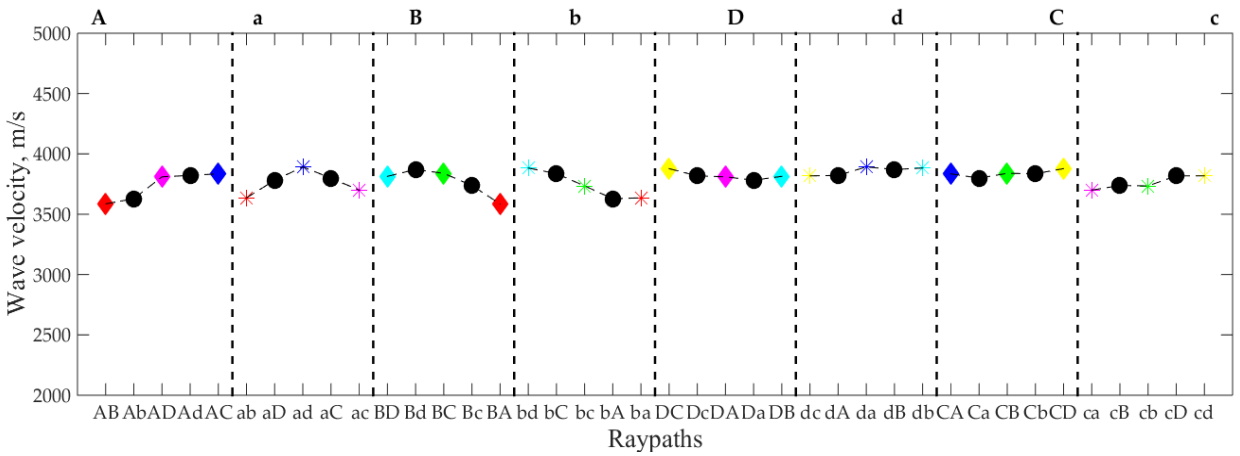

Figure 7-4: Velocities computed for each ray path for M2 (UTPole results)

Hereafter, the results are presented and analyzed grouped according to the relative position of the receiver with respect to the transmitter (angle of 180°, 135° or 90°) because, as indicated in Chapter 3 (Methodology), it was observed that the results for the attenuation present dissimilar characteristics depending on the angle. The average value, the standard deviation and the coefficient of variation are also included for the complete cross section to demonstrate the difference between the values when the section is considered as a whole, or by the relative angles. This difference is more noticeable for the attenuation than for the velocity, especially in terms of the coefficient of variation.

Table 7-2 summarizes the results of the velocity and the attenuation for case M1 and Table 7-3 for M2.

Table 7-2: Summary of the results for the case M1

Receivers	**All receivers**			**Receivers at 180**			**Receivers at 135**			**Receivers at 90**		
Parameter	μ_{all}	σ_{all}	COV_{all}	μ_{180}	σ_{180}	COV_{180}	μ_{135}	σ_{135}	COV_{135}	μ_{90}	σ_{90}	COV_{90}
Vp (m/s)	3780	96	2.54%	3781	40	1.07%	3804	76	2.00%	3754	123	3.28%
α (Np/cm)	0.366	0.065	17.89%	0.292	0.011	3.74%	0.325	0.006	1.91%	0.443	0.015	3.42%

Table 7-3: Summary of the results for the case M2

Receivers	All receivers			Receivers at 180			Receivers at 135			Receivers at 90		
Parameter	μ_{all}	σ_{all}	COV_{all}	μ_{180}	σ_{180}	COV_{180}	μ_{135}	σ_{135}	COV_{135}	μ_{90}	σ_{90}	COV_{90}
Vp (m/s)	3786	86	2.28%	3819	57	1.49%	3787	70	1.85%	3769	106	2.81%
α (Np/cm)	0.355	0.067	18.72%	0.287	0.020	7.13%	0.313	0.019	6.08%	0.432	0.023	5.25%

In both cases, the velocity presents a coefficient of variation below 4% for all angles, and the highest dispersion corresponds to the receivers at 90°.

For the attenuation, if the values are considered for the complete section, the COV is closer to 20%. However, if the averages are computed for the relative positions the COV is below 10%. As expected, there is a difference in the numerical values calculated.

Hypothesis test for the difference of the means

A difference of means hypothesis test is used to evaluate if the difference between the values is significant.

Null hypothesis $H_o: \mu_1 - \mu_2 = 0$

The null hypothesis is that there is no significant difference between the average for the whole section if the coupling system is only vacuum grease (μ_1) and the average when the proposed coupling system (duct tape and vacuum grease) is used (μ_2).

Alternative hypothesis $H_1: \mu_1 - \mu_2 > 0$

The alternative hypothesis is that there is a significant difference between the means. The significance level was chosen as 5%, because the common significance level for the comparison of the means is either 5% or 1% (Neville & Kennedy, 1966).

Table 7-4 summarizes the parameters of the hypothesis tests. In the table, μ_1 stands for the average values considering all measurements for case M1 (only vacuum grease); μ_2 represents the average for case M2 (using duct tape and vacuum grease); s_1 is the standard deviation for M1; s_2 corresponds to the standard deviation for M2; n_1 and n_2 represents the number of measurements; ν stands for the degrees of freedom; t_e is the test statistic (3-11); s_d is the standard deviation of the difference of the means (3-12); $t_{v,0.05}$ represents the critic value to compare,

which corresponds to the t-distribution value for the specific number of degrees of freedom and the level of significance of 5% (one-sided test). Finally, s_c is the combined variance of the difference computed from (3-13), because this is the method to obtain a combined variance (Neville & Kennedy, 1966) for the mean difference.

Table 7-4: Hypothesis test for the comparison of the coupling systems

Parameter	μ_2	μ_1	s_1	s_2	n_1	n_2	ν	s_d	t		$t_{38,0.05}$	Result
Velocity	3786	3780	86	96	20	20	38	28.8	0.23	<	2.02	Accept null
Attenuation	0.355	0.366	0.067	0.065	20	20	38	0.021	-0.50	<	2.02	Accept null

For both parameters, velocity and attenuation, there is not statistical evidence to reject the null hypothesis. Therefore, the null hypothesis is accepted, which means that the velocity and attenuation results for case M2 are not significantly different than those for case M1. This is considered as the demonstration that the coupling system proposed is adequate as the use of vacuum grease, but in addition has the advantage that does not stain the elements tested.

7.3 Evaluation of in-service columns

The details of each column tested are included in Appendix A. A total of 280 measurements were taken and included columns with three different diameters (0.60 m, 0.45 m and 0.35 m), four different percentages of longitudinal reinforcement (1.0%, 2.1%, 1.2% and 2.4%), two specified compressive strengths (45 MPa and 21 MPa) and two types of transverse reinforcement (ties spaced at 300 mm and spiral reinforcement with 44 mm and 64 mm pitch). Since it was the first time that the equipment was employed to test reinforced concrete columns, the aim was to cover columns of different characteristics to ascertain the effect of the different properties in the measurements of velocity, attenuation and the correlation between the signals.

7.3.1 Time signals recorded

The field data recorded are the time signals corresponding to the input signal sent to the transmitter, and the responses recorded by the receivers. Figure 7-5 is presented as an example of the time signals records obtained from UTPole software. A complete test consists of eight experiments, because each transducer is used as a transmitter once. Meanwhile, the other transducers are acting as receivers.

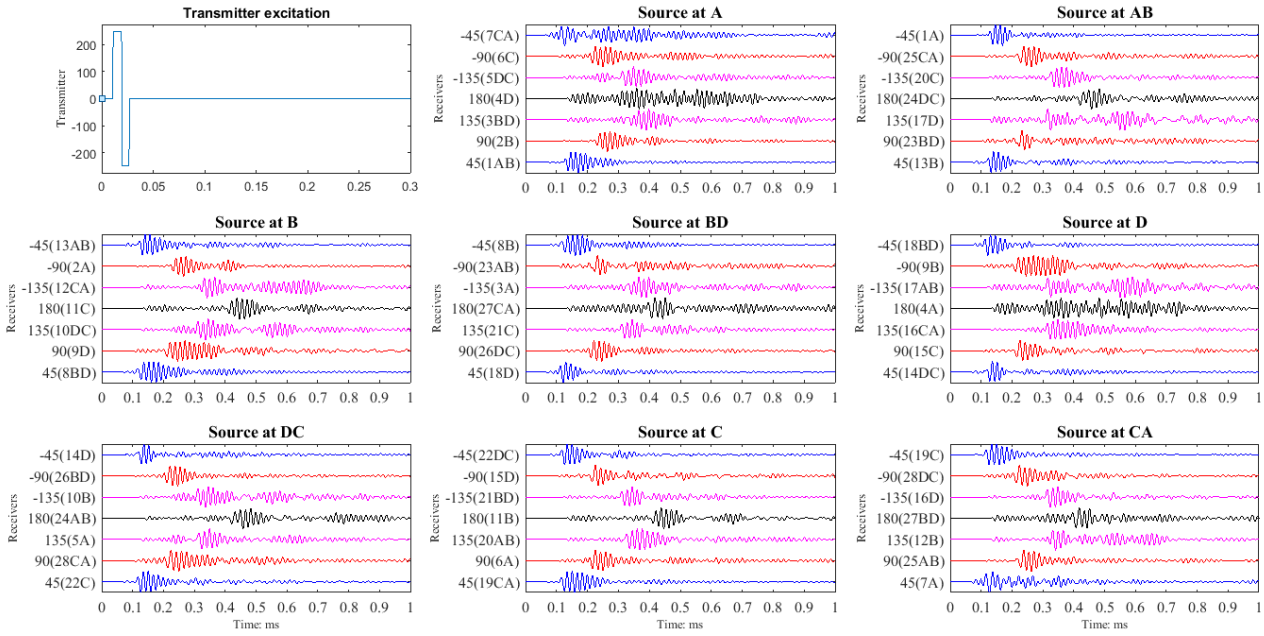

Figure 7-5: Example of the time signals results from UTPole software

The main results computed from the time signals are: the first arrival of the P-waves and the correlation between the pair of transducers. As each transducer acts as transmitter and receiver, there are two measurements involving the same two transducers. If the propagation of the wave occurs in a homogenous and sound material, it is expected that the two signals would have good correlation. Conversely, a value for the correlation below 0.5 (fixed by the software) indicates that there may be some kind of damaged area in that ray path, and it is considered as an indicator of potential damage.

7.3.2 Correlation results

To illustrate how the correlation for the signals could be considered as a first indicator of damage, Figure 7-6 shows the correlation plot for a sound column and Figure 7-7 for a column that is known to be damage.

For the column in good condition, the correlation between the signals is above 0.8 for most cases (except two).

For the damaged column on the other hand, 10 of the ray paths present a correlation below 0.8 and the software indicates that 7% of the values are below 0.5. The lower values of the correlation draw attention to certain ray paths, and in this case, the low values of correlation are

due to the existence of cracks in the vicinity of the transducers. Therefore, it is considered that the results of the correlation of the signals could be considered as an indicator of areas that may require special attention. As these results are obtained immediately in the field, it is possible to perform additional tests or document specific features that need to be considered in the evaluation of the element.

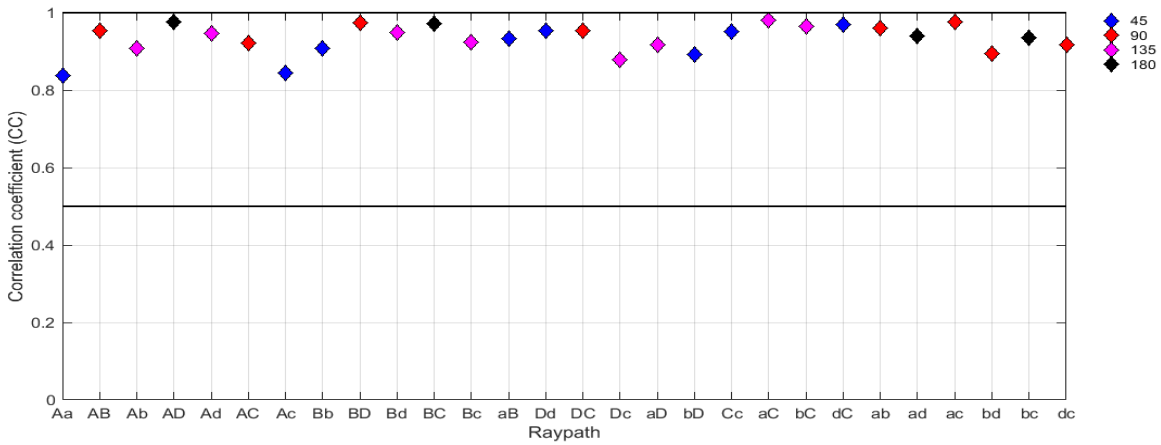

Figure 7-6: Correlation results for a sound column (STC1) obtained from UTPole software

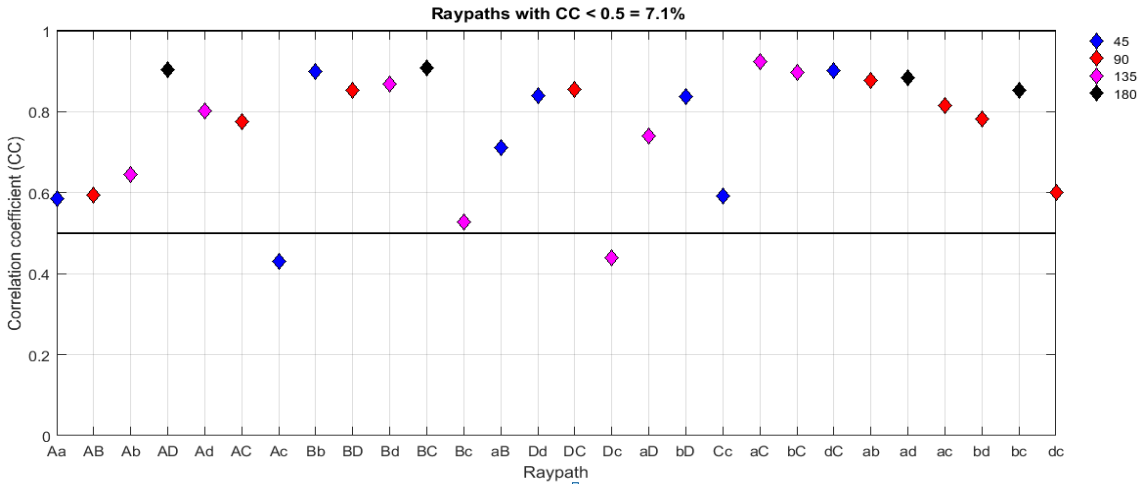

Figure 7-7: Correlation for a damaged column (CN1) obtained from UTPole software

For all measurements done, the velocities and attenuation obtained were analyzed per ray path and per cross section. Then, all the cross sections belonging to the same column were also compared. In all cases, as minimum two columns of the same type were evaluated; therefore,

the columns of similar characteristics were also grouped to evaluate the effect of the vertical and transverse reinforcement. In the following sections, only the results that were considered to illustrate a specific finding are presented. The complete data set is included in Appendix B.

7.3.3 Velocity results

As mentioned before, a common evaluation of the concrete quality based on the pulse velocity consists in the comparison of the measured value with a reference value (Krautkrämer & Krautkrämer, 1990; Ensminger& Bond, 2012; Lamond & Pielert, 2006). For example, Table 7-5 presents the criterion that has been recommended by the National Research Council of Canada until 2008, as indicated by (Saint-Pierre, Philibert, Giroux, & Rivard, 2016).

Table 7-5: Criterion to evaluate the quality of concrete based on UPV (Saint-Pierre, Philibert, Giroux, & Rivard, 2016)

Range	Quality
> 4500	Excellent
3600-4500	Good
3000-3600	Questionable
2100-3000	Poor
< 2100	Very poor

Since the minimum value of velocity computed was 4510 m/s and the maximum 5250 m/s, all the measurements would indicate that the concrete is in either good or excellent condition. However, the ranges indicated before were based in the work by (Leslie & Cheesman, 1949) which was a study of concrete dams and pavements. The ranges are intended for concrete and do not take into account the effect of the steel.

The effect of the steel on the ultrasonic velocity measured in reinforced concrete elements is well recognized (Blitz & Simpson, 1996; Bungey, 1984, ASTM C597-16). The British Standards (BS 1881:Part 203:1986) even include correction factors depending on the diameter of the reinforcing bars and the relative position of the transducers with respect to the axis of the bars. Nonetheless, the application of the correction factors is not very practical because it requires knowing in advance the position and the diameter of all the reinforcing bars in the path

between the transducers, and that information may not be available when doing the UPV test. For example, the standard ASTM C597-16 acknowledges this difficulty, and recommends avoiding measurements close to steel parallel to the direction of propagation of the ultrasonic waves. But, in the case of columns with spiral reinforcement or closely spaced ties the areas not affected by the presence of the steel would be scarce. The effect of the transverse reinforcement is not due by the diameter of the bars, but because for the test configuration used, the bars would be parallel to the direction of propagation. Therefore, for most of the measurements the velocity computed corresponds to a combination of the propagation through concrete and steel.

In Figure 7-8 the expected velocities for steel and for concrete are presented along with the measurements for a cross section of a column with ties at 300mm. The expected velocity for P-waves in steel is 5900 m/s (ASTM E494-10) and the expected velocity for concrete was computed from the equation of wave propagation and the values of modulus of elastic and density calculated for this column (see Appendix A). All the measurements lie between the expected values, which demonstrate that the velocities obtained are a combined value of the velocity of propagation in concrete and in steel. It is interesting to notice that the paths located at 90° present the highest values of the velocity and are closer to the expected value for the steel. The results suggest that the propagation of the waves may be occurring mainly through the transverse reinforcement because the calculated velocity is closer to the value expected for steel (for example ray path 15).

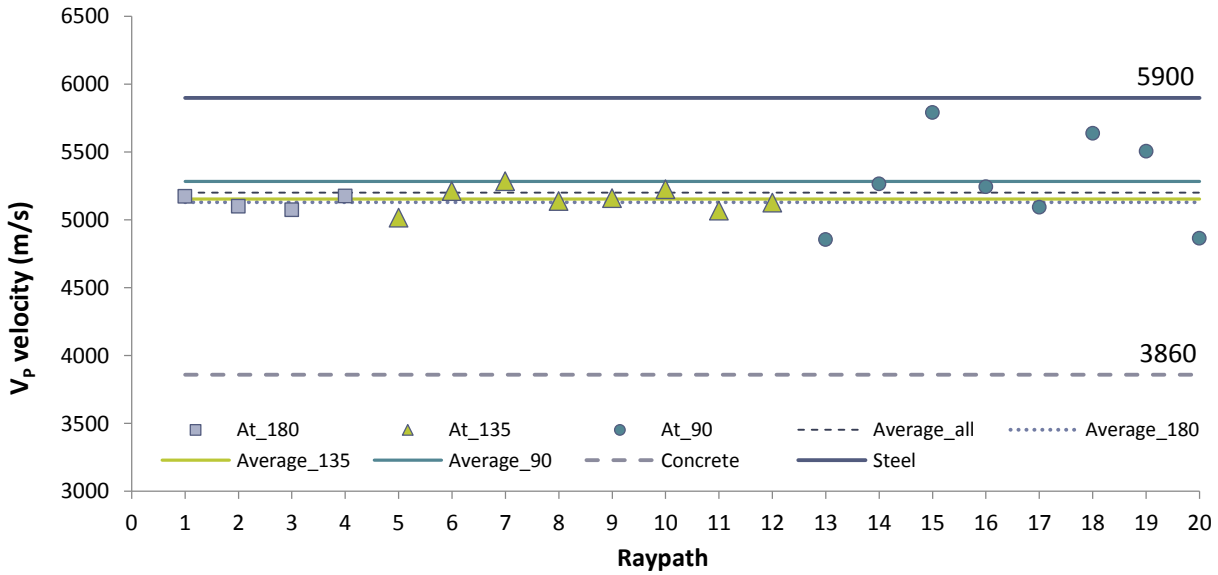

Figure 7-8: Comparison of calculated velocities and the expected values for concrete and steel for a column with ties (STC1_2)

Figure 7-9 exemplifies the case of a column with spiral reinforcement. In this case, the velocity values are less dispersed and also confirm the statement that the computed velocity is an intermediate value between the velocity of propagation through steel and through concrete. This is the expected behaviour because the pitch of the spiral in this case is 44 mm. The contact area of the transducers is 20 mm; therefore, it is very likely that the transducers would be placed over the reinforcement.

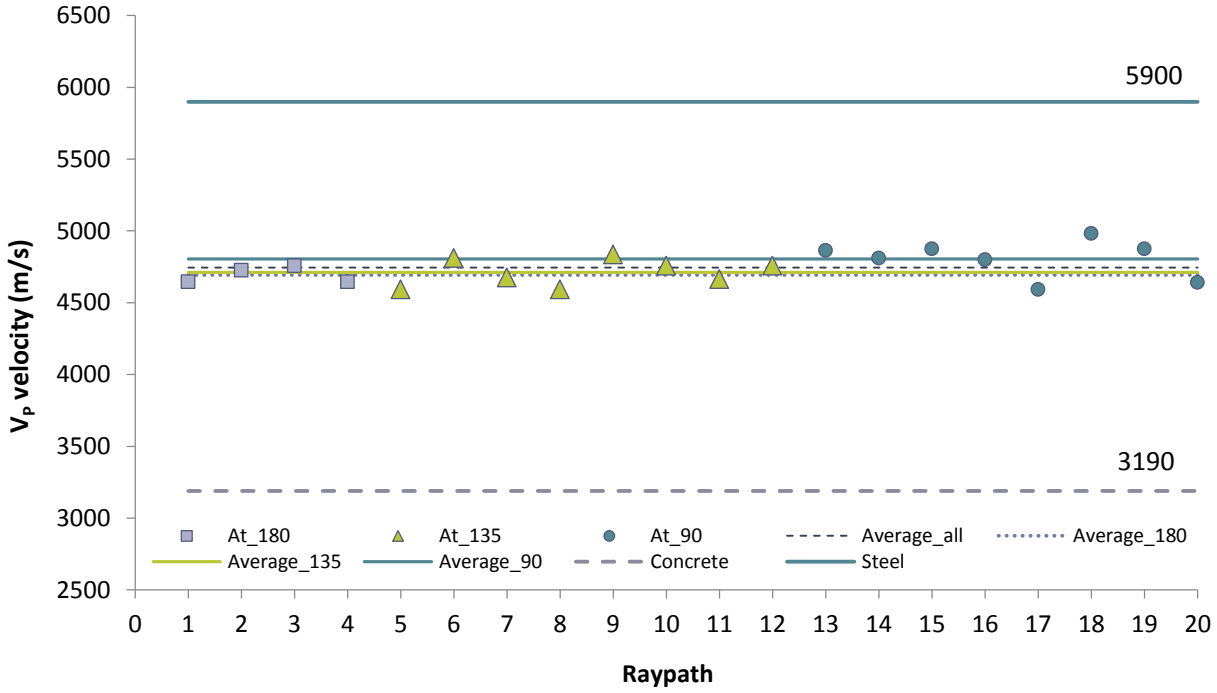

Figure 7-9: Velocity obtained for a column with spiral reinforcement (RCH3_1)

It is important to emphasize that the previous results confirm that reducing the evaluation of the quality of concrete to the comparison to reference values is inadequate. As the computed velocity is also due to the propagation in steel, a velocity above 3600 m/s does not necessary reflects a concrete of good quality. Moreover, they highlighted the importance of taking several measurements, because the results could differ significantly depending on the position of the transducers (see for example ray path 15 in Figure 7-8).

Comparison of vertical reinforcement

To appraise the effect of the percentage of vertical reinforcement in the velocity, four ratios of reinforcement were compared: 1.0%, 2.1%, 1.20% and 2.4% (see Table 3-1 or Appendix A for the details of the columns). In both cases, the ratios of reinforcement are double than the reference

columns. Figure 7-10 illustrates the cases with transverse reinforcement of stirrups and Figure 7-11 corresponds to columns with spiral reinforcement.

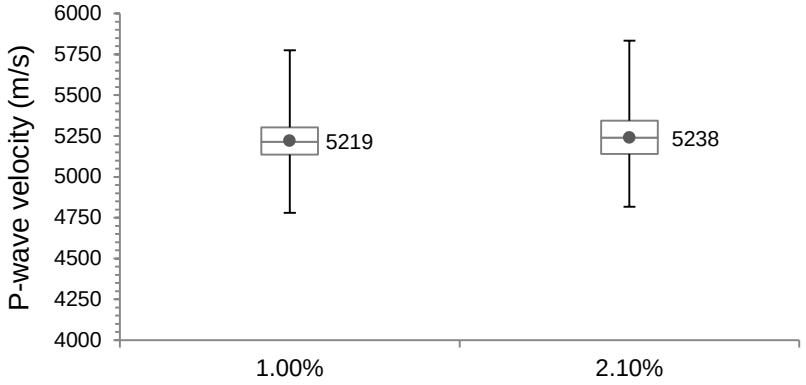

Figure 7-10: Comparison of the velocities for the reinforcement ratios of 1.0% and 2.1% (Column sections STC1-1, ST2_1,STC2,STC2_3, STC3_1 and STC3_3)

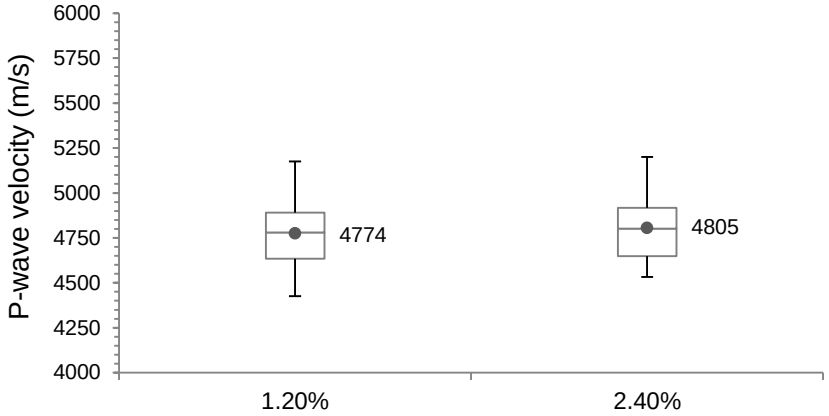

Figure 7-11: Comparison of the velocities for the reinforcement ratios of 1.2% and 2.40% (Column sections RCH1, RCH2_1, RCH2_2, RCH2_3, RCH3_1, RCH3_2 and RCH3_3)

Figure 7-10 and Figure 7-11 indicate that doubling the reinforcement ratio produces a slight increase in the average velocity. To verify if the difference between the average values was significant, hypothesis test of the difference of the means was postulated.

Null hypothesis $H_o: \mu_1 - \mu_2 = 0$

The null hypothesis is that there is no significant difference between the average velocity (μ_1) and the average when the reinforcement ratio is doubled.

Alternative hypothesis $H_1: \mu_1 - \mu_2 \neq 0$

The alternative hypothesis is that there is a significant difference between the means. The significance level was chosen as 5% and in Table 7-6 are summarized the parameters of the hypothesis tests.

In Table 7-6, μ_1 stands for the average values of 1.0% (for the columns in STC) and 1.20% (for the columns in RCH); μ_2 represents the average velocity when the reinforcement ratios are approximately double (2.10% for STC and 2.4% for RCH) ; s_1 and s_2 corresponds to the standard deviations; n_1 and n_2 represents the number of measurements; u is the test statistic from equation (3-11); σ_d is the standard deviation of the difference of the means (7-2) for a normal distribution; $z_{v,0.05}$ represents the critic value to compare that corresponds to the normal distribution value for the level of significance of 0.05 for a two-sided test.

$$u = \frac{|\overline{x_1} - \overline{x_2}|}{\sigma_d} \tag{7-1}$$

$$\sigma_d = \sqrt{\frac{s_1^2}{n_1} + \frac{s_2^2}{n_2}} \tag{7-2}$$

Table 7-6: Hypothesis test of the difference of the average velocity for different reinforcement ratios

Case	μ_1	μ_2	s_1	s_2	n_1	n_2	s_d	u		$z_{0.05}$	Result
STC	5219	5238	166	163	80	40	31.8	0.61	<	1.99	Accept null
RCH	4787	4805	165	170	80	60	28.7	0.61	<	1.98	Accept null

For both cases, there is no statistical evidence to reject the null hypothesis, which means that there is no significant difference between the average velocities. These results were expected because for the longitudinal reinforcement, the distance travelled in the steel is relatively small compared to the total length of the ray path. Therefore, the increase on the total velocity because of the propagation in steel is small.

Table 7-7 presents the average velocities computed for four of the columns considering all the cross sections evaluated in each column. These specific columns are presented because they have different reinforcement ratios, transverse reinforcement, specific compressive strength,

diameter and years in service. The purpose of presenting the results was to demonstrate the low variability in the results of the velocity. For the cases presented, the maximum coefficient of variation is 3.5%, which can be considered as small variability.

Table 7-7: Example of the velocity results averaging all the sections measured in a column

Column	All receivers			Receivers at 180°			Receivers at 135°			Receivers at 90°		
	μ_{all}	σ_{all}	COV_{all}	μ_{180}	σ_{180}	COV_{180}	μ_{135}	σ_{135}	COV_{135}	μ_{90}	σ_{90}	COV_{90}
STC2	5222	148	2.83%	5269	64	1.22%	5237	98	1.86%	5185	204	3.93%
STC3	5238	161	3.08%	5250	87	1.66%	5240	137	2.61%	5231	217	4.14%
RCH2	4807	147	3.06%	4761	111	2.33%	4796	133	2.76%	4842	172	3.55%
RCH3	4805	170	3.54%	4732	107	2.25%	4778	162	3.40%	4868	187	3.83%

7.3.4 Attenuation results

A similar comparison to the one presented for the velocity was done for the attenuation, and the results are included in Table 7-8.

Table 7-8: Example of the attenuation results averaging all the sections measured in a column

Column	All receivers			Receivers at 180°			Receivers at 135°			Receivers at 90°		
	μ_{all}	σ_{all}	COV_{all}	μ_{180}	σ_{180}	COV_{180}	μ_{135}	σ_{135}	COV_{135}	μ_{90}	σ_{90}	COV_{90}
STC2	0.0606	0.0163	26.8%	0.0419	0.0043	10.2%	0.0512	0.0034	6.61%	0.0794	0.0045	5.69%
STC3	0.0742	0.0224	30.2%	0.0486	0.0066	13.5%	0.0614	0.0036	5.87%	0.0999	0.0063	6.33%
RCH2	0.1145	0.0290	25.3%	0.0831	0.0161	19.4%	0.1028	0.0157	15.2%	0.1418	0.0189	13.3%
RCH3	0.1214	0.0257	21.2%	0.0933	0.0135	14.5%	0.1110	0.0127	11.5%	0.1459	0.0173	11.9%

The results highlight the larger variability in the attenuation measurements than in the velocity. Also show that the variability of the attenuation measurements is reduced when the relative position of the transducers is taken into consideration.

The larger variability of the attenuation with respect to the velocity is also observed in the box plots presented in Figure 7-12 and Figure 7-13. Figure 7-12 shows the results for the new columns tested and Figure 7-13 the results for the columns that have been in service for more than 50 years. In both cases, the sections with larger reinforcement ratio present larger average attenuation.

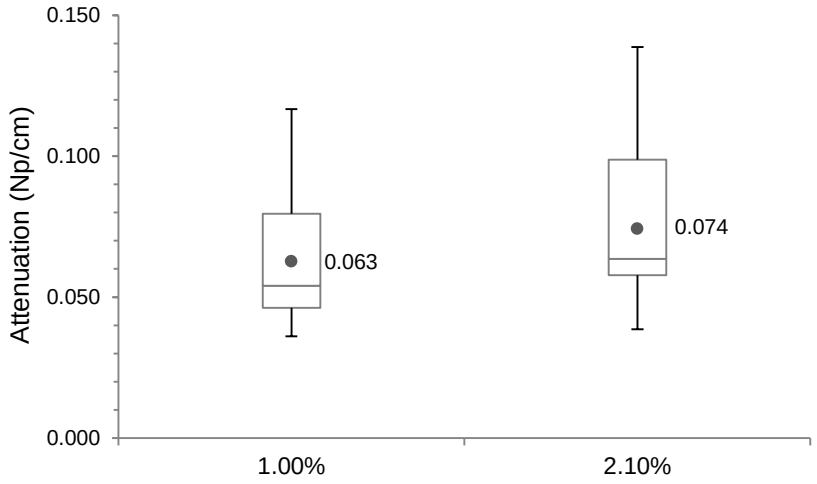

Figure 7-12: Comparison of the attenuation for the reinforcement ratios of 1.0% and 2.1% (Column sections STC1-1, ST2_1, STC2, STC2_3, STC3_1 and STC3_3)

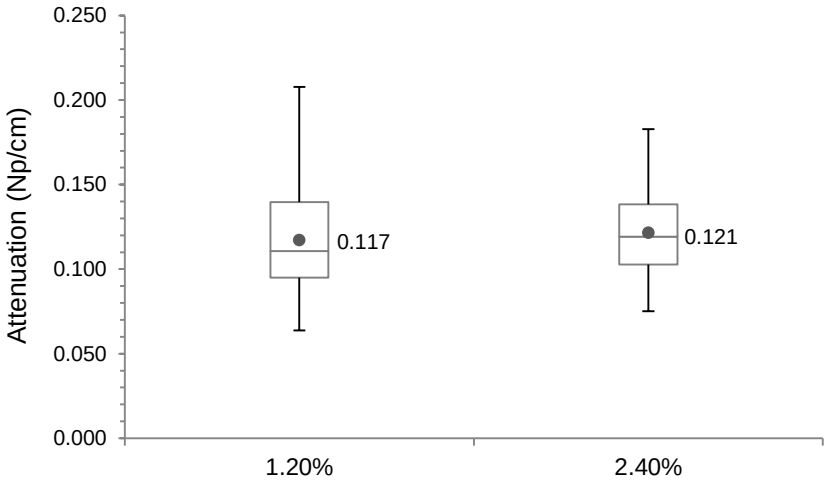

Figure 7-13: Comparison of the attenuation for the reinforcement ratios of 1.20% and 2.40% (Column sections RCH1, RCH2_1, RCH2_2, RCH2_3, RCH3_1, RCH3_2 and RCH3_3)

To evaluate if the difference between the average attenuations is significant, hypothesis test of the difference of the means was postulated. For the attenuation, the difference is evaluated for each of the positions because, as it was shown in Chapter 3, the attenuation may be different depending on the relative position of the transducers considered.

Null hypothesis $H_0: \mu_1 - \mu_2 = 0$

The null hypothesis is that there is no significant difference between the average attenuation computed for the cross sections with different reinforcement ratios.

Alternative hypothesis $H_1: \mu_1 - \mu_2 \neq 0$

The alternative hypothesis is that there is a significant difference between the average attenuation computed for the cross sections. The significance level was chosen as 5%. Table 7-9 and Table 7-10 summarize the parameters of the hypothesis tests.

In the tables, μ_1 stands for the average attenuation for the smaller reinforcement ratio; μ_2 represents the average attenuation for the reinforcement ratio that is approximately double than the reference one; s_1 and s_2 correspond to the standard deviation of the samples; n_1 and n_2 represent the number of measurements; ν stands for the degrees of freedom; t_e is the test statistic (3-11); s_d is the standard deviation of the difference of the means (3-12); $t_{\nu,0.025}$ represents the critic value to compare, which corresponds to the t-distribution value for the specific number of degrees of freedom and the level of significance of 0.025 ($\alpha/2 = 0.025$, two-sided test), and s_c is the combined variance of the difference computed from equation (3-13).

Table 7-9: Hypothesis test for the comparison of the average attenuation for the reinforcement ratios of 1.0% and 2.1% (Column sections STC1-1, ST2_1, STC2, STC2_3, STC3_1 and STC3_3)

Case	μ_1	μ_2	s_1	s_2	n_1	n_2	ν	s_d	t_e		$t_{\nu,0.025}$	Result
180º	0.042	0.049	0.004	0.007	16	8	10	2.28E-03	2.726	>	0.0643	Reject null
135º	0.052	0.061	0.006	0.004	32	16	43	1.58E-03	6.055	>	0.0631	Reject null
90º	0.084	0.100	0.011	0.006	32	16	45	3.02E-03	5.397	>	0.0631	Reject null

Table 7-10: Hypothesis test for the comparison of the average attenuation for the reinforcement ratios of 1.20% and 2.40% (Column sections RCH1, RCH2_1, RCH2_2, RCH2_3, RCH3_1, RCH3_2 and RCH3_3)

Case	μ_1	μ_2	s_1	s_2	n_1	n_2	ν	s_d	t_e		$t_{v,0.025}$	Result
180º	0.086	0.093	0.016	0.014	16	12	27	5.70E-03	1.323	>	0.0633	Reject null
135º	0.0857	0.1110	0.0152	0.0128	32	24	27	3.85E-03	6.557	>	0.0633	Reject null
90º	0.1452	0.1459	0.0195	0.0175	32	24	52	5.04E-03	0.141	>	0.0630	Reject null

In contrast to the results obtained for the velocity, for the attenuation the null hypothesis is rejected in all cases. Therefore, the increase in the reinforcement ratio has a significant effect in the attenuation measurements. These results emphasize the convenience of using various complementary parameters to evaluate the condition of the elements, because one of the parameters could be more sensitive than another to specific properties.

Likewise, the results corroborate the importance of evaluating several ray paths in each cross section. Taking several measurements per cross section reduces the possibility of not detecting a defective area because of the relative position of the transducers.

7.4 Evaluation of defective areas

The application foreseen for the testing system is to evaluate the homogeneity of concrete. To assess the adequacy of the system to detect dissimilar areas, two columns that presented defects were also evaluated.

Figure 7-14 exemplifies a column with honeycombing (voids left between the aggregates caused by inadequate consolidation ACI CT-16, 2016). Honeycombing is generally the result of improper vibration procedures when placing the concrete. Other factors that can also cause it are poor aggregate grading, inadequate workability for the placing conditions, insufficient clearance between the reinforcing steel, insufficient paste to fill the voids between aggregates, among others (Gosh, 1991). As an example of how the honeycombing is considered in structural inspections, Table 7-11 describes the criteria employed by the Ministry of Transportation of Ontario to assess the severity of the honeycombing in bridges. The sections of the elements with this type of defect usually need to be chipped out and repaired, because honeycombed concrete

would be porous (which would favour the corrosion of the reinforcement), weaker and poorly bonded to the reinforcement (Gosh, 1991).

Figure 7-14: Column tested that presents honeycombing

Table 7-11: Criteria to evaluate honeycombing in the Ontario Structure Inspection Manual (OSIM 2008)

Severity	Description
Light	Honeycombing to a depth less than 25 mm
Medium	Honeycombing to a depth between 25 mm and 50 mm
Severe	Honeycombing to a depth between 50 mm and 100 mm
Very severe	Honeycombing to a depth greater than 100 mm

Figure 7-15 presents the time signals recorded for the cross section (STC1_2). The figure can be used to visualize ray paths that require special attention because of the observed pattern. Instead of a decaying signal, as it is common in UPV tests, the time signals show several reflections (see for example when the source is at AB and CA, the receivers at 180°, 90°). This evaluation is only qualitative, but allows finding the cases that require additional analysis.

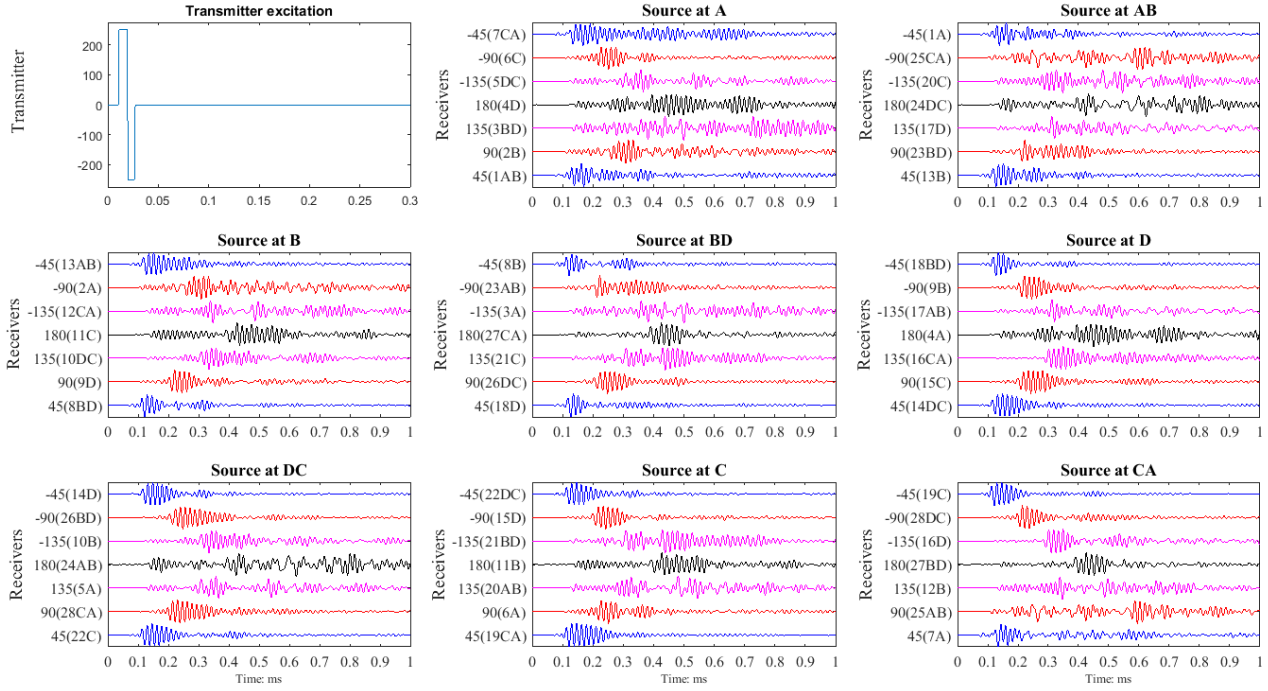

Figure 7-15: Time signals for the section with honeycombing

If the irregularities or voids are of the same order as the wavelength more dispersion from honeycombed areas is expected because there is more scattering of the wave (Lai, Wang, Kou, & Poon, 2013). Scattering is one of the components of the material attenuation, thus, it is expected that the effect of the honeycombing is more evident in terms of the attenuation than in terms of the velocity.

Figure 7-16 presents the plot of the dissimilarity indexes for the attenuation (DIA). The dissimilarity index is a measure of how much the specific value differs with respect to the expected value in a sound condition. In the figure, the dissimilarity indexes corresponding to the ray paths bd, bC, DC, Dc, db, Cb and CD indicate damaged or nonhomogeneous areas, because the value is larger than -1. Comparing the position of the ray paths with the information recorded form the visual inspection and the pictures, those ray paths cross the section with honeycombing.

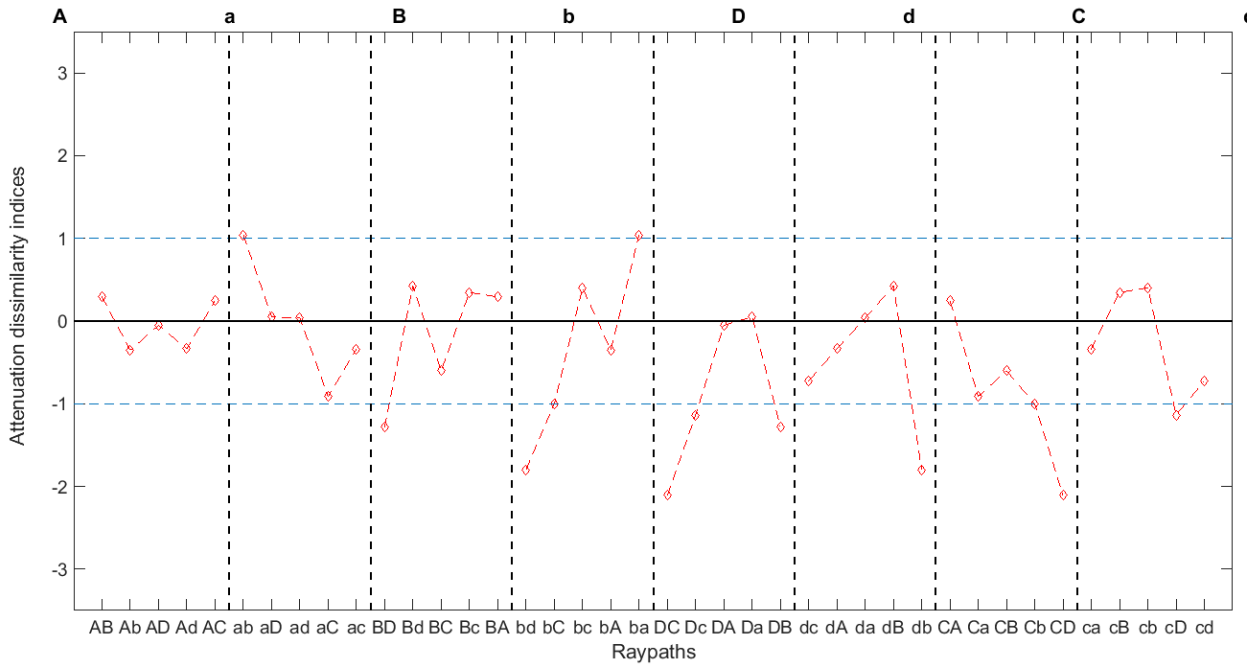

Figure 7-16: Dissimilarity indexes for the attenuation for the cross section that presents honeycombing obtained using UTPole software

To illustrate the convenience of the representation of the results through the dissimilarity indexes, Figure 7-17 includes the tomographic image from a cross section that is sound (left image) and a cross section with localized damage (image at the right).

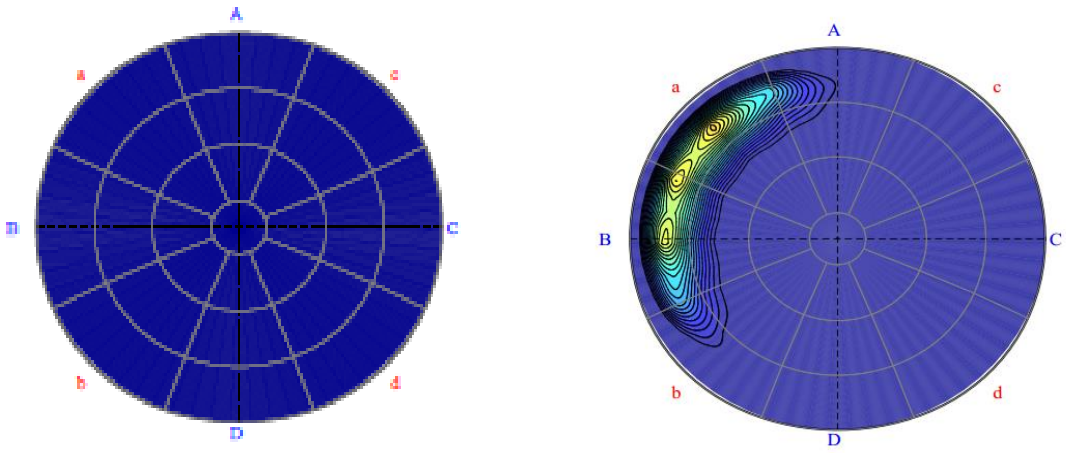

Figure 7-17: Comparison of the tomographic images of a sound section and a section with localized damage (images from the assessment report generated by the UTPole software)

As these tests were part of the verification of the functioning of the system, the evaluation of the columns in service did not include the verification of the damaged area. However, it would be interesting, in future studies, to verify the extent of the distressed area by extracting core samples.

7.5 Results from a damaged column tested in the laboratory

To validate the results, a column specimen in which the damage can be directly observed was also tested (Figure 7-18). The specimen was part of a research done by Dr. Noran Abdel-Wahab, and was available in the Nondestructive Testing Laboratory because of a previous collaborative work. The column presents corrosion of the reinforcement and longitudinal cracks caused by the expansion of corroded reinforcement (Figure 7-19).

Figure 7-18: Damaged column tested in the laboratory

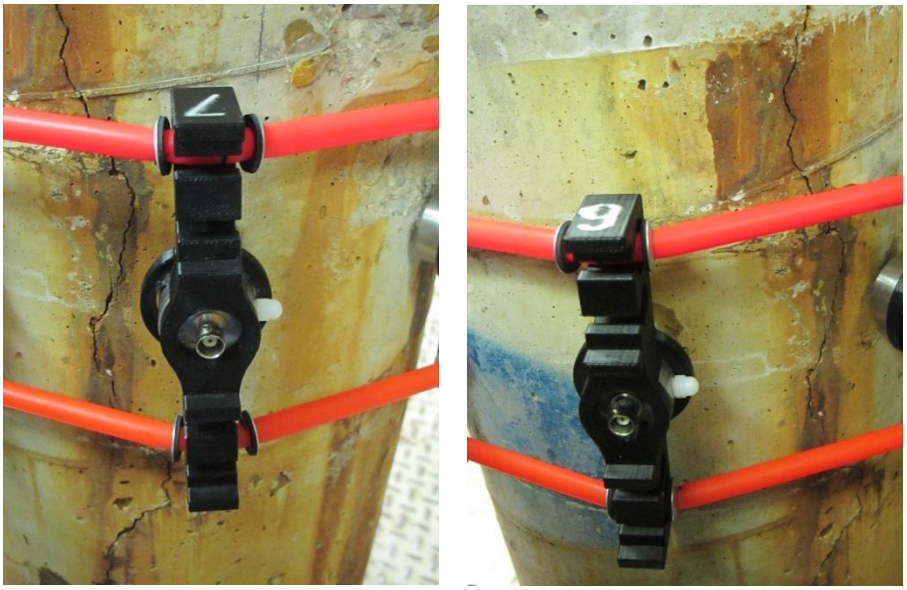

Figure 7-19: Longitudinal cracks caused by the corrosion of the reinforcement

In Figure 7-20 the dissimilarity index for the velocity (DIV), for the attenuation (DIA), for the modulus of elasticity (DIE) and the overall dissimilarity index (ODI) explained in Chapter 3 are presented. The expected values considered were the velocity and attenuation of the calibration tests. The blue horizontal lines indicate ±1 standard deviation. All the indexes indicate damage in the section, however, the velocity and modulus of elasticity suggest less damage because of the values of the dissimilarity indexes.

The attenuation is the parameter that presents larger dissimilarity indexes, which demonstrate that the attenuation is more sensitive to damage than the pulse velocity. Also, as the overall dissimilarity index is the weighted average of the indexes for the velocity and the attenuation, its values are between the results of the velocity and the attenuation. In this case, it is evident that the section is significantly damaged, and the tomographic image generated in UTPole software from the dissimilarity index shows the distribution of the damage. By comparing the image with the specimen, it was verified that the areas indicated in red correspond to the location of more concentration of damage.

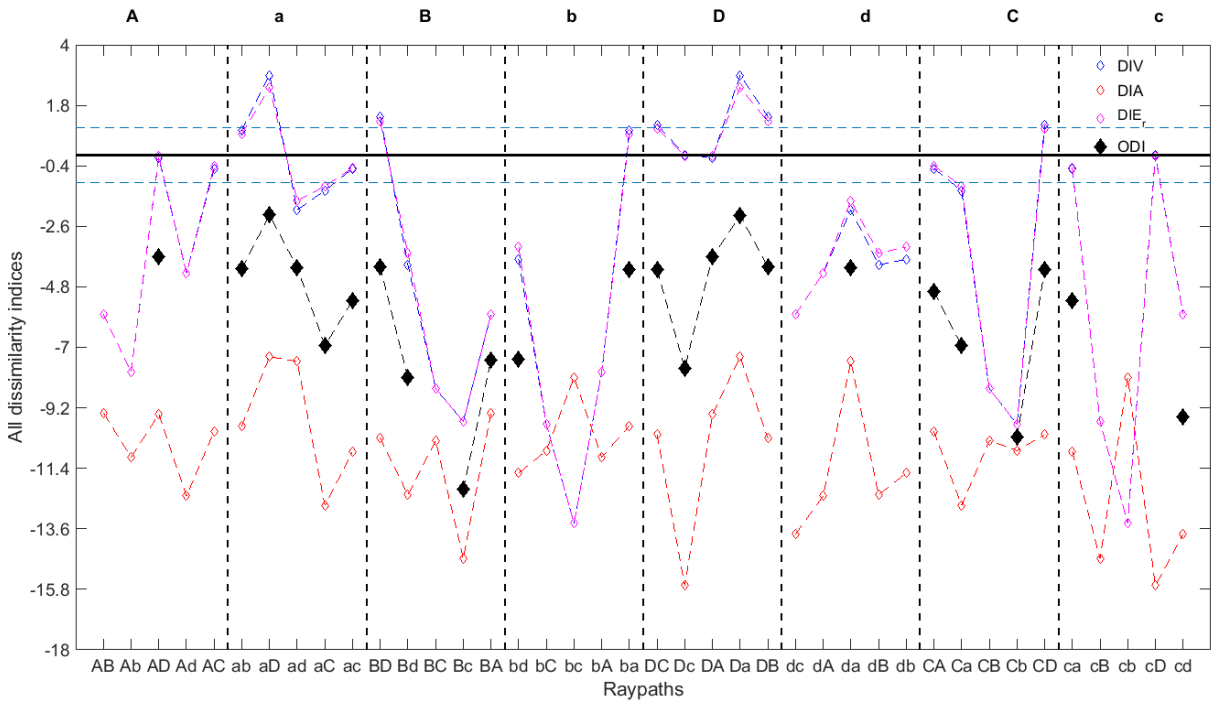

Figure 7-20: Plot of all the dissimilarity indexes for a damaged column (CN1) tested in the laboratory

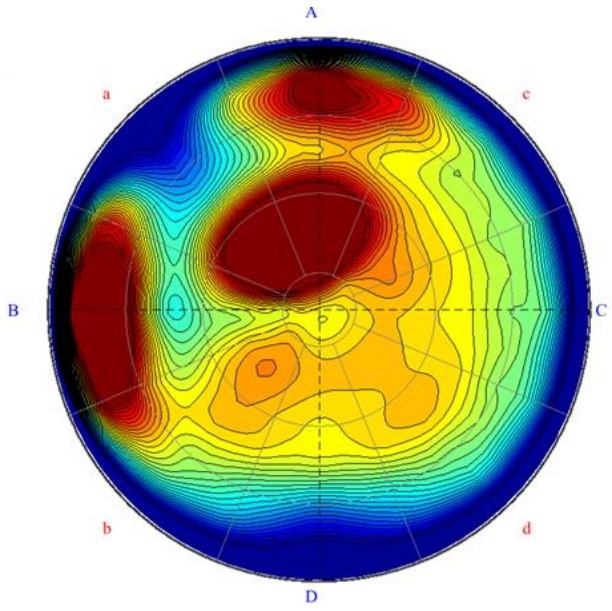

Figure 7-21: Tomographic image obtained from UTPole software for the damaged column (CN1)

7.6 Summary

This chapter presented the results from the testing of mortar and reinforced concrete elements using the field testing device built.

The evaluation of a mortar sample of known characteristics was done to evaluate the functioning of the complete field testing system (transducers array, software and electronics) and to validate the proposed coupling for the field testing.

The evaluation of a sample of in-service columns of different characteristics (diameter, longitudinal and transverse reinforcement, specified compressive strength, and years in service) had the goal of exploring the effect of different parameters on the velocity and attenuation results, and also to verify the practicality of the testing system. Also, the efficacy of the coupling proposed needed to be verified.

An important finding from the testing was that while the difference in the reinforcement ratio does not significantly change the velocity, the effect on the attenuation can be significant. This confirms the convenience of using complementary parameters and a combination of methods for the condition assessment of structural elements.

There are important differences in the material properties (the composite nature of concrete, the attenuation produced by the aggregates, the effect of the reinforcing bars) and therefore, the system needed to be verified evaluating real reinforced concrete elements. The results allowed validating that the testing device, which was developed for testing wood, can be used to test in-service concrete columns. It was verified that the UTPole system could be employed to assess the condition of in-service concrete columns with circular cross section. Columns with other geometries could also be evaluated using the same methodology, but it would require modifications on the software and the sensors array.

The results presented are an initial evaluation of the system, and further testing is needed including different types of columns to evaluate possible normalization factors.

The foreseen application of the UTPole system is to verify the homogeneity of the concrete, provided that the system is calibrated according to the characteristics of the columns tested.

Chapter 8 Conclusions and Recommendations

In this project, a new methodology for assessing the internal condition of reinforced concrete columns was evaluated. The methodology is based on the combination of two stress-wave methods and the use of a newly constructed field testing device. The two methods are the ultrasonic pulse velocity and surface wave method. Although there is vast literature about the application of the two methods to assess existing structures, there is no reference to jointly use of them, and currently there is no comprehensive method available to evaluate reinforced concrete columns.

The project consisted of a literature review and an experimental component. The literature review was focused on the inspection methods for hardened concrete, the applications of the ultrasonic and surface wave tests for structural evaluation, the combination of different NDT techniques and the probabilistic methods to evaluate the capacity of columns. The literature review allowed understanding the state of the art in inspection methods for concrete elements, the existing limitations of the methods under study and the improvements required. It also facilitated the identification of the fundamental aspects that needed to be addressed in the subsequent experimental work. The experimental work included the study of specific aspects of the NDT methods employed (sensitivity to damage, testing configurations, improvement of the system), and also the construction, testing and calibration of the field testing device.

The main findings of the work are summarized in the following sections.

8.1 Sensitivity of ultrasonic pulse velocity to internal damage

The sensitivity of the ultrasonic test to internal damage in concrete elements was evaluated through two sets of experiments: the study of freezing/thawing damage and the comparison of the velocity results from plain concrete samples before and after the uniaxial compression test.

The parameters specified in the standards for the evaluation of frost damage in concrete are the pulse velocity method and the resonance method. However, a significant change in the pulse velocity or the relative dynamic modulus (obtained from the resonance test) was not detected during the whole period of study (324 freeze/thaw cycles). The maximum reduction detected in the ultrasonic pulse velocity was 3.6%. For the relative dynamic modulus, the maximum reduction was of 8.0%. From the parameters studied to evaluate frost damage, only the attenuation was sensitive to the changes induced in the samples by more than 300 freezing/thawing cycles. The estimation of the attenuation based on the ratio of the areas below

the frequency spectrum revealed a decreasing trend in the condition of the samples with an increasing number of freeze/thaw cycles. The reduction estimated is above 50% for the three concrete mixtures studied. The reduction in the strength shown by the comparison of the cores (extracted from the specimens) and the cylinders (tested to verify the specified compressive strength) suggest that there is degradation of the condition. To confirm whether the strength reduction is due to frost damage it would be opportune to perform a petrographic analysis of the specimens. The results from this study confirm that it is convenient to incorporate the use of attenuation to overcome the limited sensitivity of the pulse velocity measurements and resonance tests. The opportuneness of wave attenuation for the assessment of damage has been studied before; however, the present work proposed a method that has the advantage that it does not require additional equipment, since the quantification of the attenuation is done from the information recorded in the pulse velocity test.

In the case of the damage induced by compression, the ultrasonic velocity results do not indicate a significant change between the values before or after the test. All specimens were loaded until the failure and all presented the longitudinal cracking that is characteristic of the compressive failure. Also when the estimated velocities were compared with reference values the results did not indicate damage. These findings confirm the insufficiency of the assessment of the condition of a concrete element based on individual measurements of pulse velocity, because the velocity does not appear to be sensitive to internal damage. In addition, the results demonstrated that an evaluation based on the comparison to reference values of pulse velocity may be inappropriate.

8.2 Surface waves testing

The objective of the research project was to develop a new methodology to inspect reinforced concrete columns based in the complementary use of surface wave testing and ultrasonic pulse velocity. The convenience of the joint use of the two techniques was justified; nevertheless, the experimental results obtained to date did not demonstrate the practicality of the proposed combination. Even though the initial objective of the surface wave investigation was not achieved, valuable results were obtained from the experimental work done.

The study of five beams tested under fatigue loading allowed evaluating different setups; assessing two types of mounting of the sensors and the ultrasonic source, and studying alternative data processing procedures.

With respect to the equipment available in the laboratory at the time, the sensors are unsuitable to perform a global and speedy evaluation as it was initially suggested. A different type of sensors (for example air-coupled sensors) or the construction of an array of accelerometers may serve to this purpose.

From the evaluated configurations, it was found that for the consistency of the tests it is necessary to maintain a constant pressure on the source transducers, and it is suggested to use a clamp or similar device to attach the source transducer. It was also verified that the compression transducers work adequately as source for the surface wave test. For the evaluation of the beams, the piezoelectric transducers with a nominal frequency of 50 kHz were appropriate. The depth that can be evaluated with this source is approximately 40 mm, which corresponded to the concrete cover. In this case, this inspection depth was suitable because the expected damage was debonding of the reinforcing bars.

With respect to the mounting of the examined accelerometers, the adhesive mounting was considered unfavourable because some of the accelerometers fell off during the fatigue loading test, and it also produced damage in the surface of the elements. On the other hand, the magnetic coupling ensured an uninterrupted mounting. However, for the application of the surface waves testing in the field, it would be convenient to build an array with the accelerometers to facilitate the installation or to utilize different sensors, for example air-coupled sensors. The verification of the adequacy of the sensors and the configuration of the array would require additional numerical and experimental work.

For the beams evaluated using the surface wave method, the frequency domain methods evaluated to process the test data provided better results than the time domain methods. The typical way of presenting the results from the surface wave tests in the frequency domain is through the dispersion curves of phase velocity as a function of frequency. Initially it was considered the variation of the phase velocity as a potential indicator of the progression of damage. Nevertheless, it was not possible to identify a clear behaviour of the phase velocity for an increasing number of fatigue cycles. Hence, three alternative methods to compare the signals recorded were evaluated: Pearson correlation, Power spectral correlation index (PSCI) and Coherence spectrum. From the methods studied the Coherence spectrum provided more information and additional investigation (experimental and numerical) is recommended. For the additional study, the data collected from the evaluation of a reinforced concrete dome is being evaluated.

8.3 New device for ultrasonic testing

An important contribution of the research project was the construction and calibration of a field testing tool for the assessment of concrete columns with a circular cross section. Other geometries could also be evaluated following the same methodology and the only modifications needed are adjustments in the software and the sensors array.

By testing a mortar sample of known characteristics, the functioning of the complete field testing system (transducers array, software and electronics) was assessed and the coupling system proposed was validated. The proposed coupling consists of duct tape and vacuum grease. The advantage of this type of coupling is that it does not stain the elements being tested, it provides adequate transmission of the ultrasonic waves, and it is easy to apply in the field.

Once the new system was verified in the laboratory, a sample of in-service columns of different characteristics (diameter, longitudinal and transverse reinforcement, specified compressive strength, and years in service) was tested. The goal of the field testing was to explore the effect of different parameters on the velocity and attenuation results, and also to verify the practicality of the system. The comparison of the measurements obtained for columns of different characteristics demonstrated the convenience of basing the evaluation in both, velocity and attenuation, because the two parameters are affected differently by the properties of the columns. While the velocity presents less variability in the results, the attenuation presented more sensitivity to damage and to the presence of the reinforcing steel. The longitudinal reinforcement did not produce a significant change in the measurements of the pulse velocity, but the measurements of attenuation were affected. It was also observed that the transverse reinforcement affects the velocity and the measured values are between the expected values for the velocity of the steel and the concrete.

The results presented are an initial evaluation of the system, and further testing is needed, including different types of columns to evaluate possible normalization factors. However, the results obtained to date showed that the new field testing device may allow reducing the inspection time without compromising reliability of data, and provides a global and also a detailed assessment of the condition of concrete elements. The proposed application of the testing device constructed is to identify areas of dissimilar characteristics and critical areas to sample by coring in reinforced concrete columns. A better assessment of the condition of the structural elements would definitely have an impact in maintenance practices and a possible reduction in costs.

References

Abraham, O., Piwakowski, B., Villain, G., & Durand, O. (2012). Non-contact, automated surface wave measurements for the mechanical characterisation of concrete. *Construction and Building Materials, 37*, 904-915.

Aggelis, A. (2009). Numerical simulation of surface wave propagation in material with inhomogeneity: Inclusion size effect. *NDT&E, 42*(6), 558-563.

Aggelis, D. G., Shiotani, T., & Polyzos, D. (2009). Characterization of surface crack depth and repair evaluation using Rayleigh waves. *Cement and Concrete Composites, 31*, 77-83.

Alyousef, R. (2012). *Fatigue behavior of GFRP prestressed concrete beams.* Research proposal, University of Waterloo, Civil Engineering.

Alyousef, R. (2016). *The Fatigue Behaviour of Tension Lap Spliced Reinforced Concrete Beams Strengthened with Fibre Reinforced Polymer Wrapping.* PhD thesis, University of Waterloo, Civil Engineering.

American Concrete Institute. (2000). *ACI 365.1R-00: Service-Life Prediction.* Farmington Hills, MI.

American Concrete Institute. (2003). *ACI 228.1R-03: In-place Methods to Estimate Concrete Strength.* Farmington Hills, MI.

American Concrete Institute. (2003). *ACI 437R-03: Strength Evaluation of Existing Concrete Buildings.* Farmington Hills, MI.

American Concrete Institute. (2003). *In-place Methods to Estimate Concrete Strength. ACI 228.1R-03.* Farmington Hills, MI.

American Concrete Institute. (2007). *ACI 364.1R-07: Guide for Evaluation of Concrete Structures before Rehabilitation.* Farmington Hills, MI.

American Concrete Institute. (2011). *ACI 318-11: Building Code Requirements for Structural Concrete and Commentary.* Farmington Mills, MI.

American Concrete Institute. (2013). *ACI 228.2R-13 : Report on Nondestructive Test Methods for Evaluation of Concrete in Structures.* Farmington Hills, MI.

American Concrete Institute. (2013). *ACI Concrete Terminology.* Farmington Hills, MI.

American Concrete Institute. (2013). *Chemical Admixtures for Concrete. ACI Educational Bulletin E4-12.* Farmington Hills, MI.

American Concrete Institute. (2013). *ACI 562M-13: Code Requirements for Evaluation, Repair, and Rehabilitation of Concrete Buildings and Commentary.* Farmington Hills, MI. .

American Society for Testing and Materials. (2008). *ASTM C666/C666M-03: Standard Test Method for Resistance of Concrete to Rapid Freezing and Thawing.* West Conshohocken, PA.

American Society for Testing and Materials. (2010). *ASTM C231-10: Standard Test Method for Air Content of Freshly Mixed Concrete by the Pressure Method..* West Conshohocken, PA.

American Society for Testing and Materials. (2010). *ASTM C143/C143M − 10a: Standard Test Method for Slump of Hydraulic-Cement Concrete.* West Conshohocken, PA.

American Society for Testing and Materials. (2010). *ASTM C469-10: Standard Test Method for Static Modulus of Elasticity and Poisson's Ratio of Concrete in Compression..* West Conshohocken, PA.

American Society for Testing and Materials. (2011). *ASTM E1316-11b: Standard Terminology for Nondestructive Examinations.* West Conshohocken, PA.

American Society for Testing and Materials. (2012). *ASTM C823-12: Standard Practice for Examination and Sampling of Hardened Concrete in Constructions.* West Conshohocken, PA.: ASTM International.

American Society for Testing and Materials. (2012). *ASTM C138-12: Standard Test Method for Density (Unit Weight), Yield, and Air Content (Gravimetric) of Concrete.* West Conshohocken, PA.

American Society for Testing and Materials. (2013). *ASTM C42-13: Standard Test Method for Obtaining and Testing Drilled Cores and Sawed Beams of Concrete.* West Conshohocken, PA.

American Society for Testing and Materials. (2015). *ASTM E6-15: Standard Terminology Relating to Methods of Mechanical Testing.* West Conshohocken, PA.

ASTM International. (2009). *ASTM C597-09: Standard Test Method for Pulse Velocity Through Concrete.* West Conshohocken.

American Society for Testing and Materials. (2016). *ASTM C597-16: Standard Test Method for Pulse Velocity Through Concrete.* West Conshohocken, PA.

American Society of Civil Engineers. (2000). *Guideline for Structural Condition Assessment of Existing Buildings.* Reston, VA.

ASTM International. (2008). *ASTM C 215-08: Standard Test Method for Fundamental Transverse, Longitudinal, and Torsional Resonant Frequencies of Concrete Specimens.* West Conshohocken.

ASTM International. (2009). *ASTM E122-09: Standard Practice for Calculating Sample Size to Estimate, With Specified Precision, the Average for a Characteristic of a Lot or Process.* West Conshohocken.

ASTM International. (2010). *ASTM C469-10:Standard Test Method for Static Modulus of Elasticity and Poisson's Ratio of Concrete in Compression.* West Conshohocken.

Balayssac, J. P., Laurens, S., Arliguie, G.; & Fortuné, I. (2008). SENSO: A French Project for the Evaluation of Concrete Structures by Combining Nondestructive Testing Methods. *On Site Assessment of Concrete, Masonry and Timber Structures International RILEM Conference(SACoMaTIS 2008)* (pp. 289-297). Varenna, Italy: RILEM.

Balayssac, J.P., Laurens, S., Arliguie, G., Breysse, D.; Gernier, V., Dérobert, X., & Piwakowski, B. (2012). Description of the general outlines of the French project SENSO-Quality assessments and limits of different NDT methods. *Construction and Building Materials, 35*, 131-138.

Berubé, S. (2008). In *Sample size effect of ultrasonic testing of geomaterials-numerical and experimental study.* MASc thesis, University of Waterloo, Civil Engineering.

Blitz, J., & Simpson, G. (1996). *Ultrasonic methods of non-destructive testing.* London: Chapman & Hall.

Breysse, D. (2010). Deterioration processes in reinforced concrete: an overview. In C. R. Maierhofer, *Non-destructive evaluation of reinforced concrete structures* (Vol. 1: Deterioration processes and standard test methods, pp. 28-56). Boca Raton, FL: Woodhead Publishing Limited.

Breysse, D. (2012). Nondestructive evaluation of concrete strength: An historical review and a new perspective by combining NDT methods. *Construction and Building Materials, 33*, 139-163.

Breysse, D., Klysz, G., Dérobert, X., Sirieix, C., & Lataste, J.F. (2008). How to combine several non-destructive techniques for a better assessment of concrete structures. *Cement and Concrete Research, 38*, 783-793.

British Standards Institution. (1991). BS 1881 Testing Concrete. Part 203. Recommendations for measurement of velocity of ultrasonic pulses in concrete. London, United Kingdom.

Bungey, J. (1984). *Special Publication: The Influence of Reinforcement on Ultrasonic Pulse Velocity Testing. SP 82-12.* Detroit: American Concrete Institute (ACI).

Canadian Standards Association. (2009). A23.1-09/A23.2-09 Test Methods and Standard Practices for Concrete. Toronto, ON, Canada.

Cascante, G. (1996). *Propagation of Mechanical Waves in Particulate Materials.* PhD dissertation, University of Waterloo, Civil Engineering, Waterloo.

Cetrangolo, G., & Popovics, J. (2010). Inspection of Concrete Using Air-Coupled Ultrasonic Pulse Velocity. *ACI Materials Journal, 107*(2), 155-163.

Chai, H.K., Aggelis, D.G., Momoki, S., Kobayashi, Y., & Shiotani, T. (2010). Single-side access tomography for evaluating interior defect of concrete. *Construction and Building Materials, 24*, 2411-2418.

Chai, H. K., Momoki, S., Kobayashi, Y., Aggelis, D. G., & Shiotani, T. (2011). Tomographic reconstruction for concrete using attenuation of ultrasound. *NDT&E International, 44*, 206-215.

Chekroun, M., Le Marrec, L., Abraham, O., Durand, O., & Villain, G. (2009). Analysis of coherent surface wave dispersion and attenuation for non-destructive testing of concrete. *Ultrasonics, 49*, 743-751.

Chevalier, Y. & Vinh, J.T. (2010). *Mechanical Characterization of Materials and Wave Dispersion:instrumentation and experiment interpretation.* London, United Kingdom: ISTE Ltd.

Cordon, W.A. & Merril, D. (1963). Requirements for Freezing-and-Thawing Durability for Concrete. *Proceedings ASTM 1963* (pp. 1026-1036). West Conshohocken, PA: ASTM International.

Dalimar Instruments. (2014, March 17). Calibration Seminar. Toronto.

De la Haza, A.O., Samokrutov, A.A., & Samokrutov, P.A. (2013). Assessment of concrete structures using the Mira and Eyecon ultrasonic shear wave devices and the SAFT-C image reconstruction technique. *Construction and Building Materials, 38*, 1276–1291.

Der Kiureghian, A. (2009). Course notes Seismic Reliability Analysis of Structures. *Lecture notes for CE193 Probabilistic Methods for Engineering Risk Analysis*. Pavia, Italy: ROSE School.

Dilek, U. (2007). Ultrasonic Pulse Velocity In Nondestructive Evaluation of Low Quality and Damaged Concrete and Masonry Construction. *Journal of Performance of Constructed Facilities, 21*(5), 337-344.

Drinkwater, B. W., & Wilcox, P. D. (2006). Ultrasonic arrays for non-destructive evaluation: A review. *NDT&E International, 39*, 525-541.

Ensminger, D., & Bond, L. (2012). *Ultrasonics Fundamentals, Technologies and Applications* (Third edition ed.). Boca Raton, Florida, United States: CRC Press.

Ferraro, C. C., Boyd, A. J., & Hamilton III, H. R. (2007). Detection and assessment of structural flaws in concrete bridges with NDT methods. *Research in Nondestructive Evaluation, 18*, 179-192.

Fisk, P., & Holster, K. (2014). Condition Assessment of Concrete Piers with Tomographic Imaging. *NDE/NDT for Structural Materials Technology for Highways and Bridges Conference* (pp. 131-137). Washington D.C., United States: The American Society of Nondestructive Testing, Inc.

Forde, M. C. (2013). Differences in International Strategy for the NDT of Concrete. In O. Büyüköztürk (Ed.), *Nondestructive Testing of Materials and Structures* (pp. 1217-1227). RILEM Bookseries 6.

Gardoni, P., Der Kiureghian, A., & Mosalam, K. M. (2002, October). Probabilistic Capacity Models and Fragility Estimates for Reinforced Concrete Columns based on Experimental Observations. *Journal of Engineering Mechanics, 128*, 1024-1038.

Garnier, V. (2012). Ultrasounds through transmission. In D. Breysse (Ed.), *Non-Destructive Assessment of Concrete Structures: Reliability and Limits of Single and Combined Techniques, RILEM State-of-the-Art Report 1* (Vol. 1, pp. 17-27). Springer.

Gaylor, D.W. & Hopper, F.N. (1969). Estimating the Degrees of freedom for Linear Combinations of Mean Squares by Satterthwaite's Formula. *Technometrics, 11*(2), 691-706.

González, M. (2014). *Investigation of Innovative Surface Characteristics of Usage on Canadian Concrete*. PhD thesis, University of Waterloo. Civil Engineering.

González, M., Safiuddin, M., Cao, J., & Tighe, S. (2013). Sound Absorption and Friction Responses of Nanoconcrete for Rigid Pavements. *Journal of the Transportation Research Board*(2369), 87-94.

Gosh, S. (Ed.). (1991). *Notes from Cement and Concrete Science.* London, united Kingdom: Thomas Telford.

Goueygou, M., Abraham, O., & Lataste, J.F. (2008). A comparative study of two non-destructive testing methods to assess near-surface mechanical damage in concrete structures. *NDT&E International, 41*, 448-456.

Graff, K. (1975). *Wave motion in elastic solids.* Columbus, United States: Ohio State University Press.

Gucunski, N., Basily, B., Kee, S.-H., La, H., Parvardeh, H., Maher, A., et al. (2014). Multi NDE Technology Condition Assessment of Concrete Bridge Decks by RABITTM Platform. *Proceedings of the Conference SMT 2014 NDE/NDTfor Highways and Bridges Structurals Materials Technology* (pp. 161-168). Washington D.C, United States: The American Society of Nondestructive Testing, Inc.

Haach, V. G. (2014). Application of ultrasonic tomography to detection of damages in concrete. In E. C. A. Cunha (Ed.), *Proceedings of the 9th International Conference on Structural Dynamics, EURODYN 2014*, (pp. 3351-3357). Porto, Portugal.

Haach, V., & Ramirez, C. (2016). Qualitative assessment of concrete by ultrasound tomography. *Construction and Building Materials, 119*, 61-70.

Hellier, C. (2001). *Handbook of Nondestructive Evaluation.* New York, United States: McGraw-Hill.

Hernández, M.G.; Izquierdo, M.A.G.; Ibáñez, A.; Anaya, J.J.; & Ullate, L.G. (2000). Porosity estimation of concrete by ultrasonic NDE. *Ultrasonics*, 531-533.

Hévin, G., Abraham, O., Pedersen, H. A., & Campillo, M. (1998). Characterisation of surface cracks with Rayleigh waves: a numerical study. *NDT&E International, 31*(4), 289-297.

Huang, Q., Gardoni, P., & Hurlebaus, S. (2009). Probabilistic Capacity Models and Fragility Estimates for Reinforced Concrete Columns Incorporating NDT Data. *ASCE Journal of Engineering Mechanics, 135*, 1384-1392.

Kalinski, M.E., Stokoe II, K.H., Jirsa, J.O., & Roesset, J.M. (1994). Nondestructive Identification of Internally Damaged Areas of Concrete Beam Unsing the Spectral Analysis of Surface Waves Method. *Transportation Research Record*(1458), 14-18.

Kim, K-S., Fratta, D., & Pincheira, J.A. (2011). Nondestructive Evaluation of Fiberglass Wrapped Concrete Bridge Columns. *Journal of Nondestructive Evaluation, 30*, 9-19.

Kirlangic, A. (2013). *Condition assessment of cemented materials using ultrasonic surface waves.* PhD. Dissertation, University of Waterloo, Civil Engineering.

Kirlangic, A.S., Cascante, G., & Polak, M.A. (2015, March). Condition Assessment of Cementious Materials Using Surface Waves in Ultrasonic Frequency range. *ASTM Geotechnical Testing Journal*, *38*(2), 139-149.

Komlos, K., Popovics, S., Nürnbergerová, T., Babál, B., & Popovics, J. S. (1996). Ultrasonic Pulse Velocity Test of Concrete Properties as Specified in Various Standards. *Cement and Concrete Composites, 18*, 357-364.

Kosmatka, S. H., Kerkhoff, B., & Panarese, W. C. (2002). *Design and Control of Concrete Mixtures* (14th edition ed.). Illinois: Portland Cement Association.

Kosmatka, S.H. Kerkhoff, R.D. & Hooton, R.J. (2011). *Design and Control of Concrete Mixtures: The Guide to Application, Methods and Materials* (8th ed.). Ottawa: Cement Association of Canada.

Krause, M., Mielentz, F., Milman, B., Müller, W., Schmitz, V., & Wiggenhauser, H. (2001). Ultrasonic imaging of concrete members using an array system. *NDT&E International, 34*, 403-408.

Krautkrämer, J., & Krautkrämer, H. (1990). *Ultrasonic Testing of Materials* (4th ed.). Berlin, Germany: Springer-Verlag.

Lai, W., Wang, Y., Kou, S., & Poon, C. (2013). Dispersion of ultrasonic guided surface wave by honeycomb in early-aged concrete. *NDT& E International, 57*, 7-16.

Lamond, J., & Pielert, J.H. (2006). *Significance of tests and properties of concrete and concrete-making materials.* Philadelphia: American Society of Testing Materials (ASTM).

Leslie, J.R., & Cheesman, W.J. (1949, September). An Ultrasoni Method of Studying Deterioration and Cracking in Concrete Structures. *Journal of the American Concrete Institute, 21*(1), 17-36.

Lesniak, A. & Nitsuma, H. (1998, November - December). Time-frequency coherency analysis of three-component crosshole seismic data for arrival detection. *Geophysics, 63*(6), 1874-1857.

Li, H. B. (2004). Life prediciton of aging wood poles and subsequent inspeciton practice - a case study. *The International Journal for Computation and Mathematics in Electrical and Electronic Engineering, 23*(1), 15-20.

Liu, L., & Guo, T. (2005). Seismic non-destructive testing on a reinforced concrete bridge column using tomographic imaging techniques. *Journal of Geophysics and Engineering, 2*, 23-31.

Maierhofer, C., Reinhardt, H-W. and Dobmann, G. (2010). *Non-destructive evaluation of reinforced concrete structrues* (Vol. 1: Deterioration processes and standard test methods). Cornwall, UK: Woodhead Publishing Limited.

Malhotra, V.M., & Carino, N.J. (2004). *Handbook o Nondestructive Testing of Concrete.* CRC press.

Meng, B., Muller, U., & Rubner, K. (2010). Components in concrete and their impact in quality: an overview. In C. Maierhofer, H.-W. Reinhardt, & G. Dobmann (Eds.), *Non-destructive evaluation of reinforced concrete structures* (Vol. 1: Deterioration processes and standard test methods, pp. 82-93). Cornwall, UK: Woodhead Publishing Limited.

Miller, R. (1973). *Factors Influencing Accelerometer Measurement Capabilities- A Practical Measurement Guide (Report 3941).* Research and Development Report, Naval Ship Reasearch and Development Center (Department of the Navy), Propulsion and Auxiliary Systems Department, Annapolis.

Ministry of Transportation of Ontario (MTO). (2008). *Ontario Structure Inspection Manual (OSIM).* Policy, Planning & Standards Division, Engineering Standards Branch, Bridge Office.

Molero, M., Aparicio, S., Al-Assadi, G., Casati, M., Hernández, M., & Anaya, J. (2012). Evaluation of freeze-thaw damage in concrete by ultrasonic imaging. *NDT&E International, 52*, 86-94.

Naik, T. R., Malhotra, V. M., & Popovics, J. S. (2004). The Ultrasonic Pulse Velocity Method. In V. Malhotra, & N.J.Carino (Eds.), *Handbook of Nondestructive Testing of Concrete* (Second edition ed.). Boca Raton, Florida: CRC Press.

Nelson, J. D., Ferraro, C. C., & Algernon, D. (2014). Full-field Visualization Techniques for High Density Ultrasound Measurements. *Proceedings of the NDE/NDT for Structural Materials*

Technology for Highways and Bridges Conference (pp. 396-403). Washington D.C., United States: The American Society of Nondestructive Testing, Inc.

Neville, A.M. & Kennedy, J.B. (1966). *Basic Statistical Methods for Engineers and Scientists.* Scranton, Pennsylvania, United States of America: International Textbook Company.

Nishiwaki, T., Adachi, K., Yangida, H., & Tamura, Y. (2008). Development of Ultrasonic Time-of-flight Computed Tomography (TOF-CT) for Inspection of Concrete. *On Site Assessment of Concrete,Masonry and Timber Structures (SACoMaTIS) 2008 International RILEM Conference* (pp. 309-317). Varenna,Italy: RILEM.

Nowak, A., Rakoczy, A.M., & Szeliga, E.K. (2005). *SP-284-6: Revised Statistical Resistance Models for R/C Structural Components.* Farmington Hills, MI: American Concrete Institute.

Nuño Ayón, J. (2011). *Método de Estimación Instantánea de Coherencia Espectral para la Identificación de Grupos de Oscilación Coherentes en Sistemas Eléctricos de Potencia.* MSc dissertation, Universidad de Guadalajara, Departamento de Ingeniería Mecánica Eléctrica, Guadalajara, Jalisco. (In Spanish)

Office of Research, Development, and Technology, Office of Infrastructure RDT. (2014, 04 13). *Federal Highway Administration Research and Technology*. Retrieved 11 04, 2014, from http://www.fhwa.dot.gov/research/tfhrc/programs/infrastructure/structures/ltbp/ltbpresearch/rabit/index.cfm

Okasha, N. M. & Aichouni, M. (2015). Proposed Structural Reliability-Based Approach for the Classification of Concrete Quality. *Journal of Materials in Civil Engineering, 27*(5).

Ould Naffa, S., Goueygou, M., Piwakowski, B., & Buyle-Bodin, F. (2002). Detection of chemical damage in concrete using ultrasound. *Ultrasonics, 40*, 247-251.

Phoon, K. K. (1999). Development of Statistical Quality Assurance Criterion for Concrete Using Ultrasonic Pulse Velocity Method. *Materials Journal*, 568-574.

Popovics, J., & Abraham, O. (2010). Surface wave techniques for evaluation of concrete structures. In C. Maierhofer, H.-W. Reinhardt, & G. Dobmann (Eds.), *Non-destructive evaluation of reinforced concrete structures* (Vol. 2, pp. 441-465). Boca Raton, Florida: CRC Press.

Popovics, J.S.,Zemajtis, J., & Shkilnik,I. (2008). *A Study of Static & Dynamic Modulus of Elasticity of Concrete.* Concrete Reasearch Council. American Concrete Institute.

Prada, J., Fratta, D., & Santamarina, J.C. (2000, December). Tomographic Detection of Low-Velocity Anomalies with Limited Data Sets (Velocity and Attenuation). *Geotechnical Testing Journal, 23*(4), 472-486.

RILEM. (2004, December). RILEM TC 176-IDC: 'Internal damage of concrete due to frost action'. *Materials and Structures, 37*, 743-753.

Rose, J. (1999). *Ultrasonic Waves in Solid Media.* Cambridge, United Kingdom: Cambridge University Press.

Ross, S. (2004). *Introduction to probability and statistics for engineers and scientists.* Elsevier Academic Press.

Safiuddin, M., González, M., Cao, J. and Tighe, S. (2014). State-of-the-art report on use of nano-materials in concrete. *International Journal of Pavement Engineering, DOI:10.1080/10298436.2014.893327*. Taylor& Francis Group.

Saint-Pierre, F.; Philibert, A.; Giroux, B.; & Rivard, P. (2016). Concrete Quality Designation based on Ultrasonic Pulse Velocity. *Construction and Building Materials, 125*, 1022-1027.

Saint-Pierre, F.,Rivard, P. & Ballivy, G. (2007). Measurement of alkali-silica reaction progression by ultrasoni waves attenuation. *Cement and Concrete Research*, 948-956.

Santamarina, J.C., & Fratta, D. (2005). *Discrete Signals and Inverse Problems.* West Sussex, England: John Wiley & Sons Ltd.

Schickert, M. (2012). Automated Ultrasonic Scanning System for Three-dimensional SAFT Imaging of Concrete Elements Using an Electronically Switched Transducer array. *2012 IEEE International Ultrasonics Symposium Proceedings* (pp. 40-43). Dresden, Germany: IEEE.

Schmer, L., & Song, S. (2007). *Ultrasonic Nondestructive Evaluation Systems. Models and Measurements.* New York, New York: Springer Science+Bussiness Media, LLC.

Setzer, M., Heine, P., Kasparek, S., Palecki, S., Auberg, R., Feldrappe, V., et al. (2004, December). RILEM TC 176-IDC: 'Internal damage of concrete due to frost action'. *Materials and Structures, 37*, 743-753.

Tallavó, F. (2009). *New Methodology for the Assessment of Decayed Utility Wood Poles Using Ultrasonic Testing.* Waterloo: University of Waterloo, Civil Engineering.

Tallavó, F. Cascante, G., & Pandey, M.D. (2011). Estimation of the Probability Distribution of Wave Velocity in Wood Poles. *Journal of Materials in Civil Engineering, 23*(1), 1272-1280.

Tallavó, F., Cascante, G., & Pandey, M.D. (2011). *A tomographic imaging method based on ultrasonic waves for the detection of decayed areas in wood poles.* Unpublished technical report, University of Waterloo.

Tallavó, F., Cascante, G., & Pandey, M.D. (2012). A novel methodology for condition assessment of wood poles using ultrasonic testing. *NDT&E International*, 149-156.doi.org/10.1016/j.ndteint.2012.08.002.

Tallavó, F., & Kalyan, E. (2014, June 11). Dynamic characterization of a ultrasonic transducer using a laser vibrometer. Unpublished technical report. Waterloo, Ontario, Canada.

Tangirala, A.K., Shah, S.L., Thornhill, N.F. (2005). PSCMAP: A new tool for plant-wide oscillation detection. *Journal of Process Control, 15*, 931-941.

Vergara, L.; Miralles, R.; Gonzálbez, J.; Juanes, F.J.; Ullate, L.G.; Anaya, J.J.; Hernández, M.G.; & Izquierdo, M.A.G. (2001). NDE ultrasonic methods to characterise the porosity of mortar. *NDT&E International*, 557-562.

Weiss, J. (2006). Elastic Properties, Creep, and Relaxation. In J. Lamond, & J. Pielert (Eds.), *Significance of tests and Properties of Concrete & Concrete-Making Materials* (pp. 194-205). ASTM International.

Welch, P. (1967, August). The Use of Fast Transform for the Estimation of Power Spectra: A Method Based on Time Averaging Over Short, Modified Periodograms. *IEEE Transactions on Audio and Electroacoustic, 15*, 70-73.

Wiggenhauser, H. (2013). Automated NDE of Structures with Combined Methods. In B. e. (eds.), *Nondestructive Testing of Materials and Structures* (pp. 753-760). Springer Netherlands.

Wu, Y. (2012). *NDT Applications for the Assessment of Asphalt Pavements, Plate Thickness, and Steel-Grout Coupling.* MSc thesis, University of Waterloo, Civil Engineering.

Yang, Y., Cascante, G., & Polak, M. A. (2009). Depth detection of surface-breaking cracks in concrete plates using fundamental Lamb modes. *NDT&E International, 42*, 501-512.

Yim, H. J., Kwak, H. G, & Kim, J. H. (2012, March). Wave attenuation measurement technique for nondestructive evaluation of concrete. *Nondestructive Testing and Evaluation, 27*(1), 81-94.

Zang, Y., Halliday, D., Jiang, P., Liu, X., & Feng, J. (2006, February). Detecting time-dependent coherence between non-stationary electrophysiological signals-A combined statistical and time-frequency approach. *Journal of Neuroscience Methods*, 322-332.

APPENDIX A

Properties of the Columns Tested

Table A-1: Geometrical information for column STC1

Location	Room 54 Science Teaching Complex
Diameter (D)	0.605 m
Details reference	UW SCB Structural Construction
Specified strength (f'_c)	45 MPa
Concrete cover	0.040 m
Longitudinal reinforcement	10 ϕ 20M
Longitudinal reinforcement %	1.0%
Transverse reinforcement	10M @ 300
Density (ρ) (Monte Carlo)	2325 kg/m^3
Number of sections tested	2
Estimated E [1]	31.5 GPa
Poisson's ratio (υ)	0.2
Estimated velocity [2]	3860 m/s

Figure A-1: Column STC1 tested in Science Teaching Complex

$(4700\sqrt{f'_c})$ [1]

$$V_p = \sqrt{\frac{E(1-\upsilon)}{\rho(1+\upsilon)(1-2\upsilon)}} \quad [2]$$

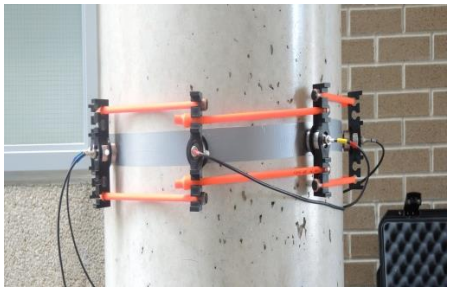

FigureA-2: Section STC1-1

Figure A-3: Section STC1-2

Table A-2: Geometrical information for column STC2

Location	Room 54 Science Teaching Complex
Diameter (D)	0.605 m
Details reference	UW SCB Structural Construction
Specified strength (f'_c)	45 MPa
Concrete cover	0.040 m
Longitudinal reinforcement	10 ϕ 20M
Longitudinal reinforcement %	1.0%
Transverse reinforcement	10M @ 300
Density (ρ) (Monte Carlo)	2325 kg/m^3
Number of sections tested	2
Estimated E [1]	31.5 GPa
Poisson's ratio (υ)	0.2
Estimated velocity [2]	3860 m/s

Figure A-4: Column STC2 tested in Science Teaching Complex

$(4700\sqrt{f'_c})$ [1]

$$V_p = \sqrt{\frac{E(1-\upsilon)}{\rho(1+\upsilon)(1-2\upsilon)}} \quad [2]$$

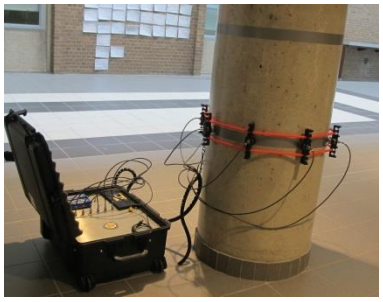

FigureA-5: Section STC2_1

FigureA-6: Section STC2_2

Figure A-7: Section STC2_2

Table A-3: Geometrical information for column STC3

Location	Room 54 Science Teaching Complex
Diameter (D)	0.605 m
Details reference	UW SCB Structural Construction
Specified strength (f'_c)	45 MPa
Concrete cover	0.040 m
Longitudinal reinforcement	12 ϕ 25M
Longitudinal reinforcement %	2.1%
Transverse reinforcement	10M @ 300
Density (ρ) (Monte Carlo)	2325 kg/m^3
Number of sections tested	3
Estimated E [1]	31.5 GPa
Poisson's ratio (υ)	0.2
Estimated velocity [2]	3860 m/s

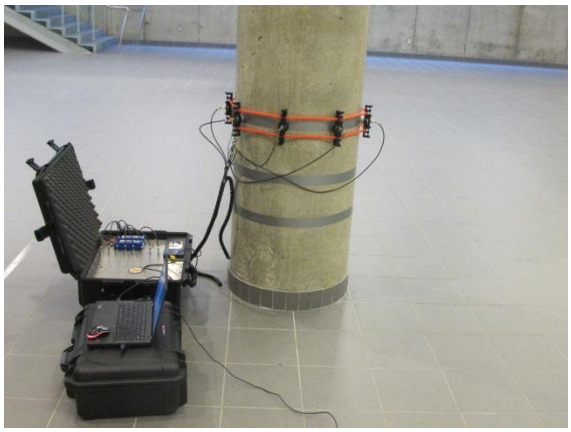

Figure A-8: Column STC3 tested in Science Teaching Complex

$(4700\sqrt{f'_c})$ [1]

$$V_p = \sqrt{\frac{E(1-\upsilon)}{\rho(1+\upsilon)(1-2\upsilon)}} \quad [2]$$

FigureA-9: Section STC3_1

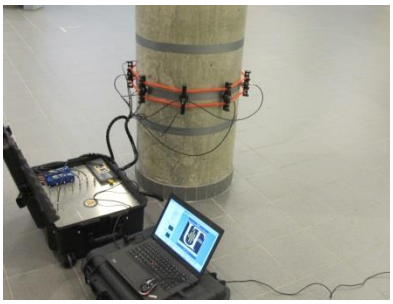

FigureA-10: Section STC3_2

Figure A-11: Section STC3_3

Table A-4: Geometrical information for column RCH1

Location	Room 218 J.R. Coutts Engineering Lecture Hall
Diameter (D)	14 in (0.357 m)
Details reference	SCAN_314R_S1_011_S_Foundation Plan & Details
Specified strength (f'_c)	3000 psi (21 MPa)
Concrete cover	3/8 in (0.01 m)
Longitudinal reinforcement	6 # 5(ϕ 15.88 mm)
Longitudinal reinforcement %	1.2%
Transverse reinforcement	$^{3}/_{8}$ @ 1 $^{3}/_{4}$ (10 M @ 44 mm)
Density (ρ) (Monte Carlo)	2325 kg/m^3
Number of sections tested	1
Estimated E [1]	21.5 GPa
Poisson's ratio (υ)	0.2
Estimated velocity [2]	3190 m/s

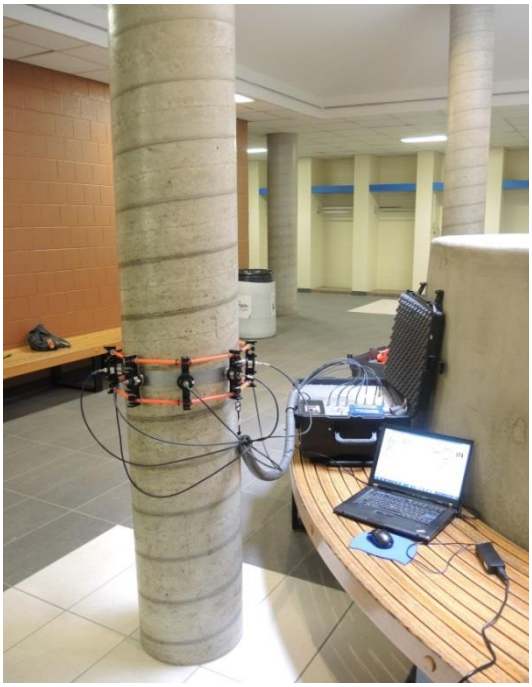

Figure A-12: Column RCH1

$(4700\sqrt{f'_c})$ [1]

$$V_p = \sqrt{\frac{E(1-\upsilon)}{\rho(1+\upsilon)(1-2\upsilon)}}$$ [2]

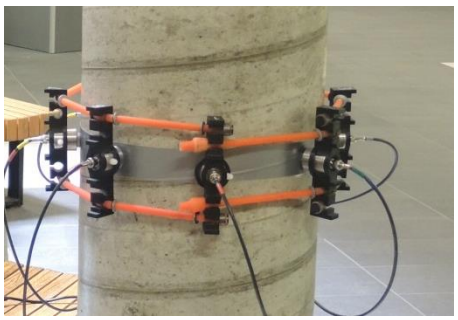

Figure A-13: Section RCH1_1

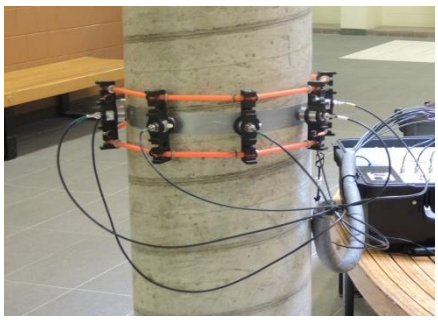

Figure A-14: Section RCH1_1

Table A-5: Geometrical information for column RCH2

Location	Room 218 J.R. Coutts Engineering Lecture Hall
Diameter (D)	14 in (0.357 m)
Details reference	SCAN_314R_S1_011_S_Foundation Plan & Details
Specified strength (f'_c)	3000 psi (21 MPa)
Concrete cover	3/8 in (0.00953 m)
Longitudinal reinforcement	6 # 5(ϕ 15.88 mm)
Longitudinal reinforcement %	1.2%
Transverse reinforcement	$^3/_8$ @ 1 $^3/_4$ (10M @ 44 mm)
Density (ρ) (Monte Carlo)	2325 kg/m^3
Number of sections tested	2
Estimated E [1]	21.5 GPa
Poisson's ratio (υ)	0.2
Estimated velocity [2]	3190 m/s

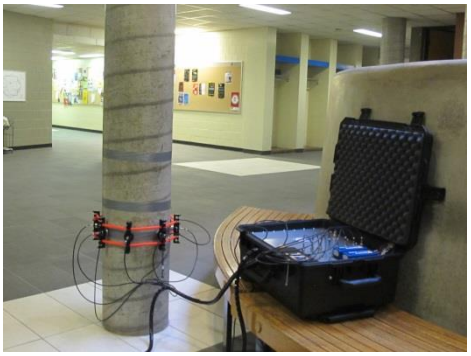

Figure A-15: Column RCH2

$(4700\sqrt{f'_c})$ [1]

$$V_p = \sqrt{\frac{E(1-\upsilon)}{\rho(1+\upsilon)(1-2\upsilon)}} \quad [2]$$

Figure A-16: Section RCH2_1

Figure A-17: Section RCH2_2

Figure A-18: Section RCH2_3

Table A-6: Geometrical information for column RCH3

Location	Room 218 J.R. Coutts Engineering Lecture Hall
Diameter (D)	18 in (0.46 m)
Details reference	SCAN_314R_S1_011_S_Foundation Plan & Details
Specified strength (f'_c)	3000 psi (21 MPa)
Concrete cover	3/8 in (0.010 m)
Longitudinal reinforcement	6 # 9(ϕ 28.65 mm)
Longitudinal reinforcement %	2.4%
Transverse reinforcement	$^{3}/_{8}$ @ 2 $^{1}/_{2}$ (10M @ 64 mm)
Density (ρ) (Monte Carlo)	2325 kg/m^3
Number of sections tested	2
Estimated E [1]	21.5 GPa
Poisson's ratio (υ)	0.2
Estimated velocity [2]	3190 m/s

Figure A-19: Column RCH3

$(4700\sqrt{f'_c})$ [1]

$$V_p = \sqrt{\frac{E(1-\upsilon)}{\rho(1+\upsilon)(1-2\upsilon)}}$$ [2]

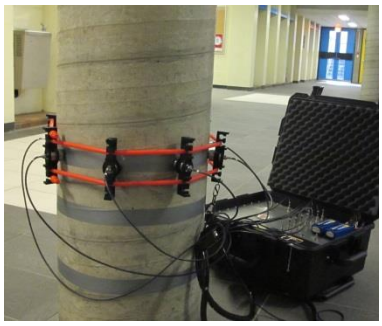

Figure A-20: Section RCH3_1

Figure A-21: Section RCH3_2

Figure A-22: Section RCH3_3

Table A-7: Geometrical information for column CN1

Location	NDT Lab
Diameter (D)	0.306 m
Details reference	Visual inspection
Specified strength (f'_c)	Unknown
Concrete cover	0.05 m
Longitudinal reinforcement	6 15M
Area of reinforcement	0.00121m²
Percentage reinforcement (ρ)	1.64 %
Transverse reinforcement	Unknown
Estimated E ($4700\sqrt{f'_c}$)	Unknown
Number of sections tested	1
Height from floor	54 cm

Figure A-23: Column CN1 NDT lab

Figure A-24: Section CN1

Figure A-25: Top view CN1

Table A-8: Geometrical information for mortar sample M1

Location	NDT Lab
Diameter (D)	0.306 m
Details reference	Berubé, S. 2008
Density	2102 kg/m^3
Poisson's ratio	0.33
Estimated E	29.5GPa
Theoretical velocity	4566 m/s
Location section	Middle section
Number of sections tested	1

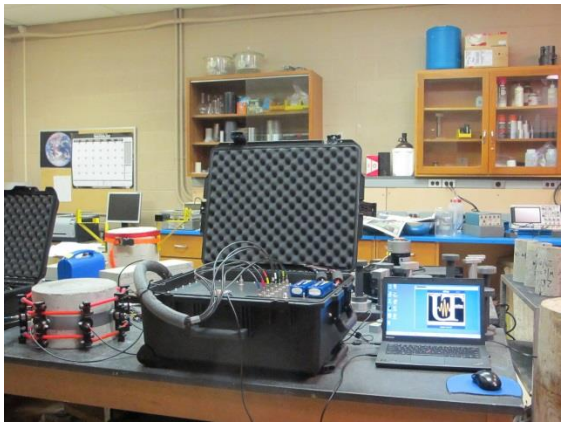

Figure A-26: Sample M1 NDT lab

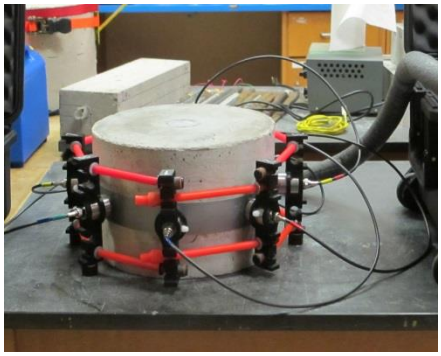

Figure A-27: Section M1

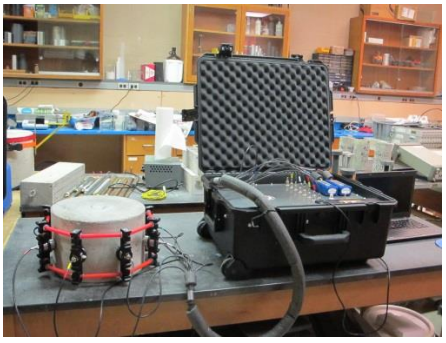

Figure A-28: Setup for testing M1

APPENDIX B

Velocity and Attenuation Results

Table B-1: Results for section STC1_1

	SECTION	STC1_1	Neper / cm	
#	RAYPATH	V_P (m/s)	α(1)	α(2)
1	AD (180)	5173	0.0449	0.0449
2	BC (180)	5102	0.0447	0.0447
3	AB-DC (180)	5074	0.0460	0.0460
4	BD-CA (180)	5176	0.0486	0.0486
5	A-BD (135)	5015	0.0522	0.0522
6	A-DC (135)	5211	0.0582	0.0582
7	B-DC (135)	5286	0.0642	0.0642
8	B-CA (135)	5138	0.0676	0.0676
9	D-CA (135)	5159	0.0561	0.0561
10	D-AB (135)	5227	0.0591	0.0591
11	C-AB (135)	5068	0.0612	0.0612
12	C-BD (135)	5127	0.0528	0.0528
13	A-B (90)	4856	0.0909	0.0909
14	B-D (90)	5265	0.0825	0.0825
15	D-C (90)	5792	0.1195	0.1195
16	C-A (90)	5245	0.0932	0.0932
17	AB-BD (90)	5093	0.0889	0.0887
18	BD-DC (90)	5638	0.1092	0.1092
19	DC-CA (90)	5507	0.1022	0.1022
20	CA-AB (90)	4864	0.0932	0.0995

Table B-2: Results for section STC1_2

	SECTION	STC1_2	Neper / cm	
#	RAYPATH	V_P (m/s)	α(1)	α(2)
1	AD (180)	5108	0.04801	0.04801
2	BC (180)	5188	0.04688	0.04688
3	AB-DC (180)	5168	0.04513	0.04513
4	BD-CA (180)	5107	0.04343	0.04343
5	A-BD (135)	5097	0.06248	0.06248
6	A-DC (135)	5186	0.05982	0.05982
7	B-DC (135)	5296	0.05885	0.05885
8	B-CA (135)	5022	0.05705	0.05705
9	D-CA (135)	5364	0.06960	0.06960
10	D-AB (135)	5177	0.06068	0.06068
11	C-AB (135)	5101	0.05940	0.05940
12	C-BD (135)	5264	0.06482	0.06482
13	A-B (90)	4924	0.09329	0.09329
14	B-D (90)	5315	0.08925	0.08925
15	D-C (90)	5561	0.11190	0.11190
16	C-A (90)	5201	0.10010	0.10010
17	AB-BD (90)	5406	0.09913	0.09913
18	BD-DC (90)	5356	0.10040	0.10040
19	DC-CA (90)	5335	0.09433	0.09433
20	CA-AB (90)	5036	0.10030	0.10030

Table B-3: Results for section STC2_2

	SECTION	STC2_1	Neper / cm	
#	RAYPATH	V_P (m/s)	α(1)	α(2)
1	AD (180)	5201	0.0387	0.0387
2	BC (180)	5215	0.0411	0.0411
3	AB-DC (180)	5185	0.0361	0.0361
4	BD-CA (180)	5347	0.0516	0.0516
5	A-BD (135)	5190	0.0500	0.0500
6	A-DC (135)	5271	0.0536	0.0536
7	B-DC (135)	5331	0.0522	0.0522
8	B-CA (135)	5062	0.0544	0.0544
9	D-CA (135)	5216	0.0521	0.0521
10	D-AB (135)	5280	0.0536	0.0536
11	C-AB (135)	5136	0.0474	0.0474
12	C-BD (135)	5310	0.0557	0.0557
13	A-B (90)	5006	0.0778	0.0778
14	B-D (90)	5386	0.0754	0.0754
15	D-C (90)	5287	0.0859	0.0859
16	C-A (90)	5140	0.0758	0.0758
17	AB-BD (90)	5196	0.0759	0.0759
18	BD-DC (90)	5335	0.0811	0.0811
19	DC-CA (90)	5325	0.0822	0.0822
20	CA-AB (90)	4913	0.0837	0.0837

Table B-4: Results for section STC2_2

	SECTION	STC2_2	Neper / cm	
#	RAYPATH	V_P (m/s)	α(1)	α(2)
1	AD (180)	5336	0.04329	0.04329
2	BC (180)	5212	0.0366	0.0366
3	AB-DC (180)	5214	0.0395	0.0395
4	BD-CA (180)	5318	0.0435	0.0435
5	A-BD (135)	5140	0.0463	0.0463
6	A-DC (135)	5175	0.0448	0.0448
7	B-DC (135)	5329	0.0485	0.0485
8	B-CA (135)	5175	0.0523	0.0526
9	D-CA (135)	5375	0.0518	0.0518
10	D-AB (135)	5216	0.0514	0.0514
11	C-AB (135)	5108	0.0446	0.0446
12	C-BD (135)	5298	0.0457	0.0457
13	A-B (90)	4996	0.0805	0.0805
14	B-D (90)	5288	0.0792	0.0792
15	D-C (90)	5297	0.0674	0.0674
16	C-A (90)	5300	0.0882	0.0882
17	AB-BD (90)	4999	0.0808	0.0808
18	BD-DC (90)	5568	0.0854	0.0854
19	DC-CA (90)	5190	0.0722	0.0722
20	CA-AB (90)	4859	0.0748	0.0748

Table B-5: Results for section STC2_3

	SECTION	STC2_3	Neper / cm	
#	RAYPATH	V_P (m/s)	α(1)	α(2)
1	AD (180)	5287	0.04378	0.04378
2	BC (180)	5244	0.0407	0.0407
3	AB-DC (180)	5294	0.0407	0.0407
4	BD-CA (180)	5370	0.0472	0.0472
5	A-BD (135)	5177	0.0537	0.0537
6	A-DC (135)	5213	0.0503	0.0503
7	B-DC (135)	5412	0.0548	0.0548
8	B-CA (135)	5132	0.0545	0.0545
9	D-CA (135)	5257	0.0504	0.0504
10	D-AB (135)	5404	0.0531	0.0531
11	C-AB (135)	5141	0.0562	0.0562
12	C-BD (135)	5335	0.0518	0.0518
13	A-B (90)	4910	0.0821	0.0821
14	B-D (90)	5460	0.0764	0.0764
15	D-C (90)	5285	0.0811	0.0811
16	C-A (90)	5088	0.0805	0.0805
17	AB-BD (90)	5137	0.0800	0.0800
18	BD-DC (90)	5399	0.0772	0.0772
19	DC-CA (90)	5290	0.0806	0.0806
20	CA-AB (90)	4779	0.0817	0.0817

Table B-6: Results for section STC3_1

	SECTION	STC3_1	Neper / cm	
#	RAYPATH	V_P (m/s)	α(1)	α(2)
1	AD (180)	5191	0.04704	0.04704
2	BC (180)	5351	0.05788	0.05788
3	AB-DC (180)	5146	0.04196	0.04196
4	BD-CA (180)	5404	0.05716	0.05716
5	A-BD (135)	5058	0.05664	0.05664
6	A-DC (135)	5175	0.06345	0.06345
7	B-DC (135)	5220	0.06004	0.06004
8	B-CA (135)	5138	0.06360	0.06360
9	D-CA (135)	5292	0.06576	0.06576
10	D-AB (135)	5246	0.05755	0.05755
11	C-AB (135)	5131	0.06246	0.06246
12	C-BD (135)	5333	0.06094	0.06094
13	A-B (90)	5080	0.10730	0.10730
14	B-D (90)	5454	0.10800	0.10800
15	D-C (90)	5345	0.10570	0.10570
16	C-A (90)	5090	0.10240	0.10240
17	AB-BD (90)	5161	0.09550	0.09550
18	BD-DC (90)	5519	0.10210	0.10210
19	DC-CA (90)	5345	0.10170	0.10170
20	CA-AB (90)	4817	0.09783	0.09783

Table B-7: Results for section STC3_3

	SECTION	STC3_3	Neper / cm	
#	RAYPATH	V_P (m/s)	α(1)	α(2)
1	AD (180)	5243	0.04608	0.04608
2	BC (180)	5237	0.04814	0.04814
3	AB-DC (180)	5179	0.03859	0.03859
4	BD-CA (180)	5251	0.05166	0.05166
5	A-BD (135)	5133	0.05783	0.05783
6	A-DC (135)	5278	0.05574	0.05574
7	B-DC (135)	5565	0.06905	0.06905
8	B-CA (135)	5068	0.06184	0.06184
9	D-CA (135)	5264	0.06302	0.06302
10	D-AB (135)	5356	0.05994	0.05994
11	C-AB (135)	5143	0.05927	0.05927
12	C-BD (135)	5435	0.06589	0.06589
13	A-B (90)	5059	0.10180	0.10180
14	B-D (90)	5567	0.10600	0.10600
15	D-C (90)	5178	0.09313	0.09313
16	C-A (90)	5142	0.08970	0.08970
17	AB-BD (90)	5275	0.10310	0.10310
18	BD-DC (90)	5502	0.10330	0.10330
19	DC-CA (90)	5247	0.09341	0.09341
20	CA-AB (90)	4919	0.08675	0.08675

Table B-8: Results for section RCH1

	SECTION	RCH1	Neper / cm	
#	RAYPATH	V_P (m/s)	α(1)	α(2)
1	AD (180)	4517	0.08132	0.08132
2	BC (180)	4425	0.09192	0.09192
3	AB-DC (180)	4517	0.10900	0.10290
4	BD-CA (180)	4592	0.09186	0.09186
5	A-BD (135)	4584	0.1016	0.1016
6	A-DC (135)	4627	0.1070	0.1070
7	B-DC (135)	4672	0.0914	0.0914
8	B-CA (135)	4525	0.1096	0.1096
9	D-CA (135)	4624	0.1040	0.1040
10	D-AB (135)	4534	0.1242	0.1242
11	C-AB (135)	4528	0.1353	0.1353
12	C-BD (135)	4627	0.0977	0.0977
13	A-B (90)	4631	0.1536	0.1536
14	B-D (90)	4890	0.1354	0.1354
15	D-C (90)	4867	0.1425	0.1425
16	C-A (90)	4816	0.1517	0.1517
17	AB-BD (90)	4778	0.1752	0.1752
18	BD-DC (90)	4833	0.1350	0.1350
19	DC-CA (90)	5025	0.1653	0.1653
20	CA-AB (90)	4870	0.1831	0.1831

Table B-9: Results for section RCH2_1

	SECTION	RCH2_1	Neper / cm	
#	RAYPATH	V_P (m/s)	α(1)	α(2)
1	AD (180)	4593	0.1179	0.1179
2	BC (180)	4890	0.076	0.07569
3	AB-DC (180)	4655	0.06384	0.06384
4	BD-CA (180)	4733	0.08609	0.08609
5	A-BD (135)	4847	0.08153	0.08153
6	A-DC (135)	4902	0.09566	0.09566
7	B-DC (135)	5077	0.09519	0.09519
8	B-CA (135)	4727	0.1174	0.1174
9	D-CA (135)	4652	0.1409	0.1409
10	D-AB (135)	4580	0.1438	0.1438
11	C-AB (135)	4683	0.08967	0.08967
12	C-BD (135)	4996	0.08956	0.08956
13	A-B (90)	4783	0.1234	0.1234
14	B-D (90)	5087	0.1734	0.1734
15	D-C (90)	4635	0.1504	0.1504
16	C-A (90)	5174	0.1693	0.1693
17	AB-BD (90)	4970	0.1285	0.1285
18	BD-DC (90)	4931	0.1151	0.1151
19	DC-CA (90)	4846	0.1392	0.1392
20	CA-AB (90)	4635	0.184	0.184

Table B-10: Results for section RCH2_2

	SECTION	RCH2_2	Neper / cm	
#	RAYPATH	V_P (m/s)	α(1)	α(2)
1	AD (180)	4913	0.09755	0.09755
2	BC (180)	4794	0.07568	0.07568
3	AB-DC (180)	4844	0.08294	0.08294
4	BD-CA (180)	4883	0.06599	0.06599
5	A-BD (135)	4898	0.09452	0.09452
6	A-DC (135)	4797	0.08711	0.08711
7	B-DC (135)	4785	0.11630	0.11630
8	B-CA (135)	4902	0.09845	0.09845
9	D-CA (135)	4895	0.10360	0.10360
10	D-AB (135)	4702	0.09814	0.09814
11	C-AB (135)	4575	0.10650	0.10650
12	C-BD (135)	4839	0.08185	0.08185
13	A-B (90)	5080	0.14220	0.14220
14	B-D (90)	5009	0.14390	0.14390
15	D-C (90)	4890	0.15880	0.15880
16	C-A (90)	4891	0.13100	0.13100
17	AB-BD (90)	4762	0.11470	0.11470
18	BD-DC (90)	5009	0.14570	0.14570
19	DC-CA (90)	4996	0.13320	0.13320
20	CA-AB (90)	4615	0.14130	0.14130

Table B-11: Results for section RCH2_3

	SECTION	RCH2_3	Neper / cm	
#	RAYPATH	V_P (m/s)	α(1)	α(2)
1	AD (180)	4688	0.10650	0.10650
2	BC (180)	4742	0.07797	0.07797
3	AB-DC (180)	4600	0.06999	0.06999
4	BD-CA (180)	4791	0.07740	0.07740
5	A-BD (135)	4777	0.10710	0.10710
6	A-DC (135)	4859	0.11170	0.11170
7	B-DC (135)	4901	0.10770	0.10770
8	B-CA (135)	4721	0.10310	0.10310
9	D-CA (135)	4890	0.10640	0.10640
10	D-AB (135)	4675	0.10020	0.10020
11	C-AB (135)	4576	0.09113	0.09113
12	C-BD (135)	4847	0.09947	0.09947
13	A-B (90)	4686	0.12900	0.12900
14	B-D (90)	4686	0.13200	0.13200
15	D-C (90)	4728	0.14890	0.14890
16	C-A (90)	4910	0.15870	0.15870
17	AB-BD (90)	4572	0.12570	0.12570
18	BD-DC (90)	4763	0.13810	0.13810
19	DC-CA (90)	4924	0.11160	0.11160
20	CA-AB (90)	4633	0.16530	0.16530

Table B-12: Results for section RCH3_1

	SECTION	RCH3_1	Neper / cm	
#	RAYPATH	V_P (m/s)	α(1)	α(2)
1	AD (180)	4810	0.10360	0.10360
2	BC (180)	4798	0.08995	0.08995
3	AB-DC (180)	4672	0.08508	0.08508
4	BD-CA (180)	4534	0.10910	0.10910
5	A-BD (135)	4548	0.13450	0.13450
6	A-DC (135)	4834	0.11810	0.11810
7	B-DC (135)	4762	0.10080	0.10080
8	B-CA (135)	4622	0.11340	0.11340
9	D-CA (135)	4805	0.10960	0.10960
10	D-AB (135)	4648	0.10040	0.10040
11	C-AB (135)	4625	0.09608	0.09608
12	C-BD (135)	4805	0.11950	0.11950
13	A-B (90)	4629	0.15710	0.15710
14	B-D (90)	4863	0.16070	0.16070
15	D-C (90)	4971	0.13800	0.13800
16	C-A (90)	4995	0.14870	0.14870
17	AB-BD (90)	4533	0.16560	0.16560
18	BD-DC (90)	4930	0.14470	0.14470
19	DC-CA (90)	4995	0.13930	0.13930
20	CA-AB (90)	4643	0.12710	0.12710

Table B-13: Results for section RCH3_2

	SECTION	RCH3_2	Neper / cm	
#	RAYPATH	V_P (m/s)	α(1)	α(2)
1	AD (180)	4645	0.07570	0.07570
2	BC (180)	4726	0.08904	0.08904
3	AB-DC (180)	4756	0.10070	0.10070
4	BD-CA (180)	4646	0.10760	0.10760
5	A-BD (135)	4593	0.12840	0.12840
6	A-DC (135)	4810	0.11570	0.11570
7	B-DC (135)	4675	0.08814	0.08814
8	B-CA (135)	4591	0.09946	0.09946
9	D-CA (135)	4834	0.10000	0.10000
10	D-AB (135)	4757	0.10330	0.10330
11	C-AB (135)	4664	0.11900	0.11900
12	C-BD (135)	4758	0.11590	0.11590
13	A-B (90)	4863	0.14410	0.14410
14	B-D (90)	4811	0.12990	0.12990
15	D-C (90)	4874	0.13170	0.13170
16	C-A (90)	4799	0.14760	0.14760
17	AB-BD (90)	4592	0.20740	0.20740
18	BD-DC (90)	4982	0.13960	0.13960
19	DC-CA (90)	4876	0.12170	0.12170
20	CA-AB (90)	4642	0.13570	0.13570

Table B-14: Results for section RCH3_3

	SECTION	RCH3_3	Neper / cm	
#	RAYPATH	V_P (m/s)	α(1)	α(2)
1	AD (180)	4913	0.09216	0.09216
2	BC (180)	4810	0.07514	0.07514
3	AB-DC (180)	4830	0.07648	0.07648
4	BD-CA (180)	4644	0.11470	0.11470
5	A-BD (135)	4676	0.12840	0.12840
6	A-DC (135)	5178	0.11160	0.11160
7	B-DC (135)	5098	0.08541	0.08541
8	B-CA (135)	4746	0.11100	0.11100
9	D-CA (135)	5068	0.12670	0.12670
10	D-AB (135)	4935	0.11110	0.11110
11	C-AB (135)	4799	0.10350	0.10350
12	C-BD (135)	4835	0.12390	0.12390
13	A-B (90)	4956	0.13680	0.13680
14	B-D (90)	5053	0.14150	0.14150
15	D-C (90)	5090	0.14340	0.14340
16	C-A (90)	5168	0.15780	0.15780
17	AB-BD (90)	4596	0.16030	0.16030
18	BD-DC (90)	5124	0.13030	0.13030
19	DC-CA (90)	5096	0.13680	0.13680

Table B-15: Summary of the velocity measurements

SECTION	All receivers			Receivers at 180			Receivers at 135			Receivers at 90		
	μ_{all}	σ_{all}	COV_{all}	μ_{180}	σ_{180}	COV_{180}	μ_{135}	σ_{135}	COV_{135}	μ_{90}	σ_{90}	COV_{90}
STC1_1	5201	222	4.26%	5131	44	0.86%	5154	82	1.59%	5283	322	6.10%
STC1_2	5211	148	2.85%	5143	36	0.70%	5188	107	2.07%	5267	192	3.65%
STC2_1	5217	118	2.27%	5237	64	1.23%	5225	86	1.65%	5199	158	3.04%
STC2_2	5220	151	2.89%	5270	57	1.09%	5227	90	1.72%	5187	212	4.09%
STC2_3	5231	165	3.16%	5299	45	0.86%	5259	106	2.01%	5169	221	4.29%
STC2	**5222**	**148**	**2.83%**	**5269**	**64**	**1.22%**	**5237**	**98**	**1.86%**	**5185**	**204**	**3.93%**
STC3_1	5225	158	3.01%	5273	107	2.04%	5199	85	1.64%	5226	217	4.16%
STC3_3	5252	164	3.12%	5228	28	0.54%	5280	157	2.97%	5236	202	3.86%
STC3	**5238**	**161**	**3.08%**	**5250**	**87**	**1.66%**	**5240**	**137**	**2.61%**	**5231**	**217**	**4.14%**
RCH1	4674	158	3.38%	4513	59	1.31%	4590	52	1.14%	4839	104	2.15%
RCH2_1	4820	175	3.63%	4718	111	2.36%	4808	165	3.42%	4883	184	3.77%
RCH2_2	4854	125	2.57%	4859	45	0.92%	4799	107	2.22%	4907	144	2.93%
RCH2_3	4748	109	2.30%	4705	71	1.51%	4781	108	2.26%	4738	117	2.46%
RCH2	**4807**	**147**	**3.06%**	**4761**	**111**	**2.33%**	**4796**	**133**	**2.76%**	**4842**	**172**	**3.55%**
RCH3_1	4751	149	3.13%	4704	112	2.38%	4706	101	2.14%	4820	176	3.65%
RCH3_2	4745	109	2.29%	4693	49	1.04%	4710	87	1.86%	4805	121	2.51%
RCH3_3	4918	179	3.65%	4799	98	2.03%	4917	170	3.46%	4980	189	3.80%
RCH3	**4805**	**170**	**3.54%**	**4732**	**107**	**2.25%**	**4778**	**162**	**3.40%**	**4868**	**187**	**3.83%**

Table B-16: Summary of the attenuation results

SECTION	All receivers			Receivers at 180			Receivers at 135			Receivers at 90		
	μ_{all}	σ_{all}	COV_{all}	μ_{180}	σ_{180}	COV_{180}	μ_{135}	σ_{135}	COV_{135}	μ_{90}	σ_{90}	COV_{90}
STC1_1	0.07191	0.02305	0.32052	0.04603	0.00156	0.03380	0.05893	0.00497	0.08436	0.09782	0.01128	11.53%
STC1_2	0.07324	0.02199	0.30019	0.04586	0.00174	0.03792	0.06159	0.00375	0.06082	0.09859	0.00632	6.41%
STC2_1	0.06121	0.01607	0.26256	0.04188	0.00588	0.14046	0.05236	0.00247	0.04713	0.07972	0.00377	4.74%
STC2_2	0.05884	0.01698	0.28861	0.04072	0.00286	0.07029	0.04818	0.00308	0.06387	0.07855	0.00640	8.14%
STC2_3	0.06183	0.01538	0.24873	0.04308	0.00271	0.06301	0.05310	0.00200	0.03758	0.07994	0.00194	2.43%
STC2	**0.0606**	**0.0163**	**26.85%**	**0.0419**	**0.0043**	**10.24%**	**0.0512**	**0.0034**	**6.61%**	**0.0794**	**0.0045**	**5.69%**
STC3_1	0.075751	0.022646	0.298956	0.05101	0.006758	0.13248402	0.061305	0.002929	0.047782	0.10256625	0.00411	4.01%
STC3_3	0.072712	0.0214362	0.294809	0.046118	0.004782	0.10369414	0.0615725	0.004073	0.066149	0.09714875	0.006773	6.97%
STC3	**0.0742**	**0.0224**	**30.22%**	**0.0486**	**0.0066**	**13.49%**	**0.0614**	**0.0036**	**5.87%**	**0.0999**	**0.0063**	**6.33%**
RCH1	0.124179	0.0296305	0.238611	0.092763	0.008884	0.09576629	0.10884125	0.013446	0.123536	0.155225	0.016795	10.82%
RCH2_1	0.119027	0.0335974	0.282269	0.08588	0.020093	0.23396655	0.10671375	0.022727	0.212974	0.1479125	0.023837	16.12%
RCH2_2	0.110972	0.0262003	0.236099	0.08054	0.011515	0.142978	0.09830875	0.010183	0.103578	0.13885	0.012065	8.69%
RCH2_3	0.113398	0.0254338	0.224288	0.082965	0.013948	0.16811685	0.10335	0.005983	0.057891	0.1386625	0.016787	12.11%
RCH2	**0.1145**	**0.0290**	**25.31%**	**0.0831**	**0.0161**	**19.37%**	**0.1028**	**0.0157**	**15.24%**	**0.1418**	**0.0189**	**13.34%**
RCH3_1	0.123066	0.023776	0.193198	0.096933	0.009769	0.10078243	0.1115475	0.011828	0.106037	0.14765	0.012128	8.21%
RCH3_2	0.120032	0.0278565	0.232076	0.09326	0.012116	0.12991209	0.1087375	0.012288	0.113006	0.1447125	0.02491	17.21%
RCH3_3	0.138318	0.1031353	0.745642	0.17566	0.223189	1.27057584	0.11270125	0.013248	0.117545	0.1452625	0.010409	7.17%
RCH3	**0.1214**	**0.0257**	**21.20%**	**0.0933**	**0.0135**	**14.47%**	**0.1110**	**0.0127**	**11.45%**	**0.1459**	**0.0173**	**11.87%**